REPUBLIC OF TÜRKİYE
HARRAN UNIVERSITY
GRADUATE SCHOOL OF NATURAL AND APPLIED SCIENCES

DOCTORATE THESIS

LOAD-DEFORMATION BEHAVIOR OF SELF-COMPACTING GEOPOLYMER CONCRETE FILLED STEEL TUBES UNDER AXIAL LOADING

ESAMADDIN MSAEED MULAPEER MULAPEER

DEPARTMENT OF CIVIL ENGINEERING

Şanlıurfa
2024

REPUBLIC OF TÜRKİYE
HARRAN UNIVERSITY
GRADUATE SCHOOL OF NATURAL AND APPLIED SCIENCES

DOCTORATE THESIS

LOAD-DEFORMATION BEHAVIOR OF SELF-COMPACTING GEOPOLYMER CONCRETE FILLED STEEL TUBES UNDER AXIAL LOADING

ESAMADDIN MSAEED MULAPEER MULAPEER

DEPARTMENT OF CIVIL ENGINEERING
Thesis Supervisor: Prof. Dr. KASIM MERMERDAŞ
Thesis Co-Supervisor: Assoc. Prof. Dr. Radhwan ALZEEBAREE

Şanlıurfa
2024

ACKNOWLEDGEMENT

My heartfelt and sincere thanks to the Almighty God Allah, who granted me all these graces to fulfil this task and supported me throughout my life.

First, I would like to thank Prof. Dr. Kasım Mermerdaş, who offered me years of supervision, guided me during the research process, and gave me valuable guidance, advice, encouragement, and extensive experience during the entire research and dissertation writing stages.

I want to express my deep gratitude and appreciation to my participant's supervisor, Assist. Prof. Dr. Radhwan Alzeebaree, who provided me with a lot of advice and guidance during the experimental work and the preparation of the research.

I want to thank my wife, Avin Rafiq, who always helps and supports me in my research, my life, and all my family members.

I would like to extend special thanks to my brother,Assist. Prof. Dr. Mohamed Tahir Mulapeer, who guided me and facilitated the conduct of some laboratory tests on the mechanics of materials.
I also want to thank my father and mother for their prayers, patience, support, and tolerance.
Finally, I would like to thank my colleague, a PhD candidate, Nadhim Hamah Sor, whose presence was always necessary during my doctoral studies.

CONTENTS

ABSTRACT

DOCTORATE THESIS

LOAD-DEFORMATION BEHAVIOR OF SELF-COMPACTING GEOPOLYMER CONCRETE FILLED STEEL TUBES UNDER AXIAL LOADING

ESAMADDIN MSAEED MULAPEER MULAPEER

HARRAN UNIVERSITY
GRADUATE SCHOOL OF NATURAL AND APPLIED SCIENCES
DEPARTMENT OF CIVIL ENGINEERING

Thesis Supervisor: Prof. Dr. KASIM MERMERDAŞ
Thesis Co-Supervisor: Assoc. Prof. Dr. Radhwan ALZEEBAREE
Year:2024, Page : 104

In this thesis load-deformation behavior of the self-compacting geopolymer concrete (SCGC) filled composite columns was investigated. To achieve the aim of the study, the experimental study was designed as a two-stage program. The first one is the determination of proper mix proportions for geopolymer concrete to attain self-compatibility criteria conforming to EFNARC with a proper mechanical property. For this purpose, three types of coarse aggregate with three different grades were used for SCGC. The effect of aggregate type and size on the fresh and hardened properties of produced SCGCs was investigated. Two different base materials, blast furnace slag and fly ash, were used to produce self-compacting geopolymer concrete. Fresh properties were tested as per EFNARC requirements. A total of eighteen mixtures were produced. Compressive strength developments were investigated at ages 7 days, 14 days, 28 days, and 90 days. The second stage covers an experimental study regarding composite columns filled with self-compacting geopolymer concrete of the highest mechanical properties. To achieve this, concrete-filled steel tubes (CFST) were produced. The deformation performance of the produced composite columns and the load-carrying capacity were investigated. The research involved fabricating sixteen specimens of CFST with two length-to-diameter (L/D) ratios (short and long), four different tube diameters, and two different wall thicknesses. Self-compacting geopolymer concrete with a compressive strength of 45 MPa was used to ensure optimal compaction. The specimens were then subjected to axial load tests to examine their load-deformation characteristics, ultimate strength, shortening curves, and failure modes. The ultimate loading capacity of the columns was compared with two design codes, the American code ANSI/AISC 360-16 and European specifications for composite structural design for steel structures EC4. The test results show that the ultimate loading capacity increased with increasing the tube thickness; overall, the code provisions accurately predicted the capacity of the columns. The factors of L/D and relative slenderness are crucial and directly influence the behavior of CFST. However, the D/t ratio proved to have no significant effect on the column's behavior.

KEYWORDS: Self-compacting geopolymer concrete, Fresh state properties, Concrete-filled steel tube column, Load-deformation behavior

ÖZET

DOKTORA TEZİ

EKSENEL YÜKLEME ALTINDA KENDILIĞINDEN YERLEŞEN GEOPOLIMER BETON DOLGULU KOMPOZIT ELIK TÜP KOLONLARIN YÜK-DEFORMASYON DAVRANIŞLARI

ESAMADDIN MSAEED MULAPEER MULAPEER

HARRAN ÜNİVERSİTESİ
FEN BİLİMLERİ ENSTİTÜSÜ
İNŞAAT MÜHENDİSLİĞİ ANABİLİM DALI

Tez Danışmanı: Prof. Dr. KASIM MERMERDAŞ
Tez Eş-Danışmanı: Assoc. Prof. Dr. Radhwan ALZEEBAREE

Yıl:2024, Sayfa : 104

Bu tezde, kendiliğinden yerleşen geopolimer beton (KYGB) dolgulu kompozit kolonların yük-deformasyon davranışı incelenmiştir. Araştırmanın amacına ulaşabilmesi için deneysel çalışma iki aşamalı bir program olarak tasarlanmıştır. Bunlardan ilki, geopolimer betonun EFNARC'a uygun ve yeterli mekanik özelliğe sahip kendiliğinden yerleşebilirlik kriterlerini sağlayacak karışım oranlarının belirlenmesidir. Bu amaçla KYGB için üç farklı gradasyona sahip üç tip iri agrega kullanılmıştır. Agrega türü ve boyutunun üretilen KYGB'lerin taze ve sertleşmiş özelliklerine etkisi araştırılmıştır. Kendiliğinden yerleşen geopolimer beton üretiminde yüksek fırın cürufu ve uçucu kül olmak üzere iki farklı temel malzeme kullanılmıştır. Taze özellikler EFNARC gereksinimlerine göre test edilmiştir. Toplam on sekiz karışım üretilmiştir. Basınç dayanım gelişimleri 7 günlük, 14 günlük, 28 günlük ve 90 günlük yaşlarda incelenmiştir. İkinci aşama, en yüksek mekanik özelliklere sahip kendiliğinden yerleşen geopolimer betonla doldurulmuş kompozit kolonlara ilişkin deneysel bir çalışmayı kapsamaktadır. Bunun için beton dolgulu çelik tüp (BDÇT) üretilmiştir. Üretilen BDÇT'lerin deformasyon performansı ve yük taşıma kapasitesi araştırılmıştır. Araştırma, iki uzunluk-çap (L/D) oranına (kısa ve uzun), dört farklı tüp çapına ve iki farklı cidar kalınlığına sahip on altı BDÇT numunesinin üretilmesini içermektedir. En iyi kompaksiyon sağlamak için 45 MPa basınç dayanımına sahip kendiliğinden yerleşen geopolimer beton kullanılmıştır. Numuneler daha sonra yük-deformasyon özelliklerini, nihai mukavemetlerini, kısalma eğrilerini ve hasar modlarını incelemek için eksenel yük testlerine tabi tutulmuştur. Kolonların nihai yükleme kapasiteleri, iki tasarım koduyla; Amerikan ANSI/AISC 360-16 ve çelik yapılar EC4 için kompozit yapısal tasarıma ilişkin Avrupa spesifikasyonlarıyla karşılaştırılmıştır. Test sonuçları, çelik tüp kalınlığının artmasıyla nihai yükleme kapasitesinin arttığını göstermektedir. Genel olarak, standartlardaki bağıntıların kolonların kapasitesini doğru bir şekilde tahmin ettiği tespit edilmiştir. L/D ve göreceli narinlik faktörleri çok önemlidir ve BDÇT'lerin davranışını doğrudan etkilemiştir. Ancak D/t oranının kolonun davranışı üzerinde önemli bir etkiye sahip olmadığı görülmüştür.

ANAHTAR KELİMELER: Kendiliğinden yerleşen geopolymer beton, Taze özellikler, Beton dolgulu çelik tüp kolon, Yük-deformasyon davranışı

INDEX OF FIGURES

INDEX OF TABLES

ABBREVIATIONS

Ac : Cross-sectional Area of Concrete

ACI : American Concrete Institute

Ag : Gross Cross section

AISC : American Institute of Steel Construction

As : Cross-Sectional Area of Steel

ASTM : American Society for Testing and Materials

CaO : CaOCalcium oxide

CFST : Geopolymer Self-Compacting Concrete Filled Steel Tube

D/L : Diameter-to-length ration

D/t : Diameter to thickness ratio

Ec : Modulus of Elasticity of Concrete Cross-Sectional

EC4 : European Specifications for Composite Structures

Es : Modulus of Elasticity of Steel Section

F : Maximum load

FA : Fly ash

GGBS : ground granulated blast furnace slag

GPC : Geopolymer concrete

GSCC : Geopolymer self-compacting concrete

Ic : Concrete Cross-sectional Moment of Inertia

Ic : Concrete Cross-sectional Moment of Inertia

Is : Steel Shape moment of Inertia

KOH : Potassium hydroxide

M : Molar

MgO : Magnesium oxide

NaOH : sodium hydroxide

Nu : Ultimate Experimental Loading

OPC : Ordinary Portland Cement

Pe : Euler Critical Load

Pn : Nominal Compressive Strength

Pno : Composite Cross-Section Strength

SCC : Self-compacting concrete

SI : Strength Index

1. INTRODUCTION

1.1. General

In recent years, there has been a growing emphasis on developing sustainable and innovative construction materials and techniques to address the challenges of urbanisation, infrastructure development, and environmental sustainability. Concrete is a fundamental construction material, but its production and use contribute significantly to carbon emissions and energy consumption. As a result, researchers and engineers have been exploring alternative materials and methods that can reduce the environmental footprint of concrete structures.

Reducing greenhouse gas emissions, particularly carbon dioxide, has become a paramount objective in various human endeavours, and implementing sustainable development projects plays a central role in achieving this goal. In addition to utilising innovative technology for structural innovation in infrastructure construction, embracing the "low carbon" concept is imperative. The widespread use of concrete in construction operations heavily relies on Portland cement as a binding agent in concrete mixtures. However, cement manufacturing consumes substantial energy, contributing to approximately 10% of global carbon dioxide emissions. Reports indicate that the production of each ton of cement leads to the release of about one ton of CO_2, and the cement production industry is experiencing an annual growth rate of approximately 3% (Hardjito and Rangan, 2005).

New research recommends innovative alternatives to environmentally friendly materials to reduce the environmental problems associated with the construction industry (Wallah and Rangan, 2006; Wang et al., 2023; Golewski, 2023a). The production of geopolymer concrete, a sustainable and environmentally friendly alternative to ordinary Portland concrete, has gained significant traction (Lata, 2019; Golewski, 2023b; Golewski, 2023c). The mechanical and chemical properties of geopolymer concrete are superior to ordinary Portland concrete, including high compressive strength, low creep, good bonding with steel, good resistance to acid sulfate, and better fire resistance (Lata, 2019; Golewski, 2023b; Golewski, 2023c; Golewski, 2023d; Güneyisi et al., 2014; Temuujin et al., 2010).

As in the case of ordinary concrete, the problem of compaction in geopolymer concrete exists. To obtain geopolymer concrete with good compaction, it is possible to produce self-compacting concrete (SCC). Commonly, self-compacted concrete is used in civil engineering structures, especially in precast industries, high-rise

buildings, and congested reinforcement structures. The main features of self-compacted concrete are good workability, flowability, passing, and filling ability without causing bleeding and/or segregation. Self-consolidating geopolymer concrete can be considered a new and good invention in the concrete sector, as it is an advanced and environmentally friendly type of concrete that includes geopolymer and self-concrete concrete characteristics (Zrar et al., 2023; Gülşan et al., 2019). There are limited or very few studies on self-consolidating geopolymer concrete. To learn more about the factors that affect the characteristics of geopolymer concrete in its fresh or hard state, further investigation must be conducted to evaluate its properties and the factors that affect it.

High-performance reinforced concrete elements, especially columns, have been extensively used to construct skyscraper structures. It is well-established that as the concrete's strength increases, its ductility tends to decrease, thereby elevating the potential for sudden structural failures. Composite materials have become imperative to address the challenge of maintaining the ductility of concrete members, especially in high-rise buildings requiring exceptionally high strength (Lai et al., 2016). Concrete-filled steel tubes (CFTs) have gained widespread use as mega columns in towering structures like Goldin Finance 117 (597 m, Tianjin, China), SEG Plaza (356 m, Shenzhen, China), and the Two Union Square Utilizing high-strength materials, such as steel with a yield stress of at least 525 MPa and concrete with a compressive strength of at least 70 MPa, in construction offers the advantage of reducing the dimensions and weight of structural members while simultaneously increasing available space and structural span. A lot of research has been done on high-strength square concrete-filled tube (CFT) members. Some of the authors who have contributed are Sakino et al. (2004), Varma et al. (2005), Yong and Ellobody (2006), Xiong et al. (2017), Tao et al. (2021), Lai and Varma (2018), Wang et al. (2022), Z. Lai et al. (2018), and Wang et al. (2022)

Many experiments are being done on composite columns. For example, (Yan et al., 2023) did experiments on high-strength concrete-filled steel tube short columns and found that enclosing the steel tube could greatly increase the columns' ductility and compressive strength . Research has concluded that composite materials improve their properties compared to individually-used components. The strength of confined concrete and the corresponding stresses increase linearly as the actual confinement rates increase (Khan et al., 2020; Al-Saadi et al., 2018; Khan et al., 2016). So far, no studies have examined the mechanical properties of self-compacting geopolymer concrete filled steel tubes. One study investigates the

behaviour of recycled geopolymer concrete-filled steel tubular columns under axial loading (Shi et al., 2015). However, the other studies are limited to axial compression tests and mainly consider using conventional ordinary Portland cement concrete.

1.2. The aim of the study

This study investigates the fresh properties and compressive strength of self-compacting geopolymer concrete as an environmentally friendly alternative to conventional Portland cement concrete, and then uses self-compacting geopolymer concrete to produce composite columns by filling steel tubes with self-compacting geopolymer concrete and examines the deformation behavior of composite columns when axially loaded.

1.3. Thesis Organization

This thesis consists of seven chapters:

Chapter 1 covers an introduction to general information about the study topic and the main aims of the study.

Chapter 2 includes a brief review of the literature on the main content of this study.

Chapter 3 covers the properties of the materials used in this study, the preparation of materials with mixed proportions, the method of casting, the curing condition, and the testing procedures.

Chapter 4 presents the testing results.

Chapter 5 presents a detailed discussion of the test results.

Chapter 6 summarises all the results and discussions and briefly gives the study's conclusion.

Chapter 7 includes the general recommendations related to this study.

2. PREVIOUS STUDIES

2.1. Introduction

This chapter primarily examined the environmental impacts of the industrialising process of ordinary Portland cement, explored alternatives for OPC, and discussed the production of specialised concrete forms using these alternatives. The text provides a comprehensive overview of numerous studies conducted on geopolymer concrete, examining its application in concrete technology and its incorporation as a component in composite materials.

2.2. Ordinary Portland cement concrete and the environment

Concrete, an essential construction component, is the second most widely consumed commodity globally, following water. Cement is the main compound of concrete. Projections indicate that the demand for cement, a key input in concrete production, will rise from 4.2 billion metric tonnes (MT) to 6.2 billion MT by 2050.

According to a report from Malhotra (1999), Malhotra and Ramezanianpour (2004), the critical determinant of the environment is the quantity of CO_2 emissions. Certain activities in the industrial area, such as cement production, cause substantial greenhouse gas emissions, considerably impacting global warming. Tradable emissions refer to the economic processes expected to assist governments worldwide in achieving the emissions reduction targets established by the Kyoto Protocol in 1997. An approximate value of $10 can be assigned to each tonne of emissions.

The processes involved in cement manufacturing contribute around 7% of the emissions from greenhouse gases worldwide, or nearly 1.35 billion metric tonnes per year. Cement is ranked as the third most energy-intensive building material, behind steel and aluminium (Malhotra and Ramezanianpour, 2004).

Cement production is increasing by approximately 3% annually (McCaffrey, 2002). For each tonne of cement produced, approximately 1 tonne of carbon dioxide (CO_2) is emitted into the environment throughout this process. Carbon dioxide (CO_2) is generated due to burning fossil fuels and removing carbon from limestone in the kiln, as Roy mentioned (Roy, 1999).

Figure 2.1 illustrates the geographical utilisation of cement over ten years,

with 1997 serving as the reference year (Szabo et al., 2003). The majority of growth occurs in emerging regions. China and India have had the most substantial economic expansion. By 2030, their consumption of global cement production will reach over 50%. China's consumption will peak by 2020 and remain steady until 2030. This is because of the postulated equation for cement consumption, which follows an inverted U-shape hypothesis (Szabó et al., 2003).

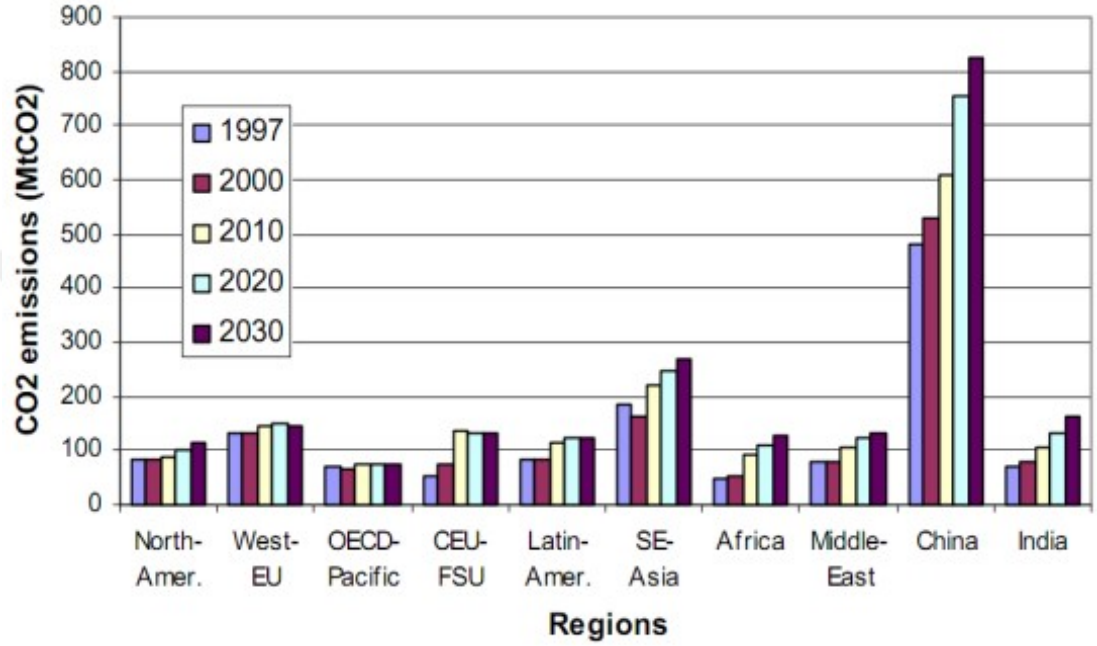

Figure 2.1. Estimation of global carbon dioxide emissions

2.3. Geopolymer concrete

Geopolymer is an inorganic polymer related to the polymers' family and forms a polymeric Si-O-Al framework in zeolite shape. The word "geopolymer" was first coined by Joseph Davidovits, a French chemist, in 1978. It involves the formation of aluminosilicate polymers in a high pH environment, leading to the development of a non-crystalline microstructure. In their 1998 study, Young et al. (1998) specified polymers as a class of substances composed of extensive molecules comprising several repetitive units known as monomers. The molecular composition of a unit governs the material properties of massive molecules. The amorphous state, also known as the non-crystalline state, is characterised by the complete absence of uniformity in atomic packing.

Geopolymer binder is a cementitious substance with reduced carbon dioxide emissions. The production of CO_2 is not contingent upon the calcination of limestone. This breakthrough can decrease 80% of the CO_2 greenhouse gas

emissions from the concrete industry (Young et al., 1998).

The chemical reaction between alkali polysilicates and Al_2SiO_5 results in the formation of structures with three-dimensional polymeric sialate linkages (Si-O-Al-O), which transition from an amorphous to a semicrystalline state (Davidovits, 1994). The term "sialate tetrahedral arrangements" refers to the organisation of atoms in a tetrahedral shape. The name "alkali silica-oxo-aluminate" is used to describe this arrangement. Figure 2.2 in Davidovits' work clarifies that the alkali elements involved in this arrangement are potassium, lithium or calcium, and sodium (Davidovits, 1988).

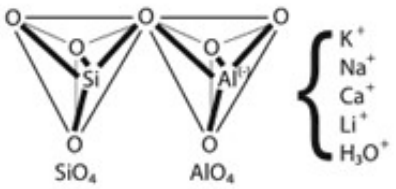

Figure 2.2. Arrange tetrahedrons in a Sialate structure

When exposed to hydroxide ions (-OH), the compound Al_2SiO_5 undergoes dissolution, a key step in forming polymers. Subsequently, ominous ions combine with monomers to create polycondensed structures, forming polymers (Hardjito and Rangan, 2005).

Natural sources of Al_2SiO_5 include spinel, andalusite, micas, clay, and kaolinite. Waste industrial materials, such as slag, fly ash, silica fume, and rice husk, can be sources of resources. Geopolymerization often involves using a solution containing aqueous alkaline colloidal polysilicates containing different types of sodium-based silica (Brykov, 2004; Rahi et al., 2014b).

In their study, Jang and Lee (2016) contributed significantly to our understanding of geopolymer strength development. They examined the characteristics effect of fly ash and the development of geopolymer strength made from FA. They observed a significant retardation in the development of high strength in the geopolymer. FA's chemical and physical properties were analysed using an X-ray fluorescence, particle size analyser, and X-ray diffraction tests. The researchers employed a range of analytical methods, including (SEM) scanning electron microscopy with (EDS) energy-dispersive X-ray spectroscopy, (MIP) mercury intrusion porosimetry, and (FT-IR) Fourier-transform infrared spectroscopy, to fully

understand the connection between the microstructure, strength development, and reaction products based on the maturity of the geopolymer (Jang and Lee, 2016). The study determined that the features of FA substantially impacted the qualities of geopolymer.

2.3.1. Geopolymerization

Geopolymerization, often referred to as polycondensation, is an intricate process responsible for the creation of geopolymers. It has been the subject of study for several decades. Nevertheless, this matter needs a more comprehensive understanding (Provis and Van Deventer, 2009). Although several research studies have been conducted on geopolymerization, further research is required to comprehensively examine the composition and characteristics of geopolymers. The geopolymerization process includes creating spatial structures from aluminosilicate source materials. These structures are amorphous or sub-crystalline and share similarities with zeolites (Koleżyński et al., 2018). Geopolymerization consists of Si-O-Al as polymeric structures. The structures mentioned consist of chains of tetrahedra made of AlO_4 and SiO_4 (Nguyen and Škvára, 2016). The tetrahedra chain comprises oxygen atoms shared between water molecules and metal cations such as calcium, sodium, lithium, potassium, or lithium. (Roy, 1999). Geopolymers and zeolites are distinguished by their amorphous forms at room temperature. Describing geopolymers is challenging due to their diverse morphologies, topologies, and compositions. (Koleżyński et al., 2018).

The process of geopolymerization comprises the subsequent primary steps (Koleżyński et al., 2018; Nguyen and Škvára, 2016; Fletcher et al., 2005):

1. Dissolution (deconstruction)

2. The process of oligomerisation.

3. Geopolymerization creates a solid substance by combining aluminosilicate minerals with an alkaline activator without using traditional cement.

Figure 2.3 illustrates the conceptual framework of several steps of the geopolymerization process presented by Duxson et al. (2006) (Duxson et al., 2006).

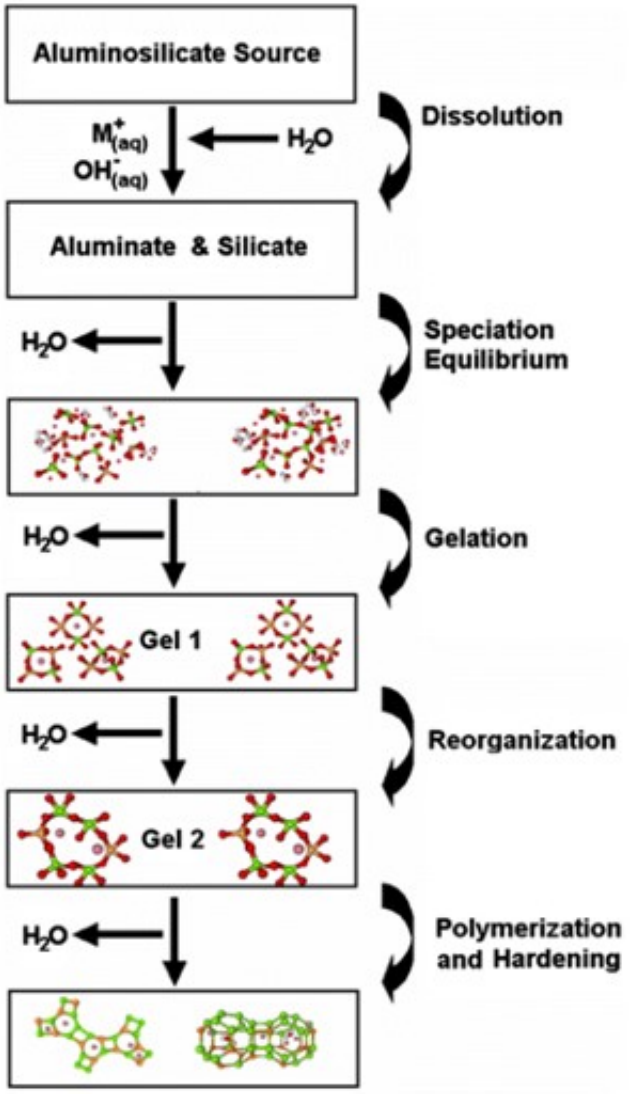

Figure 2.3. Geopolymerization process

2.3.2. Geopolymer base materials

A paste agent is necessary to remove the cement component from concrete, such as in geopolymer concrete. This paste is created by activating aluminosilicate with an alkaline regime. The aluminosilicate is called geopolymer base material. The primary components of geopolymer concrete are predominantly composed of byproducts such as pulverised granulated blast furnace slag, fly ash, silica fume, rice husk ash, and similar elements. Moreover, waste glass powder (Tho-In et al., 2018; Zhuang et al., 2016), phosphate sludge (Moukannaa et al., 2018), and red mud (Hu et al., 2018) were utilised in the production of geopolymer concrete as a foundational substance. These pozzolanic components enhanced the durability of geopolymer concrete (Golewski, 2023a; Golewski, 2023b). The base materials' physical properties, such as particle size and shape of particles, impact the properties of

geopolymer concrete when in its fresh state. Particles with a more rounded shape result in better workability. Additionally, geopolymer concrete's hardened properties are influenced by the chemical composition of the base materials.

Fly ash is produced as a byproduct of coal combustion and is considered an industrial waste material. It is collected mainly at power station plants and is widely available globallyThe aluminosilicate substance is classified as a pozzolan due to its ability to chemically react with calcium hydroxide $Ca(OH)_2$ and generate cementitious compounds. The fly ash can be categorised based on the kind of combustion burned coal. Class F fly ash is obtained from burning bituminous coals and anthracite, while fly ash produced from burning lignite coals and sub-bituminous coals is categorised as Class C. The constituents of fly ash Class F differ in terms of their composition. Their concentrations of silicon dioxide (SiO_2) and Aluminium oxide (Al_2O_3) are higher, but CaO is less than 10%. On the other hand, Fly ash Class C has a Calcium Oxide (CaO) content of over 10% and shows significant self-hardening characteristics (ASTM C618, 2012).

CaO improves the chemical reaction and strengthens geopolymerization (Diaz et al., 2011). The reactivity of fly ash depends on the silicon dioxide (SiO_2) ratio and its intrinsic features (Hemmings et al., 1989).

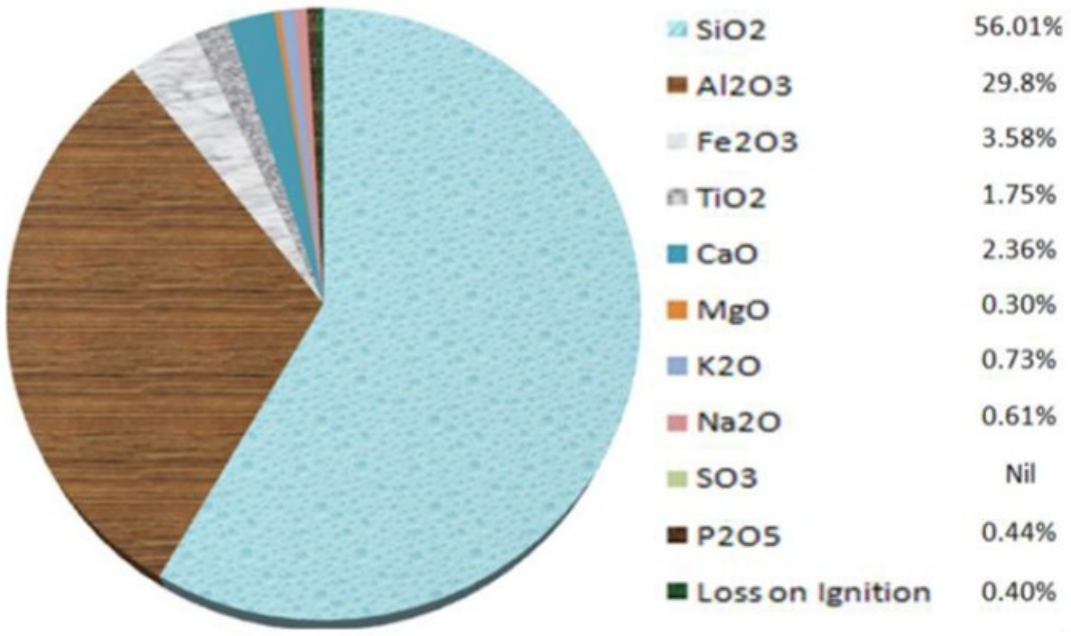

Figure 2.4. Fly ash chemical ingredients

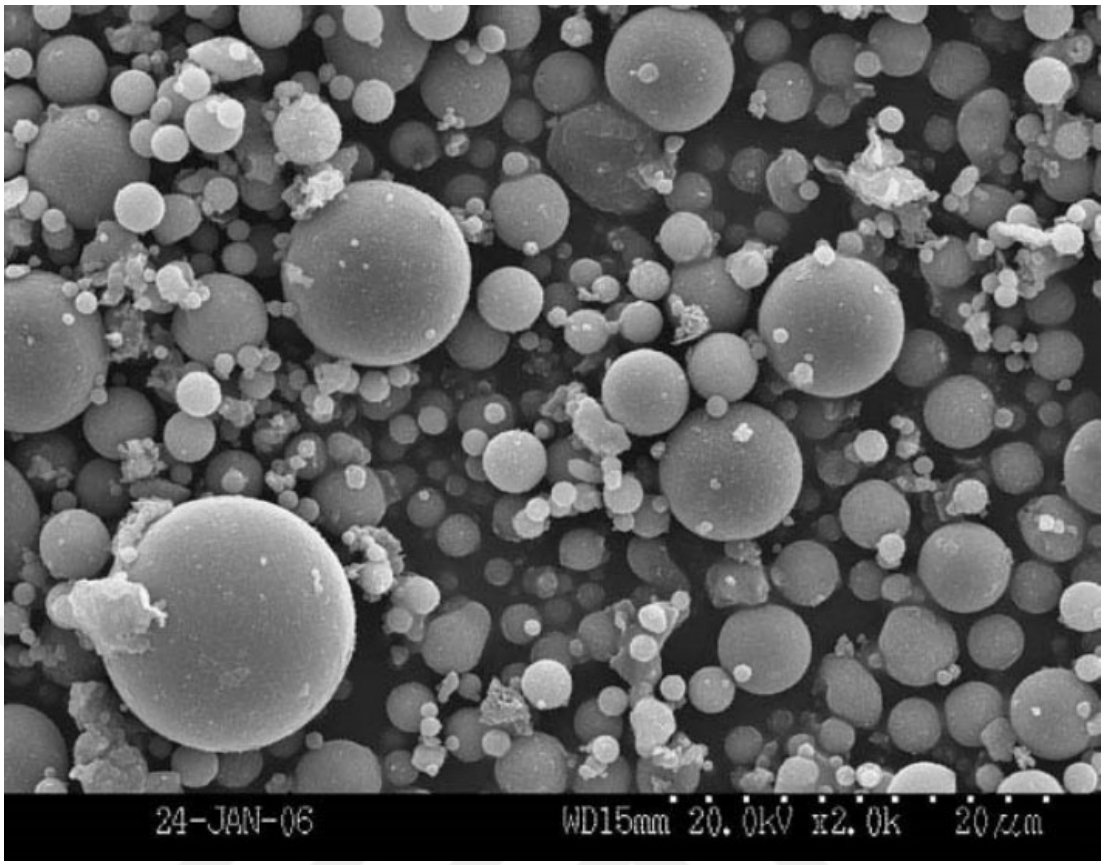

Figure 2.5. Fly ash microstructure

Including GGBFS in geopolymer significantly improves its compressive strength, which can be attributed to two factors.: i) the higher silicon/aluminium (Si/Al) ratio content in GGBFS accelerates the chemical reactivity with the activator compared to FA, which shows slower reactivity. and ii) the higher silicon/aluminium (Si/Al) ratio in GGBFS improved the microstructure of the geopolymer matrix by increasing the number of stronger Si-O-Si bonds (Resheidat and Alzyoud, 2008).

2.3.3. Geopolymer alkaline activator

The primary solution of alkali polysilicates consists of sodium silicate (Na_2SiO_3) and sodium hydroxide (NaOH). This solution is commonly employed in synthesising geopolymers based on fly ash (FA). Van Jaarsveld et al. (2002) concluded that the geopolymer production process mainly involves combining an alkaline solution, such as sodium hydroxide (NaOH) or potassium hydroxide (KOH), with sodium silicate (Na_2SiO_3) or potassium silicate (Ki_2SiO_3).

The choice of an activator is crucial in the formation of geopolymer products. The inclusion of soluble silicate in the alkaline activator significantly accelerates the rate of the reaction. This behaviour is observed when using sodium silicate (NaOH)

or potassium silicate (KOH) instead of simply alkaline hydroxides. (Palomo et al., 1999).

Xu and Van Deventer (2000) and Van Jaarsveld et al. (2002) demonstrated that the addition of sodium silicate (Na_2SiO_3) solution to the sodium hydroxide (NaOH) solution, resulting in an alkaline activator, the alkaline solution enhances the interaction with the base material. Through examining the geopolymerization process of Si-Al as a natural mineral, it was found that the KOH solution generally caused less mineral dissolution compared to the NaOH solution. Therefore, NaOH is considered to be superior.

The formation of the geopolymeric material structure is currently progressing through stages that are indistinguishable and parallel to each other. The first stage in forming the structure involves dissolving aluminium silicate (Al_2SiO_5) in a strongly alkaline solution obtained from the base material. In the second stage, the precursors are broken down to form a geopolymer composed of covalent linkages with a Si-O-Al-O composition. In the third stage, the oligomers undergo polycondensation, creating a three-dimensional framework composed of silicate (SiO_4) and nitrogen oxoanion (AlO_4) tetrahedra interconnected by oxygen ions. This process also involves the simultaneous elimination of H_2O. During the last phase, the solid particles bond and subsequently solidify, forming a polymeric structure (Giannopoulou and Panias, 2007).

Alkaline component ratio and concentration directly affect geopolymer concrete's compressive strength, NaOH's molarity, the ratio of Na_2SiO_3, and the alkali-to-base material ratio (Shilar et al., 2022; Zribi et al., 2019). Based on research, the ideal NaOH molarity recommended ranges (10–12), with a sodium silicate to sodium hydroxide (Na_2SiO_3/NaOH) ratio of 2.5 producing the maximum value of compressive strength and an alkali ratio to base materials of 0.55 (Shilar et al., 2022; Mathew and Issac, 2020).

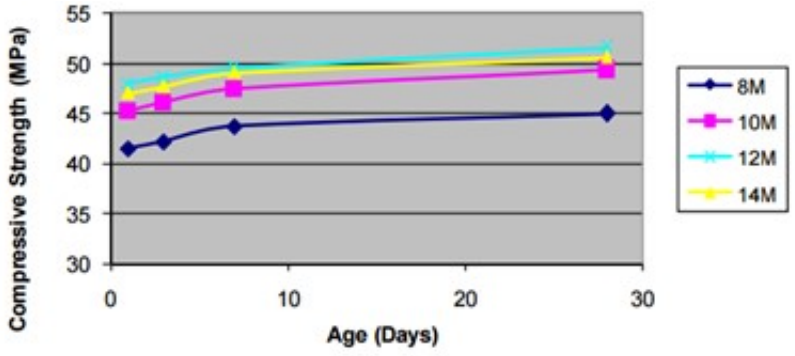

Figure 2.6. Effect of NaOH molarity on the geopolymer concrete compressive strength

Increasing the concentration (molarity) of sodium hydroxide (NaOH) or the ratio of sodium silicate to sodium hydroxide (Na_2SiO_3/NaOH) enhances the alkali viscosity and reduces geopolymer concrete's fluidity (Shilar et al., 2022; Mathew and Issac, 2020).

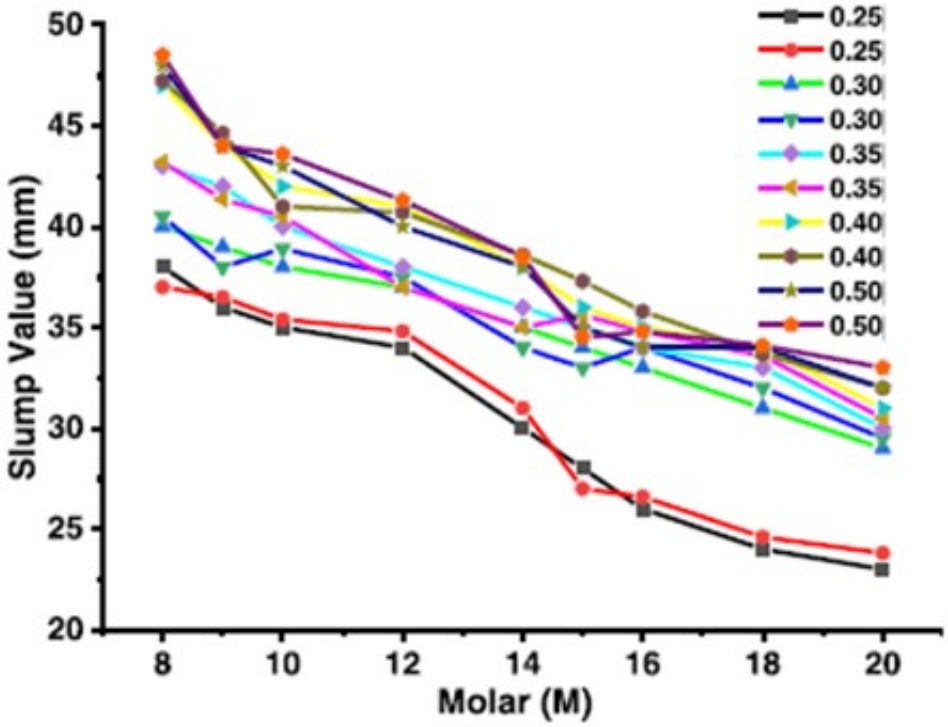

Figure 2.7. NaOH molarity effect on slump by variation of alkali/base material ratio

2.3.4. Curing regimes

During the geopolymerization process, curing temperature plays a crucial role. The optimal curing temperature should range from the surrounding temperature to 100°C (Nuruddin et al., 2011). Higher curing temperatures accelerate the

dissolving, polymerisation, and hardening processes in geopolymerization. Geopolymer samples showed ideal mechanical properties when curred at 60°C Therefore, this curing temperature is the ideal curing temperature for geopolymer curing. For example, Mo et al. (2014) demonstrated that geopolymer samples with metakaolin exhibited satisfactory compressive strength when exposed to a curing temperature of 60°C for 7 days. Salehi et al. (2017) did an experiment in which they exposed samples of sodium hydroxide (NaOH) and sodium silicate (Na_2SiO_3) based geopolymer to temperatures ranging from 25 to 80°C over 7 days to facilitate curing. The findings indicated that the geopolymer concrete achieved its maximum compressive strength when exposed to a temperature of 70°C for 48 hours (Nuruddin et al., 2011).

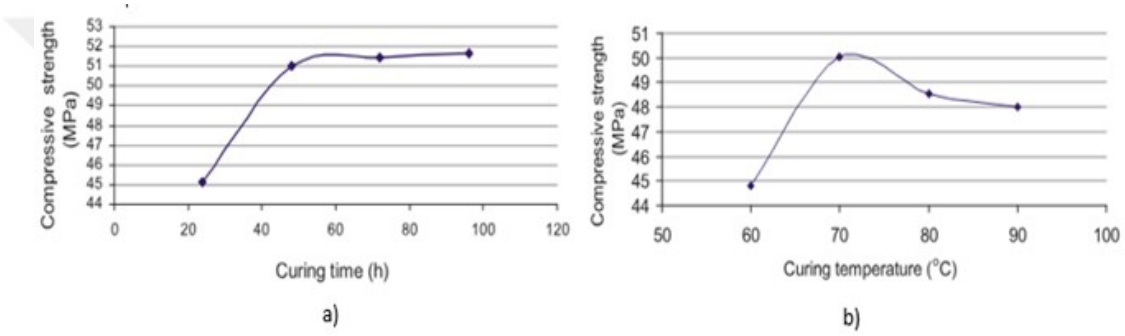

Figure 2.8. Curing time, b) curing temperature effect on GPC compressive strength

2.4. Self-compacting concrete

Nearly all concretes depend primarily on achieving complete compaction. When dealing with extensive and intricate structures, it can be challenging to guarantee complete compaction. Inadequate compaction greatly diminishes the ultimate performance of concrete, even with a good mix design. The proper placement of new concrete necessitates trained workers to achieve sufficient compaction, yielding the concrete's intended durability, strength, and durability in the hardened state (Resheidat and Alzyoud 2008; Erniati et al., 2006). When concrete is manufactured and deposited at construction sites under less-than-ideal conditions, employing normal vibration techniques may present a hazard to workers and give rise to issues regarding the durability and lifespan of the concrete (Hemant et al., 2009). An effective approach to address these challenges is the utilisation of SCC (Erniati et al., 2006; Hemant et al., 2009; Okamura and Ouchi, 1998).

Self-compacting concrete (SCC) is a concrete type that can be compacted through all areas of the moulds or formwork only due to its weight. Developing SCC

aims to achieve sufficient compaction and enable concrete placement in constructions with densely packed reinforcing and limited space. SCC, or self-compacting concrete, is widely acknowledged to have originated in 1980 in Japan as a direct response to the scarcity of experienced workers and the demand for enhanced durability. A researcher states that the necessity for SCC was initially recognised in 1986, and in 1988, the initial prototype was created. (Ouchi 2000) SCC has numerous advantages and benefits compared to conventional concrete. The benefits of using this method include enhanced concrete quality, decreased construction duration, simplified casting in crowded reinforcements, consistent and thorough consolidation, reduced noise levels, improved bond strength without vibration, decreased overall expenses, and a setting that is more secure and free from potential hazards (Resheidat and Alzyoud 2008; Dubey and Kumar, 2012; Druta, 2003).

An inherent challenge with normal concrete is the requirement for external energy for compaction. This can be acquired on-site through vibrating pokers, tables, or other alternative techniques in concrete factories.

SCC is a significant and influential development in concrete technology that greatly influences concrete practices. Originating in Japan, this technology was first used in the early 1990s and has quickly gained global acceptance in the building industry. SCC is a recently developed substance requiring new placement methods. It offers unique perspectives and inventive advancements to traditional concrete technology.

Concrete works traditionally prefer fresh mixes for greater ease of handling and placement. Consistently achieving a higher level of consistency will make the fresh combination more fluid, as Bartos (1992) stated. Nevertheless, this objective can only be accomplished by augmenting the volume of water in the combination or by amplifying the quantity of cement paste. In the early phases of the development of standard concrete, it was recognised that maintaining a high level of consistency (workability) was crucial (EN 206-1 2000).

Self-compacting geopolymer concrete (SCGC) is a significant and innovative development in concrete technology. It is a novel form of concrete that can be placed without vibration and is made by removing regular Portland cement.

2.4.1. Fresh properties

Characteristics of interest to any discussion of new SCC are those that affect its status and compactness. With these characteristics, SCC shines and distinguishes itself from other types of concrete. The characteristics of SCC are related to its fresh properties. Concrete concrete has three main new properties: fillability, passability and segregation resistance, and must be secured during transport and after pouring (Pade, 2005). These characteristics are interconnected and linked to each other. Any change in one property will generally lead to different properties. In other words, poor packing capacity and high separation resistance can lead to insufficient passing ability, i.e. blocking.

Concrete construction often uses fresh concretes with a moderate-low slump (Bartos, 1992). Realising the maximum strength of these concretes after hardening is highly dependent on obtaining complete compaction. Vibration has traditionally been the most prevalent technique for compacting conventional concrete. This is achieved by using vibrating tables, exterior vibrators, and internal (poker) vibrators.

The main characteristics that define self-compacting concrete are:

The flowing ability refers to a substance's capacity to effectively occupy all spaces and corners of the formwork in which it is placed.

The passing ability is to navigate through a densely packed structure without generating any disconnection or blockage among its components.

Resistance to segregation refers to the capacity to keep the larger particles in a mixture suspended, ensuring that the material remains uniform and consistent.

Self-compacting concrete can easily obtain high strength values but requires more paste than traditional concrete. As a result, there is a reduction in the elastic modulus. Increasing the quantity of fine particles is crucial for effectively mixing self-compacting concrete. The workability of aggregates is significantly affected by their geometric properties, which are widely recognised (Sosa et al., 2021). To achieve self-compacting concrete, i-aggregate content is limited, ii-reduced water is used, and iii-chemical admixtures such as superplasticisers are used (Bartos, 1992; Sosa et al., 2021).

2.4.2. Mix proportioning

To achieve self-compatibility, it is imperative to maintain robust packing capacity, practical obstacle-overcoming capabilities, and adequate separation resistance. However, the self-consolidating concrete (SCC) needs to possess a high degree of fluidity in its initial state to effectively occupy all the remote areas of the moulds while bearing its weight and passing through the substantial reinforcement without encountering any hindrance or detachment. Implementing a systematic approach to determine the optimal quantity of materials and additives is crucial to attaining the objective of self-compatibility. The three basic guidelines (Okamura and Ouchi, 2003) provided are depicted in Figure 2.9.

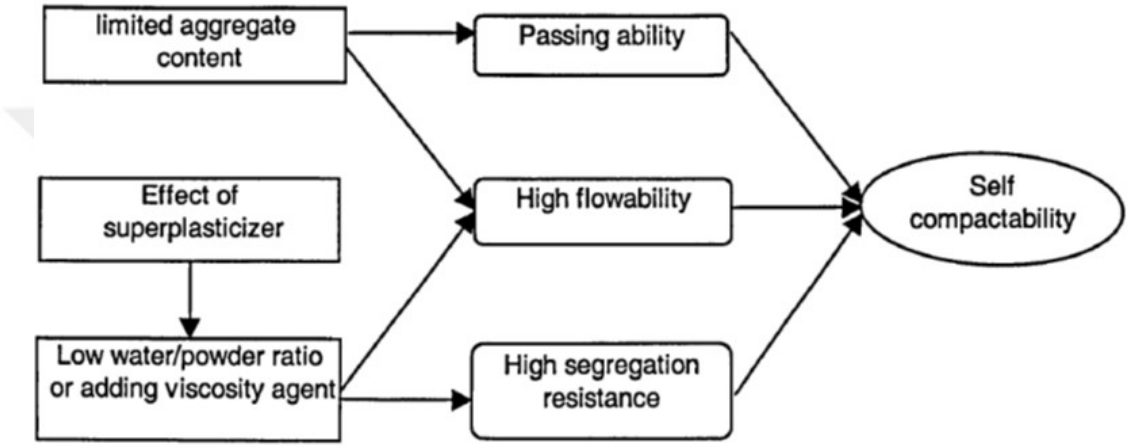

Figure 2.9. The three fundamental principles for achieving self-compacting concrete

Supercritical cement (SCC) exhibits a low water-to-powder ratio, indicating a high powder concentration. This characteristic is necessary to decrease the amount of free moisture and enhance the viscosity. This was the inaugural SCC prototype constructed. The SCC mixtures utilised in this methodology exhibit sensitivity to variations in constituent materials due to their elevated powder concentration. As a result of its low water-to-binder ratio, it is anticipated that this concrete will exhibit elevated strength, reduced shrinkage, and diminished permeability. Additives such as cement replacement materials (CRMs) and fillers are generally employed to substitute Portland cement and regulate the heat-induced hydration process.

2.4.3. Aggregate

Typically, aggregates comprise approximately 70-77% of the total volume of normal concrete and are obtained in fine and coarse aggregates. Self-compacting concrete aggregate content must be limited to achieve the required flowability. The mechanical properties such as tensile strength, compressive strength, and modulus of elasticity of self-compacting geopolymer concrete SCGC using a 10mm maximum

coarse aggregate exhibit greater values than the geopolymer concrete utilising a 20mm maximum size of coarse aggregate. This is due to the decreased maximum dimension of the coarse aggregate, resulting in an increased surface area. Consequently, the load applied to the concrete enhances the bonding strength in the transition zone (ITZ) surrounding the aggregate particles. Moreover, the influence of the coarse aggregate on compressive strength revealed that using crushed limestone in the mixtures resulted in greater mechanical properties, compressive strength and flexural strengths and a higher modulus of elasticity compared with crushed gravel (Khaleel et al., 2011).

This behaviour can be connected to the influence of chemical interaction and particles' more uneven surface texture, which results in a stronger binding between the aggregate and paste. Furthermore, the findings suggest that mixtures containing crushed gravel exhibit greater values for modulus of elasticity in addition to greater compressive strength and flexural strength than those containing uncrushed coarse gravel. The roughness of crushed gravel surfaces may explain this difference compared to uncrushed gravel surfaces. With fixing the water to powder (W/P) ratio and superplasticiser dosage, the flowability of self-compacting concrete (SCC) decreases by increasing the maximum size of coarse aggregate and the change in surface texture of coarse aggregate, such as using crushed type (Khaleel et al., 2011).

2.4.4. Superplasticiser

Superplasticiser achieve good self-compacting concrete flowability by reducing the water-to-cement (w/c) ratio or adding additional water. According to previous research definitions, the superplasticiser is a linear polymer with sulphuric groups linked to the polymer backbone at intervals (Nuruddin et al., 2011). Nuruddin et al. (2011) (Nuruddin et al. 2011) concluded that increasing the superplasticiser dosage up to 6% of the total volume of base material improved compressive strength at a fixed NaOH molarity.

An FESEM examination was conducted to evaluate the microstructural features of SCGC, with a particular focus on its ITZ. As the proportion of SP increased, the thickness of the ITZ dropped. The gap between the paste and aggregate resulted from an inadequate dosage, making them less malleable and reducing the concrete's strength. However, an increase in the percentage of SP to 6% or 7% led to the observation of improved refinement of the ITZ and the discontinuation of microcracks upon entering the ITZ. As a result, the strength was

greater than using 3%, 4%, and 5% SP dosage (Nuruddin et al., 2011).

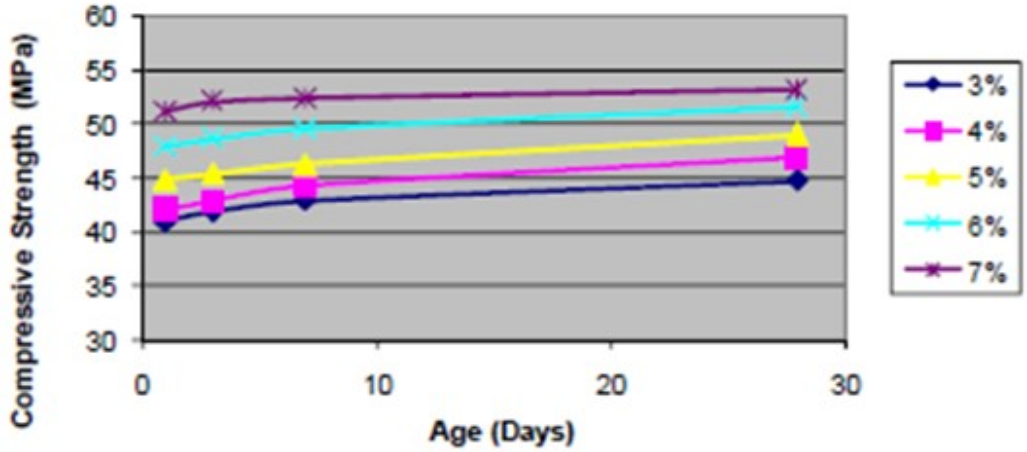

Figure 2.10. Effect of superplasticiser amount on geopolymer concrete's compressive strength

2.5. Concrete filled composite columns

2.5.1. General

Recently, there has been an increasing focus on developing sustainable and innovative construction materials and techniques to address the challenges of urbanisation, infrastructure development, and environmental sustainability. Concrete is a fundamental construction material, but its production and use contribute significantly to carbon emissions and energy consumption. Consequently, scientists and engineers have been investigating alternate materials and techniques that can diminish the ecological impact of concrete structures. High-strength concrete has been widely used in constructing skyscrapers, particularly for columns, due to the rapid growth of urbanisation and the associated challenges. It is well established that as the concrete's strength increases in resisting, its ductility tends to decrease, thereby elevating the potential for sudden structural failures. Composite materials have become imperative to address the challenge of maintaining the ductility of concrete members, especially in high-rise buildings requiring exceptionally high strength (Lai et al., 2016).

By conducting numerical studies and experimental experiments, it was revealed that the ductility and strength of composite members exceed those of reinforced concrete or steel members. This improvement in concrete steel-filled tubes (CSFT) as a composite materials' performance is achieved due to the good

confinement provided by the steel pipe's lateral support for the concrete fill. The lateral support provides additional energy to the filled concrete, and the pipe's ductility properties also improve the hole member ductility. (Lai et al., 2014).

2.5.2. Experimental considerations

Concrete-filled steel tubes have gained widespread use as mega columns in towering structures in Tianjin, China, in the Goldin Finance Building, consisting of 117 floors with a total height of 597 m, and also in SEG Plaza, with a height of 356 m, the same in Shenzhen, China. The Two Union Square used high-strength materials, steel yield stress of more than 525 MPa and high compressive strength with fc of more than 70 MPa in construction, reducing the dimensions and weight of structural members while increasing the available structural span and more space.

Two notable issues have been identified in this body of research: (i) In comparison to circular steel tubes, which uniformly confine the infill concrete, Square steel tubes offer a restricted level of confinement due to non-uniform confining pressure (Al-Saadi et al., 2018; Khan et al., 2020; Lai, Yan, et al., 2023). (ii) Using ultra-high performance concrete (UHPC) or high-strength concrete, concrete-filled steel tube square short columns with high strength display a brittle behaviour and a decrease in strength after reaching the peak. (Xiong et al., 2017; Lai, Yan, et al., 2023).

Many studies and investigations are being conducted on composite columns; studies and research on concrete-filled steel tube short columns with high strength have been conducted, concluding that confined steel tubes could significantly improve ductility and compressive strength (Khan et al., 2016). Research has concluded that composite materials improve their properties compared to individually-used components. The strength of the confined material and the related stresses exhibit a linear increase as the level of confinement increases (Khan et al., 2020; Al-Saadi et al., 2018; Khan et al., 2016). So far, no studies have examined the mechanical properties of self-compacting geopolymer concrete filled steel tubes. One study investigates the behaviour of recycled aggregate geopolymer concrete-filled steel tubes subjected to axial loading (Shi et al., 2015). However, the other studies are limited to axial loading tests and mainly consider using conventional ordinary Portland concrete.

Shi et al. (2015) conducted a study to determine the ductility enhancement of

geopolymer concrete-filled steel tube columns compared to geopolymer concrete columns and empty steel tubes. They achieved this by effectively confining the geopolymer concrete filled steel tube and comparing the results with the predicted strength capacity of the columns based on theoretical calculations using the mechanical characteristics of the materials. The researchers concluded that the improved model strongly correlated with the test results.

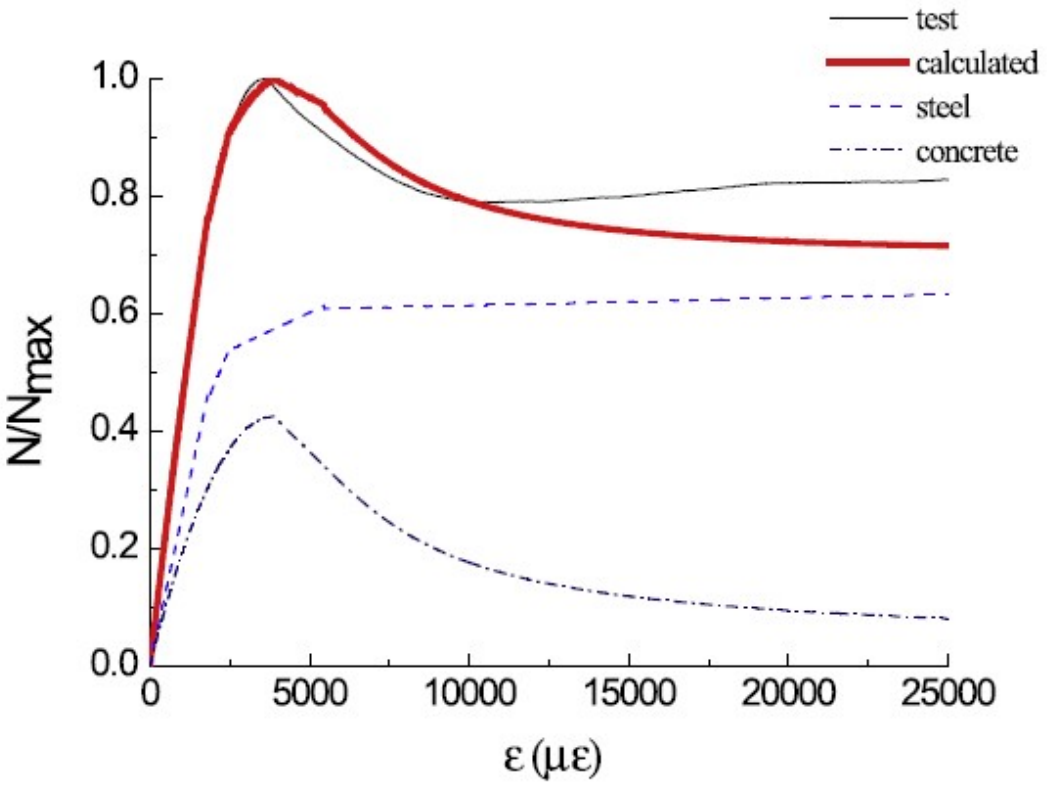

Figure 2.11. Stress-strain sample of GCFST

The enhancement of the ductility of composite materials relies on the mechanical characteristics of the concrete core, steel tube yield strength, and geometrical dimensions of the composite material, particularly the length of the steel tube, the diameter of the steel tube, and the thickness of the steel tube. According to De Oliveira et al. (2009), the concrete sample with a lower ratio of length to diameter (L/D) has a better strength capacity than the specimen with a higher (L/D) ratio when considering the value strength of the concrete core; the maximum strength capacity increased as the diameter-to-thickness (D/t) ratio decreased (Mustapha et al. 2021).

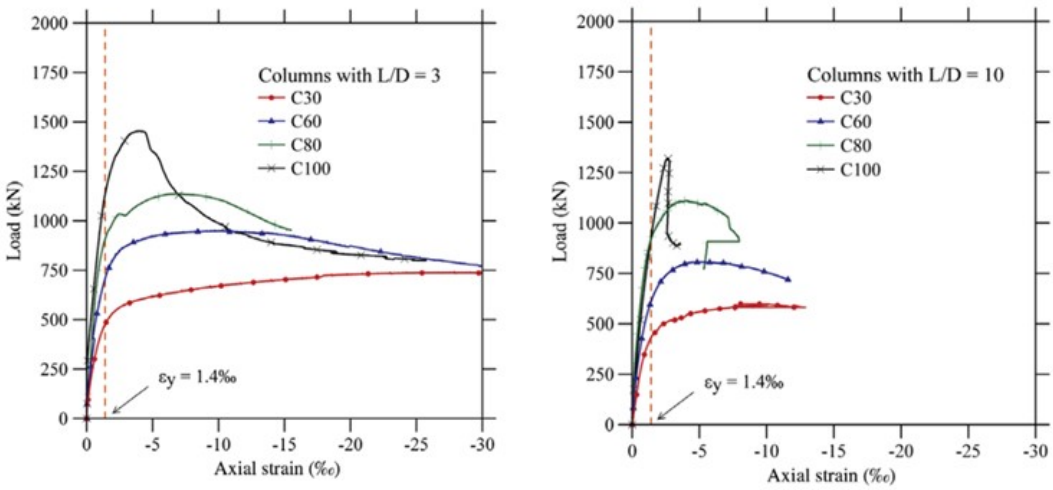

Figure 2.12. Load capacity of conventional concrete filled steel tubes with different D/L and same compressive strength

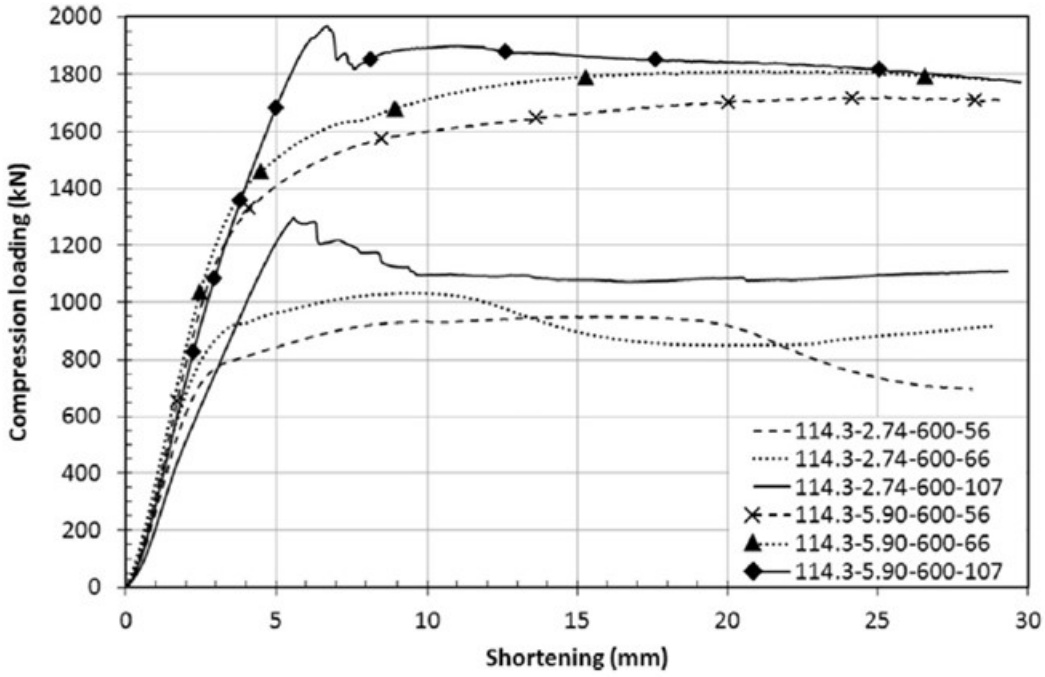

Figure 2.13. Load capacity of conventional concrete filled steel tube of different D/t ratios

2.5.3. Theoretical analysis and design specifications

In the past several decades, considerable advancements have been achieved in developing composite materials combining steel and concrete. Consequently, extensive research has investigated the calculating methods and theories for concrete-filled steel tube (CFST) columns (Nuruddin et al., 2011; Khaleel et al., 2011; Shi et al., 2015; De Oliveira et al., 2009). Design criteria are employed to predict the increased axial load capacity of concrete-filled steel tubes (CFST) or geopolymer

concrete-filled steel tubes (GCFST) columns. Eurocode 4 (EC 4 2004) utilises the limit state design methodology to guarantee safety and functionality by integrating partial safety factors for material properties and load. The American legal system The AISC (AISC 360-16 2016) methodology, based on the design of structural steels, permits the use of either the allowable stress design or the limit state. Furthermore, AISC increases the concrete stress level to appropriately consider the restraining hoop force.

Mustapha et al. (2021), from a study of the performance of FA and SF sefl-compacting concrete steel-filled tube columns with two different ratios of diameter to thickness (D/t) and two different yield strengths of steel tubes, concluded that Eurocode 4 accurately approximates the test results. The mean value is 0.927, and the standard deviation from the mean is 0.073. The ACI forecast, on the other hand, exhibits a conservative approach with an average value of 1.341 and a standard deviation of 0.089.

Table 2.1. Comparison of experimental results with EC4 and ACI prediction

Specimen	N_{EXP} (kN)	N_{EC4} (kN)	N_{ACI} (kN)	N_{EXP}/N_{EC4}	N_{EXP}/N_{ACI}
C5AR	1286.30	1261.94	866.38	1.019	1.485
C5BR	1243.70	1261.94	866.38	0.986	1.436
C4AR	1109.20	1111.08	780.00	0.998	1.422
C4BR	1132.70	1111.08	780.00	1.019	1.452
C3AR	937.20	949.40	691.73	0.987	1.355
C3BR	898.20	949.40	691.73	0.946	1.298
C5AP	1176.70	1430.10	881.73	0.823	1.335
C5BP	1165.70	1293.76	868.59	0.901	1.342
C4AP	1022.20	1161.16	794.51	0.880	1.287
C4BP	975.20	1144.34	782.31	0.852	1.247
C3AP	826.70	984.13	694.13	0.840	1.191
C3BP	859.70	984.13	694.13	0.874	1.239

Ekmekyapar and Al-Eliwi (2016), performed a study on the behaviour of circular concrete-filled steel tube columns; they used two different D/t ratios and concluded that they displayed the minimum permissible thicknesses for circular tubes made of S355 European steel according to the EC4 (Eurocode 4 2004) and AISC (AISC 360-16 2016) standards. From Figure 2.14, it is evident that AISC 360-10 specifically addresses relatively lower thicknesses. AISC 360-10 exhibits a prominent characteristic. EC4 imposes a stringent tube thickness restriction to

prevent the negative consequences of local buckling, which is not the case in AISC 360-10. The disparity is significant, even when comparing the compact section limit of AISC (AISC 360-16 2016) to the thickness limit of EC4 (Eurocode 4 2004).

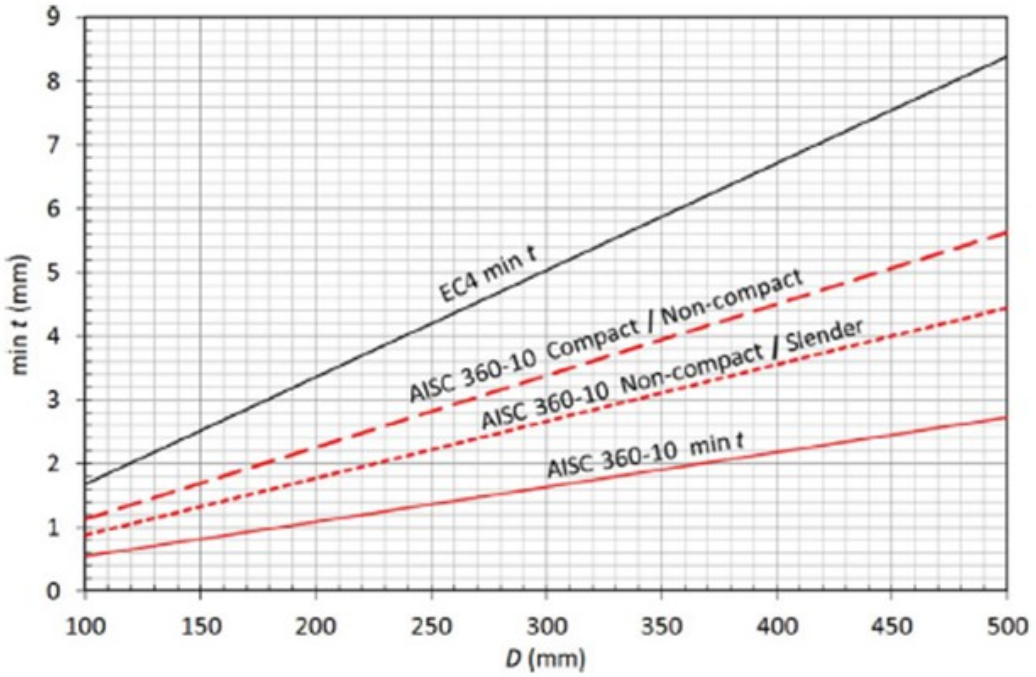

Figure 2.14. Differences in allowed circular tube thickness between EC4 and AISC360-10

De Oliveira et al. (2009) conducted a study on the axial loading capacity of concrete-filled steel tubes (CFST) with four varying diameter-to-length (D/L) ratios. The researchers conducted a comparison between the experimental results and four international codes. They determined that the standard codes yielded precise results for columns with higher length-to-diameter (L/D) ratios. Nevertheless, in the case of shorter columns, the codes inaccurately predicted how much the load capacity of concrete-filled steel tubes (CFST) would increase due to the confinement effect, especially as per EC4 (European Code 2004).

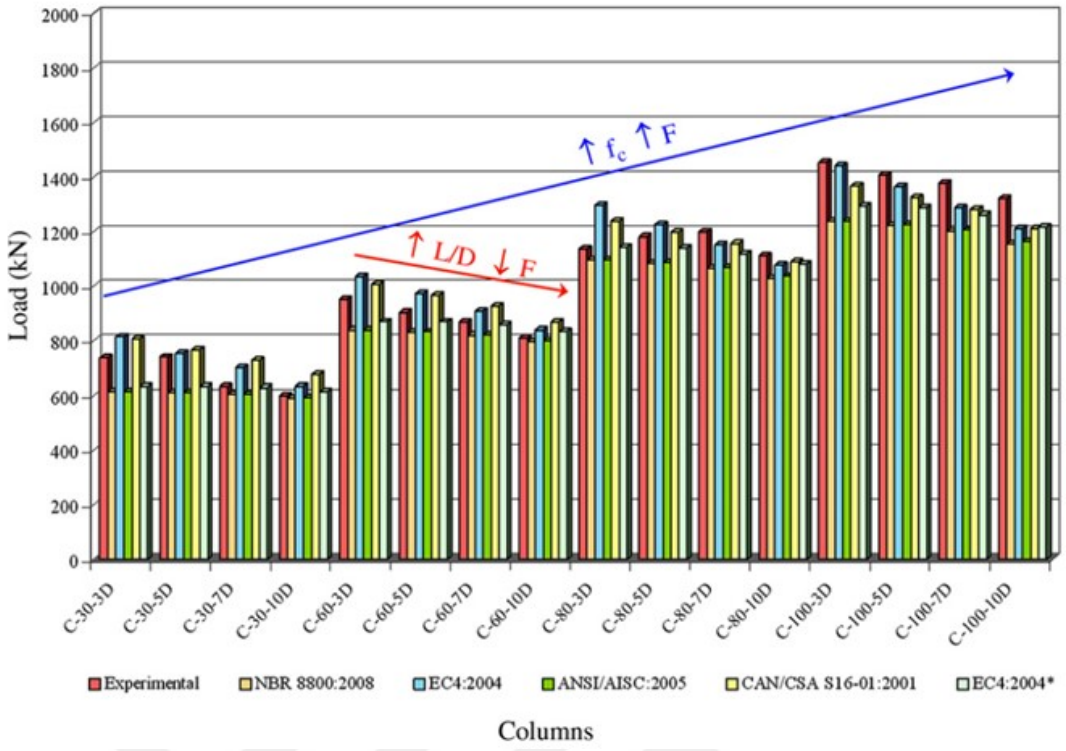

Figure 2.15. Comparison of experimental results with experimental results and codes

The main aim of this part of the study is to examine the new model of composite material, an environmentally friendly alternative to normal concrete composite material, and compare the experimental results with international codes. The same parameters used for normal concrete composite material were considered in this study: two L/D and eight D/t ratios were considered.

3. MATERIALS AND METHODS

3.1. Materials

3.1.1. Base materials

This research used ground-granulated blast furnace slag and fly ash as base materials.

3.1.1.1. Ground granulated blast furnace slag

Ground granulated blast furnace slag was used as a base material for producing self-compacting geopolymer concrete. GGBS was provided by the local construction material supplier (DCP Company Erbil); the table below shows the chemical and physical properties of the GGBS.

Table 3.1. GGBS's Physical and chemical characteristics

Chemical and physical	GGBS
SiO_2	36.40
Al_2O_3	11.39
CaO	34.12
Fe_2O_3	1.69
SO_3	0.49
MgO	10.30
K_2O	3.63
Na_2O	0.35
Loss on ignition	1.64
Specific gravity	2.79
Blaine fineness (m^2/Kg)	418

3.1.1.2. Fly ash

Fly ash ASTM (C 618 class C) was used in this study as a part of the base

material provided by the local construction material supplier (DCP Company Erbil); the table below shows the fly ash's physical and chemical properties.

Table 3.2. FA's Physical and chemical characteristics

Chemical and physical	Fly ash
SiO_2	44.96
Al_2O_3	15.59
CaO	15.75
Fe_2O_3	12.09
SO_3	0.10
MgO	7.86
K_2O	2.51
Na_2O	0.38
Loss on ignition	1.58
Specific gravity	2.29
Blaine fineness (m^2/Kg)	378

3.1.2. Aggregates

3.1.2.1. Fine aggregates

The fine aggregate employed in this study was natural sand sourced from the Great Zab River's quarry. It had a fineness modulus of 2.78, a specific gravity of 2.61, and an absorption rate of 0.95%.

3.1.2.2. Coarse aggregates

This study examined the impact of the type and size of coarse aggregate on the fresh and hardened properties of SCGC. Three types of locally available coarse aggregate were used: crushed river gravel (with a fineness modulus of 4.16, specific gravity of 2.68, and absorption of 1.03%), crushed marble (with a fineness modulus

of 4.32, specific gravity of 2.57, and absorption of 0.91%), and a combination of both aggregates in equal proportions. Furthermore, three different grades of coarse aggregate were utilised, specifically (4-9) mm, (4-12) mm, and (4-16) mm, respectively. Fig. 3.1 and Fig. 3.2 display collections of items, while Figure 3.3 illustrates the grading of the aggregate.

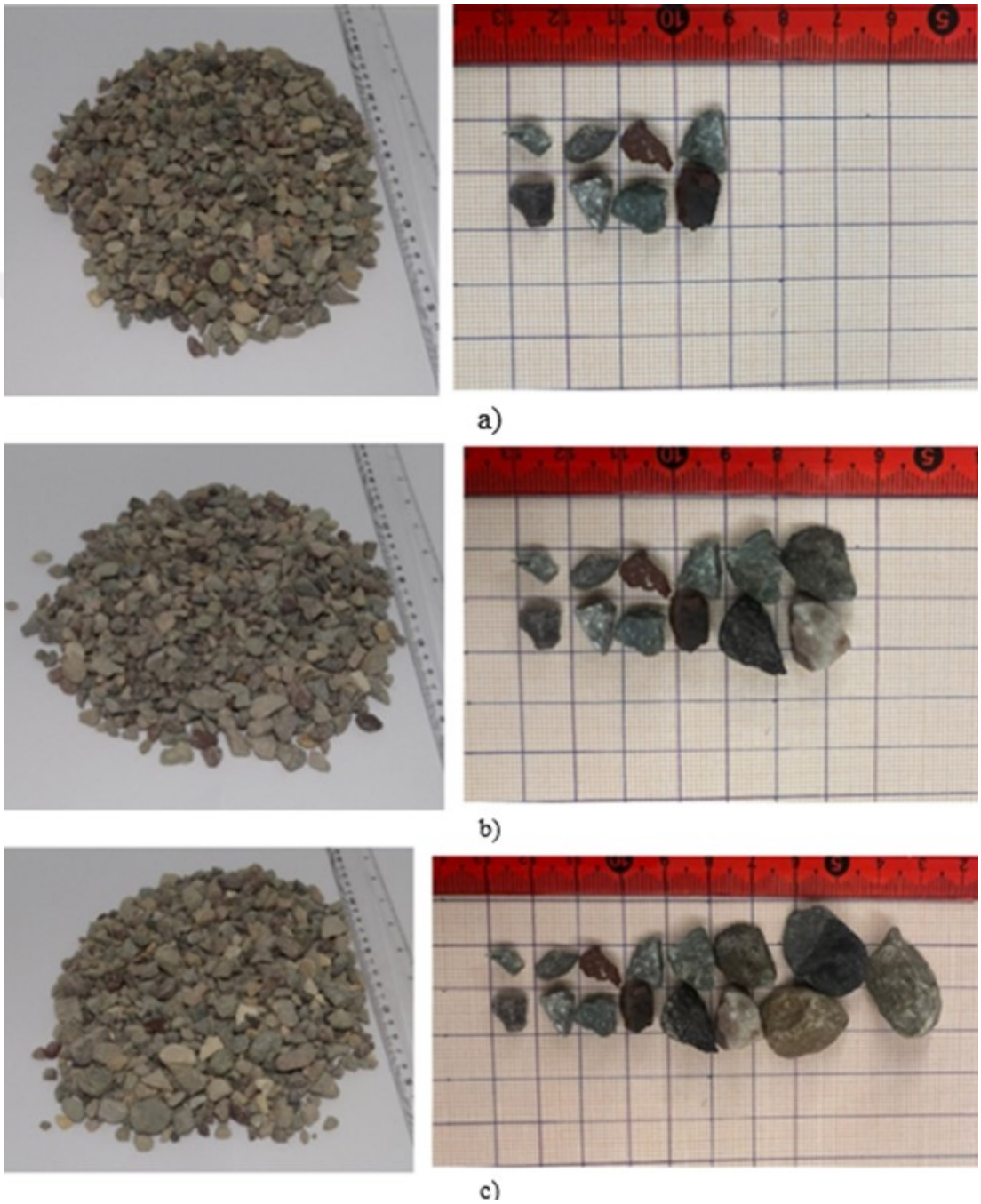

Figure 3.1. Crushed gravel maximum size a) 9 mm b) 12 mm c) 16 mm

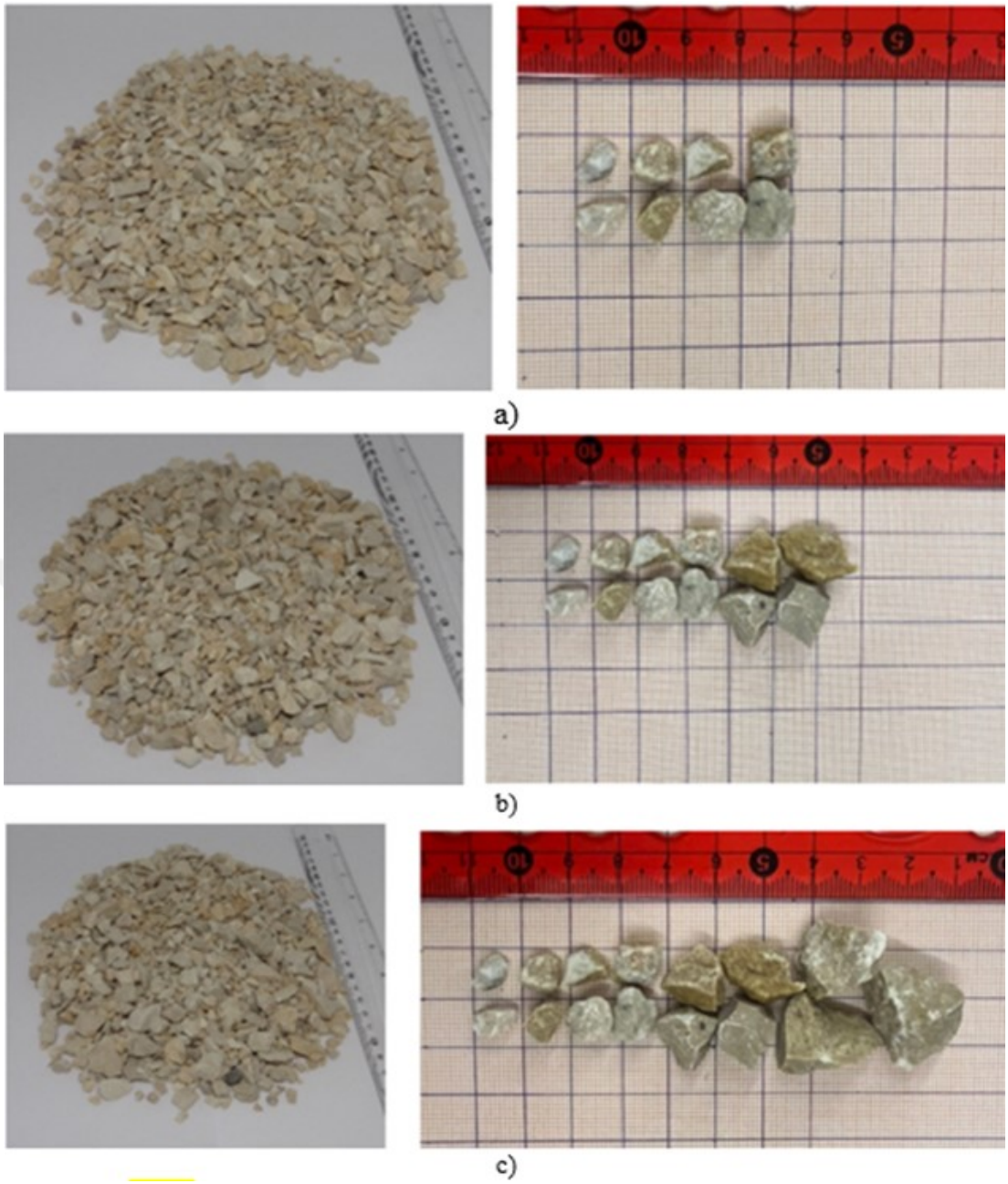

Figure 3.2. Crushed marble maximum size a) 9 mm, b) 12 mm, c) 16 mm

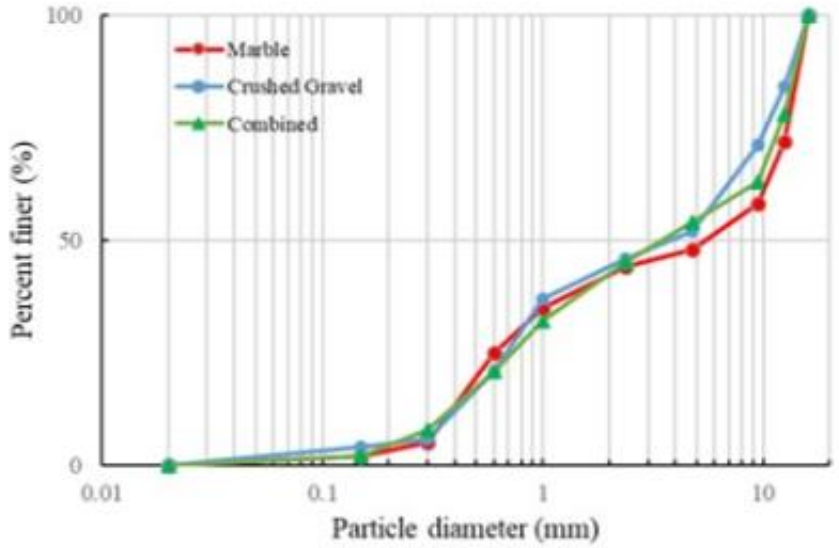
100
50
0
Percent finer (%)
Marble
Crushed Gravel
Combined
0.01
0.1
1
10
Particle diameter (mm)

a)

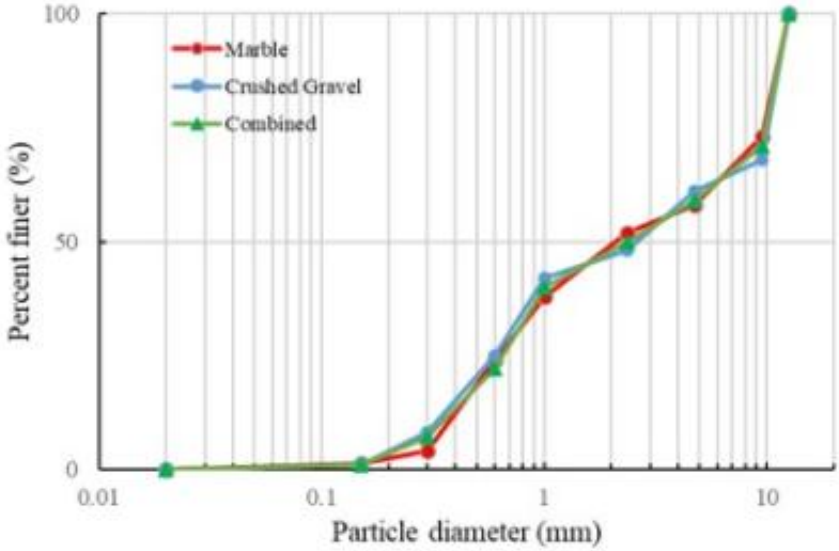
100
50
0
Percent finer (%)
Marble
Crushed Gravel
Combined
0.01
0.1
1
10
Particle diameter (mm)

b)

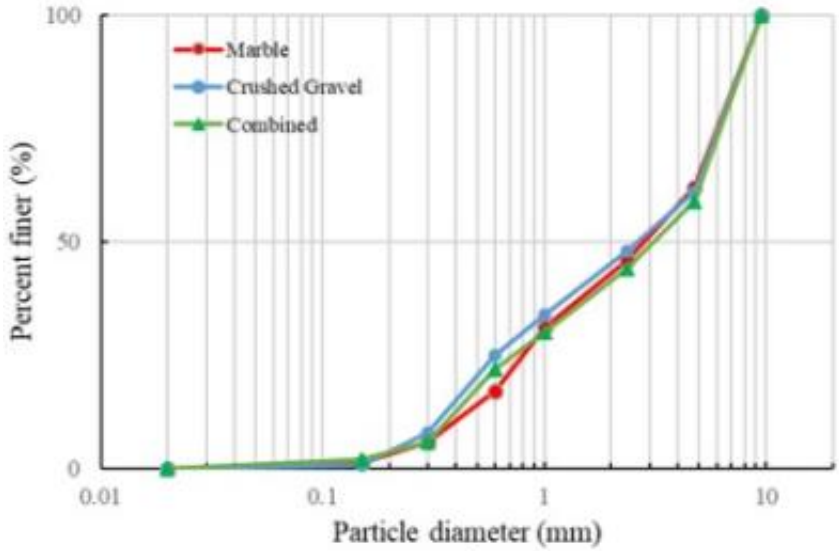
100
50
0
Percent finer (%)
Marble
Crushed Gravel
Combined
0.01
0.1
1
10
Particle diameter (mm)

c)

Figure 3.3. Sieve analysis of a) Combined natural sand with coarse aggregates 16mm b) Combined natural sand with coarse aggregates 12mm c) Combined natural sand with coarse aggregates 9mm

3.1.2.3. Aggregate crushing strength

The crushing strength of aggregates was measured to describe their features. The crushing strength of aggregates was measured in compliance with BS 812 (Part 110: 1990). To perform this test, the aggregate particles with sizes ranging between 9 and 16 mm were chosen, and then, a single aggregate particle was placed between two parallel plates to apply the diametrical load to the particle, as demonstrated in Fig. 3.4 A device with a 1000 kg capacity was used to apply the point load. A statistically determined number of representative particles was tested. In this study, the crushing strength, referred to as the crushing value, is the mean of the strength values obtained from testing these aggregate particles. Fig. 3.5 demonstrates the crushing load of the loaded aggregate particles. The crushing strength of the aggregate particles compressed from two opposing locations was calculated using the equation provided. The resulting crushing strength values may be seen in Fig. 3.6.

$$\sigma_{Crushing}=\frac{2.8F}{\Pi x^2} \tag{3.1}$$

Where *F* and x are the crushing load (in N) and the distance between loading points, namely pellet diameter (in mm), respectively.

Figure 3.4. Point load testing machine

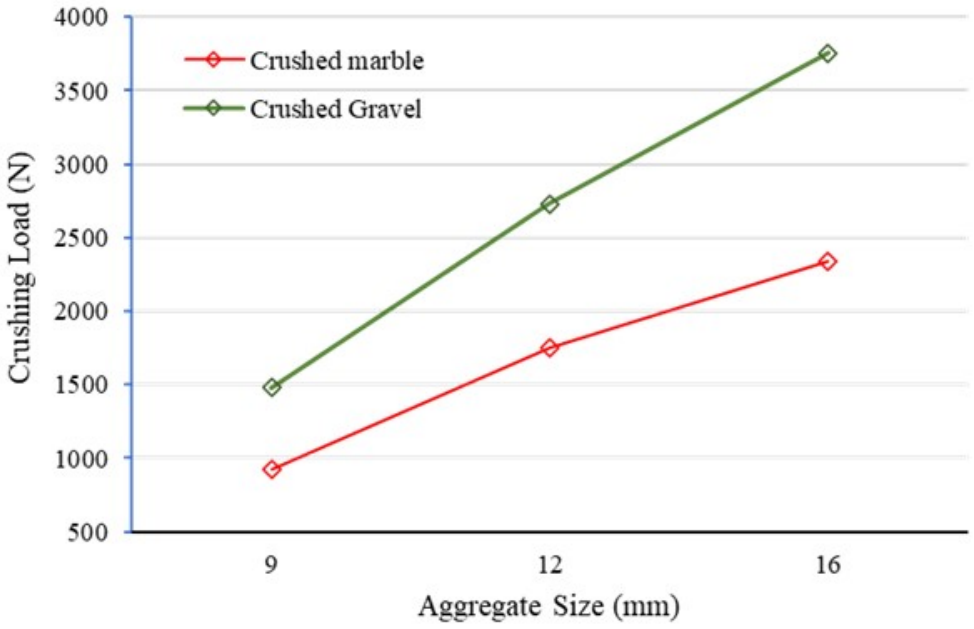

Figure 3.5. Aggregate crushing load

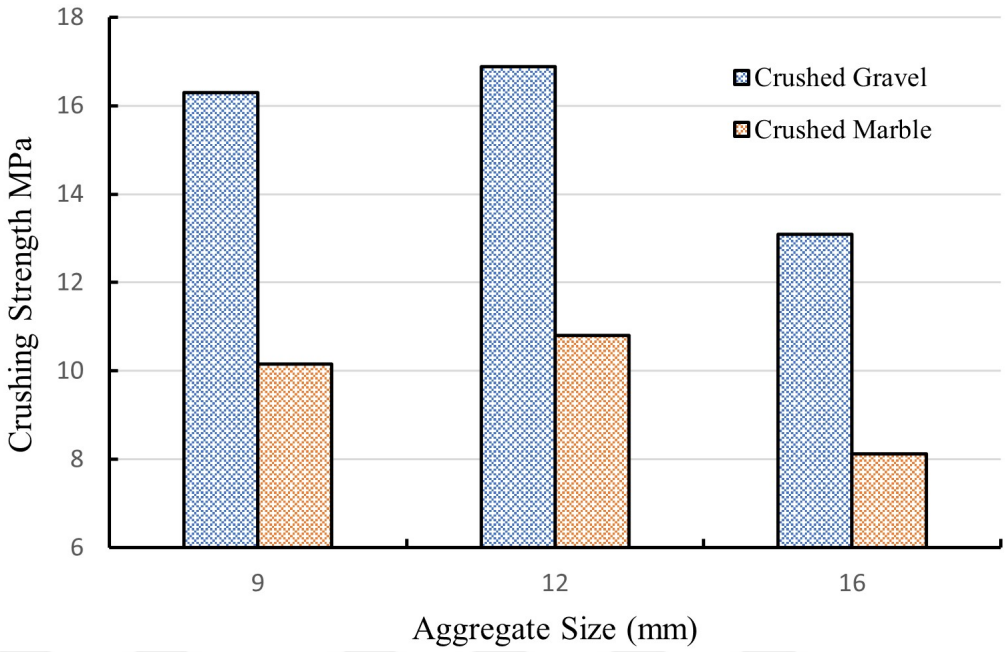

Figure 3.6. Aggregate crushing Strength

3.1.3. Alkali activators

This study utilized a combination of Na_2SiO_3 (sodium silicate) solution and NaOH (sodium hydroxide) solution as an alkaline activator to produce SCGC. The sodium silicate was acquired according to the product datasheet, which specified the chemical composition as follows: Na_2O: 13.7%, SiO_2: 29.4%, and water: 55.9% by mass. The sodium hydroxide solution had a specific gravity of 1.48 g/cc and a viscosity of 400 cp at a temperature of 20 ^oC. The sodium hydroxide (NaOH) was in the form of technical-grade flakes, measuring around 3 mm in particle size and with a specific gravity of 2.15. The pH value was 14. The molar mass is 40 grammes per mole. According to the product datasheet, the sodium hydroxide has a purity of 98%. This information was obtained from the supplier, DCP Company Erbil. To achieve satisfactory mechanical properties in self-consolidating geopolymer concrete, the researchers chose a molarity of 12M based on earlier studies conducted on geopolymer concrete (Fletcher et al., 2005; Duxson et al., 2006; and Deb et al., 2014).

The NaOH solution was made by dissolving NaOH flakes in water. The dispersion of NaOH solids in a solution is dictated by the concentration of the solution, which is expressed in terms of molarity (M). The inquiry entails using NaOH with a concentration of 12M, corresponding to a mass of 381 g per kilogramme. To create a solution weighing 1 kilogramme, you will need 381 grammes of NaOH flakes and 619 grammes of water.

3.1.4. Superplasticizer

To obtain high flowability and achieve self-consolidating standards without segregation and/or bleeding, a solution of polycarboxylate ether-type superplasticiser (SP) with 1.06 specific gravity was added to all mixes at a proportion of 6% of the weight of base material.

Table 3.3. Properties of superplasticizer

Properties	Superplasticizer
Name	Glenium 51
Colour tone	Dark brown
State	Liquid
Specific gravity (kg/1)	1.06
Chemical Description	Polycarboxylate ether

3.2. SCGC Sample preparation

3.2.1. Mixing

First, fine and coarse aggregates with FA and GGBS were blended for 2.5 minutes to produce self-consolidating geopolymer concrete. Later, the alkali activator, superplasticizer, and extra water were added to the mixture in one minute and mixed for another 2 minutes. Afterwards, fresh concrete was mixed for 3 minutes to ensure homogeneity and uniformity. Fig. 3.9 shows the mixing process of self-compacting geopolymer concrete.

Figure 3.9. Mixing of SCGC

3.2.2. Casting

Using self-compacting geopolymer concrete eliminates the compaction effort for the testing cubes, cylinder moulds for testing compressive strength, and steel tubes. After finishing the mixing process, the moulds were prepared, and fresh self-compacting geopolymer concrete was poured on the modules; later, the modules were covered with a plastic cover to prevent evaporation of the alkaline solution and left at room temperature for curing; the same process was applied for steel tube filled self-compacting geopolymer concrete. Figs. 3.10 and 3.11 illustrate the casting of testing moulds and steel tubes, respectively.

Figure 3.10. Casting cube samples for testing the compressive strength of SCGC

Figure 3.11. Casting steel tube-filled self-compacting geopolymer concrete

3.2.3. Curing

After the concrete was produced, the samples were cast with self-compacting geopolymer concrete. The modules were covered with a plastic cover to prevent evaporation of the alkaline solution and left at an ambient temperature that did not exceed 20 ± 2 °C for 24 hours. The samples were de-moulded, covered again with a plastic cover, and left at ambient temperature until the testing date, which was at ages 7, 14, 28, and 90 days. Compressive strength tests were conducted on cubic specimens (100x100x100 mm) at ages 7, 14, 28, and 90 days using the ASTM C39 standard.

The same curing procedure was applied to the steel tube-filled self-compacting geopolymer concrete.

Figure 3.12. Ambient curing of cube samples

Figure 3.13. Ambient curing of steel tube filled self-compacting geopolymer concrete

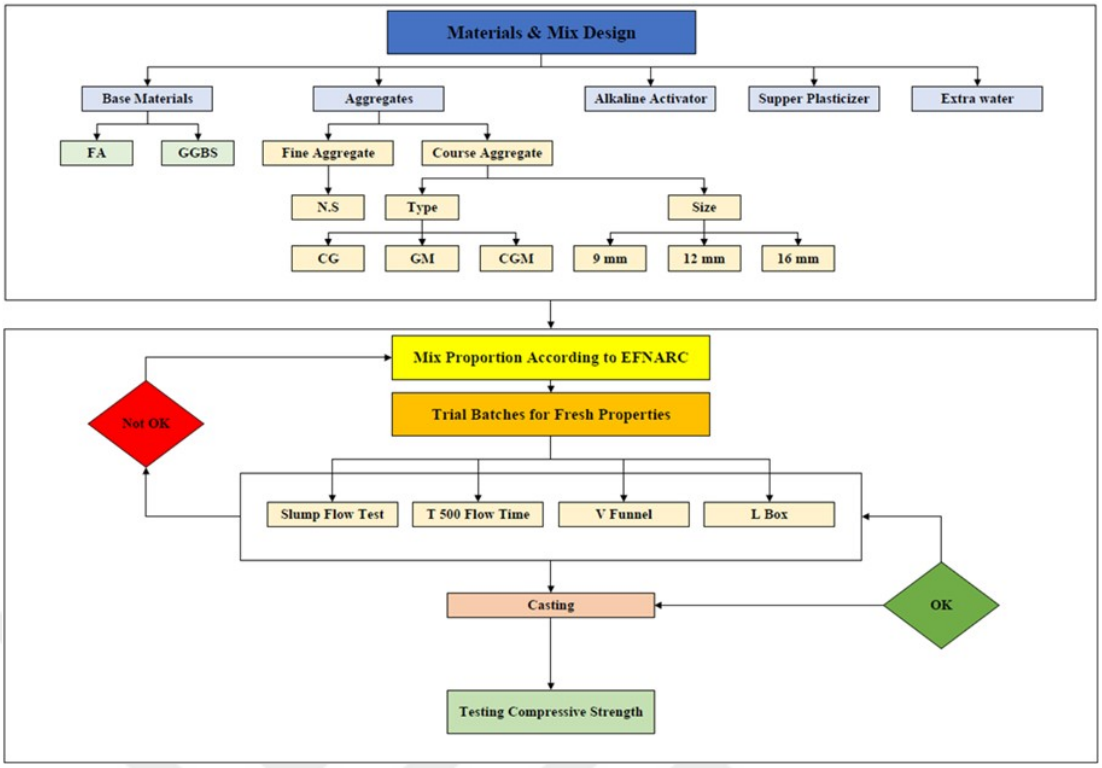

Figure 3.14. Schematic presentation of the experimental program

3.3. Preparation of steel tubes for composite columns

In this study, four different tube diameters, two different wall thicknesses, and two length-to-diameter (L/D) ratios (short and long) (Ekmekyapar & Al-Eliwi, 2016; Li et al., 2015) were used to examine how self-compacting geopolymer concrete behaved under axial load.

The steel tube specimens were prepared from mild circular hollow steel cold-formed tubes with a length of 6 m; four different outer diameter D steel tubes, 101 mm, 114 mm, 127 mm, and 139 mm, were used, with two thicknesses of 3 mm and 6 mm for each cross-section, according to ASTME8/E8M-16. The tensile strength of the steel tube was obtained, as illustrated in Table 3.5. A cold-cutting machine cut the steel tubes straight during specimen preparation to obtain and control the accurate length.

Table 3.5. Mechanical properties of steel tubes

Tube thickness	Elastic modulus *E* (GPa)	Yield strength (MPa)
3 mm	200	330
6 mm	200	450

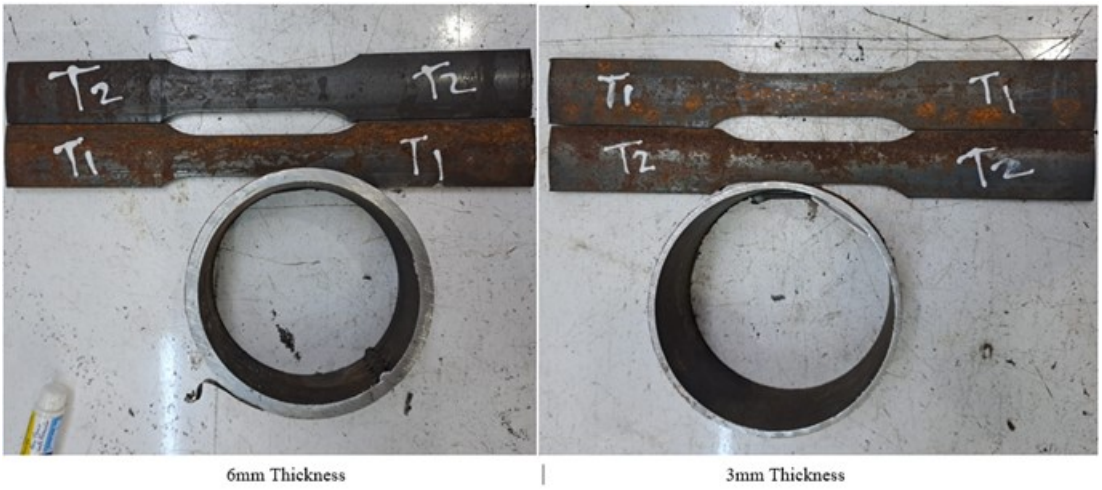

Figure 3.7. Sample preparation for testing mechanical properties of steel tube

As illustrated in Table 3.5, the groups' quality depends on the steel tube thickness; the yield strength of the 3mm thickness is 350 MPa, and that of the 6mm is 458 MPa. This is to examine the column's behaviour with high and low confinement factors (ξ) in Equation 1. Several studies have used the confinement factor as a practical parameter to characterise a column's confinement capability. This factor is employed for circulators and rectangular columns (Ekmekyapar & Al-Eliwi, 2016).

$$\xi = \frac{Asfy}{Acfc} \tag{3.2}$$

Where ξ is the confinement factor, fc is the compressive strength of the concrete, fy is the yield strength of the steel tube, and As and Ac are the cross-sections of the steel tube and concrete, respectively.

Based on the L/D ratio, the specimens were classified into two groups: L/D = 4.5 and L/D=2.0; according to the literature, when L/D > 4 is classified as long, and L/D ≤ 4 is classified as short (Ekmekyapar and Al-Eliwi, 2016; Li et al., 2015), a cold cutter was used to cut the specimens to get an accurate length, before casting, the inside surface of the specimens was cleaned properly to ensure appropriate interaction between the SCGC and the steel tubes. Sixteen SCGC steel tube columns were manufactured, as shown in Table 3.6. To hold the fresh SCGC during casting, the base of the steel tubes was closed by a 2 mm-thick plate using silicon to connect the plate with the base of the steel tubes. The top of the steel tubes was left empty, about 5mm during SCGC pouring and later was filled with high-strength stone

powder for levelling the top of specimens. Before testing, the bottom plate was removed from the specimens, and the top was levelled with high-strength stone powder. The specimens were left for curing at a lab ambient temperature of 23 ±2 oC for 28 days. Fig. 3.7 shows the specimens.

Table 3.6. Columns properties

Column	L/D	t (mm)	D (mm)	L(mm)	*fy* MPa	*fc* MPa	*SI*
SCGC-C-101-3-202	2.0	3	101	202	330	45	1.24
SCGC-C-101-6-202	2.0	6	101	202	450	45	1.3
SCGC-C-101-3-454	4.5	3	101	454	330	45	1.18
SCGC-C-101-3-454	4.5	6	101	454	450	45	1.31
SCGC-C-114-3-228	2.0	3	114	228	330	45	1.26
SCGC-C-114-6-228	2.0	6	114	228	450	45	1.2
SCGC-C-114-3-513	4.5	3	114	513	330	45	1.27
SCGC-C-114-6-513	4.5	6	114	513	450	45	1.22
SCGC-C-127-3-254	2.0	3	127	254	330	45	1.13
SCGC-C-127-6-254	2.0	6	127	254	450	45	1.11
SCGC-C-127-3-572	4.5	3	127	571	330	45	1.16
SCGC-C-127-6-572	4.5	6	127	571	450	45	1.09
SCGC-C-139-3-278	2.0	3	139	278	330	45	1.06
SCGC-C-139-6-279	2.0	6	139	278	450	45	1.03
SCGC-C-139-3-625	4.5	3	139	625	330	45	1.09
SCGC-C-139-6-625	4.5	6	139	625	450	45	1.10

Figure 3.8. Steel tubes

3.4. Mix proportions

A constant total binder amount of 500 kg/m^3 was used to produce different series of SCGC mixtures. According to the base materials, the first group contains 100% GGBS, and the second group contains 50% GGBS with 50% fly ash. The aggregate types were crushed gravel and marble; the compensation of crushed gravel with crushed marble was 50% for each. Table 3.4 illustrates the amount of each component as a weight for 1 m^3 of concrete. As shown in Table 3.4, six test series on 216 specimens were designed in this study as follows:

Series A: 36 SCGC specimens CG; crushed gravel, 100S; 100% GGBS, (9, 12, 16) maximum aggregate size.

Series B: 36 SCGC specimens CM; crushed marble, 100S; 100% GGBS, (9, 12, 16) maximum aggregate size.

Series C: 36 SCGC specimens CGM; combined crushed gravel and marble, 100S; 100% GGBS, (9, 12, 16) maximum aggregate size.

Series D: 36 SCGC specimens CG; crushed gravel, 50S; 50% GGBS, 50F; 50% FA, (9, 12, 16) maximum aggregate size.

Series E: 36 SCGC specimens CM; crushed marble, 50S; 50% GGBS, 50F; 50% FA, (9, 12, 16) maximum aggregate size.

Series F: 36 SCGC specimens CGM; combined crushed gravel and marble, 50S; 50% GGBS, 50F; 50% FA, (9, 12, 16) maximum aggregate size.

Table 3.4. Mixture proportion of self-consolidating geopolymer concrete

#	Mix ID	Base Material	Base Material Type		Fine Aggregate	Coarse Aggregate		S.H	S.S	M	S.P	Addition Water
			GGBS	FA	N. S	CG	CM					
		Kg/m³	Kg/m³	Kg/m³	Kg/m³	Kg/m³	Kg/m³	Kg/m³	Kg/m³		%	%
1	CG-100S-9	500	500	0	790	699	0	71	179	12	6	10
2	CG-100S-12	500	500	0	790	699	0	71	179	12	6	10
3	CG-100S-16	500	500	0	790	699	0	71	179	12	6	10
4	CM-100S-9	500	500	0	790	0	673	71	179	12	6	10
5	CM-100S-12	500	500	0	790	0	673	71	179	12	6	10
6	CM-100S-16	500	500	0	790	0	673	71	179	12	6	10
7	CGM100S-9	500	500	0	790	350	337	71	179	12	6	10
8	CGM-100S-12	500	500	0	790	350	337	71	179	12	6	10
9	CGM-100S-16	500	500	0	790	350	337	71	179	12	6	10
10	CG-50S-50F-9	500	250	250	758	671	0	71	179	12	6	10
11	CG-50S-50F-12	500	250	250	758	671	0	71	179	12	6	10
12	CG-50S-50F-16	500	250	250	758	671	0	71	179	12	6	10
13	CM-50S-50F-16	500	250	250	758	0	646	71	179	12	6	10
14	CM-50S-50F-16	500	250	250	758	0	646	71	179	12	6	10
15	CM-50S-50F-16	500	250	250	758	0	646	71	179	12	6	10
16	CGM-50S-50F-9	500	250	250	758	335	323	71	179	12	6	10
17	CGM-50S-50F-12	500	250	250	758	335	323	71	179	12	6	10
18	CGM-50S-50F-16	500	250	250	758	335	323	71	179	12	6	10

Referring to previous studies, the Na_2SiO_3/NaOH ratio lies in the range of 1.5–2.5 (Ouchi, 2000) for economic reasons, and a ratio (Na_2SiO_3/NaOH) of 1/2.5 was utilised in current research.

3.5. Introduction

This chapter comprehensively explains the various materials' respective quantities and qualities. It explains the mix preparation of self-compacting geopolymer concrete (SCGC) and the mix proportions, the type and grading of aggregate used in this research, the dosage of base materials, and the alkali used. Moreover, it explains the preparation of steel tubes and their geometrical and mechanical properties.

The mixing, casting, and curing methods were explained to determine SCGC's mechanical properties and the steel tube preparation, casting, and curing methods.

3.6. Testing procedure

3.6.1. Fresh state tests on SCGCs

Fresh state tests were performed on the produced SCGCs for all mixes after mixing to ensure passing ability and flowability requirements were fulfilled without bleeding and segregation.

3.6.1.1. Fresh unit weight of SCGC

A digital scale was utilised to measure the weight of the moulds before and after casting to determine the fresh unit weight of self-compacting geopolymer concrete by ASTM C138. Additionally, callipers were employed to verify the dimensions of the moulds before the casting process.

Figure 3.15. Fresh unit weight of SCGC

3.6.1.2. Slump flow test on SCGC

This test evaluates the ability of fresh SCC to flow freely horizontally under its weight without external restrictions or obstructions. This test cannot verify whether the concrete will pass between the reinforcement rebars for distances, but it may be an indicator to detect free flow quality. To measure the ideal flow duration, a T_{500} test must be performed, representing a measure of viscosity. This test can be performed on-site directly, and two persons are required during the test to determine the time and diameter of the flow. The EFNARC requirements propose three classes of flow categories according to the final spread.

Table 3.7. Slump flow classes according to EFNARC

SCC Class	Slump flow diameter [mm]
SF1	550-650
SF2	660-750
SF3	760-850

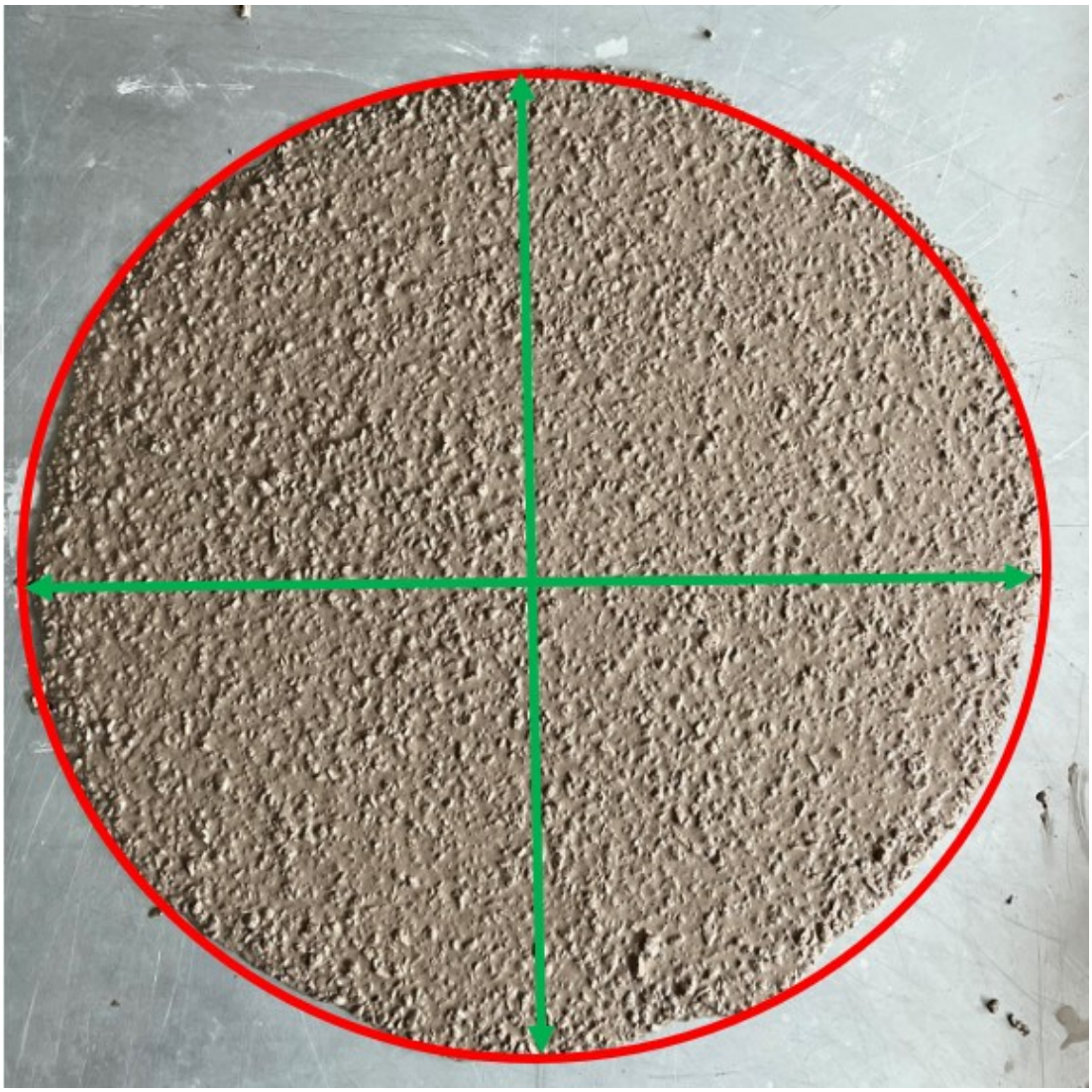

Figure 3.16. Flow test

3.6.1.3. V-funnel test on SCGC

This test was developed for the first time in Japan. This test evaluates fresh SCC's filling capacity with a maximum opening volume of 20 mm. It is also an indicator for adjusting the powder and water content added to concrete and a good predictor of viscosity. The test is performed by filling the V-shaped funnel with about 12 litres of fresh SCC. The time taken for the flow through the V-funnel is measured, and the duration is recorded as the filling time. Some factors may affect

the flow duration, including the size or content of coarse aggregate or a high-viscosity mixture. The flow duration represents the filling ability of SCC, and according to EFNARC requirements, there are two categories for time.

Table 3.8. Viscosity classes according to EFNARC

SCC class	500mm spread time T_{500} [sec]	V-funnel time [sec]
VS1/VF1	≤ 2	≤ 8
VS2/VF2	> 2	9-25

Figure 3.17. V-Funnel test

3.6.1.4. L-box test on SCGC

The passing ability of the SCGC mixes was measured by the L-Box test from the passing of fresh SCGC between narrow openings bars spaced (41±1) by dividing the SCGC height of the horizontal section by the height of the vertical section after the end of the SCGC floe. Table 3.9 presents the limits of the fresh state performance of SCC mixes according to the EFNARC committee's specifications.

Table 3.9. Passing classes according to EFNARC

SCC class	Passing ability
PA1	≥ 0.80 with 2 bars
PA2	≥ 0.80 with 3 bars

Figure 3.18. L-Box test

3.6.2. Compressive strength test

To determine the compressive strength of self-compacting geopolymer concrete cubes, the test was conducted on 100x100x100 mm cubes using a hydraulic testing machine with a capacity of 3000 kN. It followed the guidelines outlined in ASTM C39 and was performed on specimens 7, 14, 28, and 90 days old at 0.5 kilonewtons per second loading rate. The compressive strength was determined by taking the average of three samples for each age test.

Figure 3.19. Compressive strength test machine

3.6.3. Axial loading test of CFST

The study investigates the load-deformation behaviour of the columns, the deformation mode, and the failure mode after the maximum load capacity. All columns were tested using a 300-tonne compression machine in the College of Engineering, Saladin University, Erbil laboratory. A longitudinal strain gauge was

attached to the middle of the column to record the deformation of the columns, and three LVDTs were installed to measure the vertical and transverse displacement of the columns. A laser levelling instrument was used to check the alignment of the columns under the testing machine to ensure the eccentricity of the load. A data logger was used to record the data on steel tube deformation and vertical and lateral displacement every second. The displacement of the hydraulic compression machine was controlled manually at a constant rate of 0.5 mm/min for all tested samples.

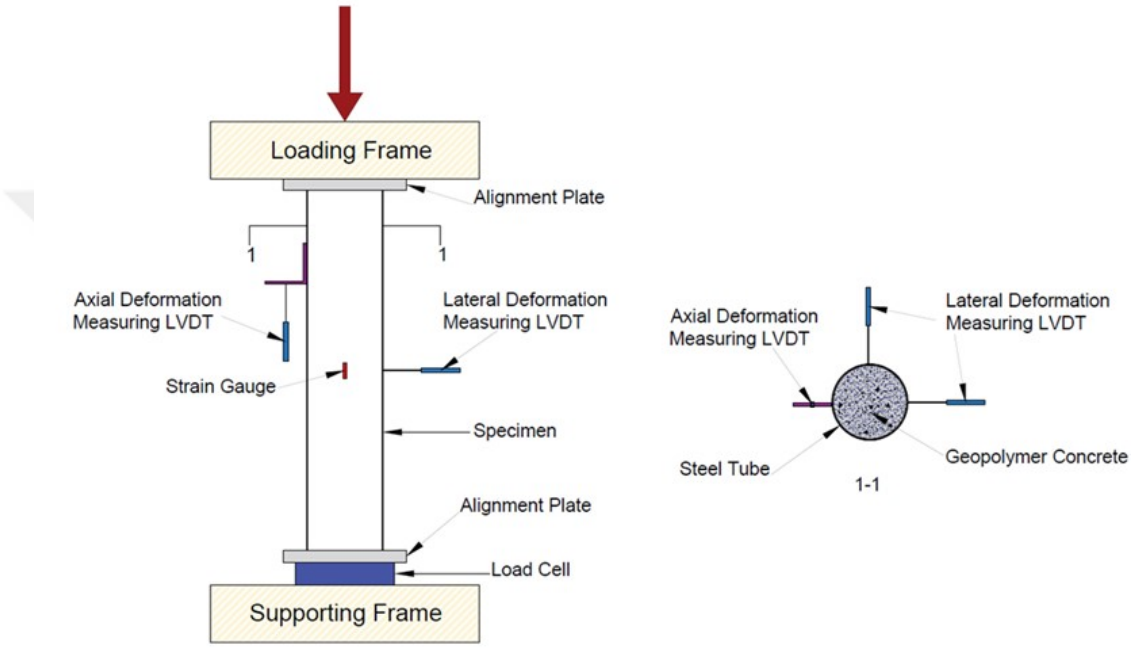

Figure 3.20. Schematic testing procedure

Figure 3.21. Axial loading machine

4. FINDINGS

4.1. Fresh Properties of SCGCs

4.1.1. Fresh unit weight

Table 4.1 shows the results of the fresh unit weight of self-compacting geopolymer concrete for all mixes.

Table 4.1. Fresh unit weight of SCGC

#	Mix No.	Base Material %	Mix Code	Test Result Kg/m^3
1	M1	*CG-100S*	CG-100S-9	2375
2	M2		CG-100S-12	2373
3	M3		CG-100S-16	2393
4	M4	*CM-100S*	CM-100S-9	2338
5	M5		CM-100S-12	2314
6	M6		CM-100S-16	2352
7	M7	*CGM-100S*	CG-M100S-9	2330
8	M8		CGM-100S-12	2321
9	M9		CGM-100S-16	2352
10	M10	*CG-50S-50F*	CG-50S-50F-9	2358
11	M11		CG-50S-50F-12	2341
12	M12		CG-50S-50F-16	2323
13	M13	*CM-50S-50F*	CM-50S-50F-16	2317
14	M14		CM-50S-50F-16	2308
15	M15		CM-50S-50F-16	2331
16	M16	*CGM-50S-50F*	CGM-50S-50F-9	2298
17	M17		CGM-50S-50F-12	2284
18	M18		CGM-50S-50F-16	2318

4.1.2. Slump flow test and T500 mm

Slump flow test and T_{500} for all mixes were performed; table 4.2 shows the results of slump flow test, while table 4.3 shows the results of T_{500}.

Table 4.2. Flow slump test results

#	Mix No.	Base material %	Mix Code	Test Result mm
1	M1	*CG-100S*	CG-100S-9	685
2	M2		CG-100S-12	705
3	M3		CG-100S-16	714
4	M4	*CM-100S*	CM-100S-9	658
5	M5		CM-100S-12	684
6	M6		CM-100S-16	687
7	M7	*CGM-100S*	CG-M100S-9	662
8	M8		CGM-100S-12	691
9	M9		CGM-100S-16	704
10	M10	*CG-50S-50F*	CG-50S-50F-9	778
11	M11		CG-50S-50F-12	782
12	M12		CG-50S-50F-16	804
13	M13	*CM-50S-50F*	CM-50S-50F-16	726
14	M14		CM-50S-50F-16	768
15	M15		CM-50S-50F-16	762
16	M16	*CGM-50S-50F*	CGM-50S-50F-9	742
17	M17		CGM-50S-50F-12	772
18	M18		CGM-50S-50F-16	768

Table 4.3. T500 mm test results

#	Mix No.	Base material %	Mix Code	Test Result Sec.
1	M1	*CG-100S*	CG-100S-9	5.65
2	M2		CG-100S-12	5.12
3	M3		CG-100S-16	4.25
4	M4	*CM-100S*	CM-100S-9	5.91
5	M5		CM-100S-12	5.76
6	M6		CM-100S-16	5.63
7	M7	*CGM-100S*	CG-M100S-9	5.78
8	M8		CGM-100S-12	5.52
9	M9		CGM-100S-16	5.14
10	M10	*CG-50S-50F*	CG-50S-50F-9	2.23
11	M11		CG-50S-50F-12	2.11
12	M12		CG-50S-50F-16	2.07
13	M13	*CM-50S-50F*	CM-50S-50F-16	4.08
14	M14		CM-50S-50F-16	3.65
15	M15		CM-50S-50F-16	3.26
16	M16	*CGM-50S-50F*	CGM-50S-50F-9	3.78
17	M17		CGM-50S-50F-12	3.45
18	M18		CGM-50S-50F-16	3.11

4.1.3. V-Funnel Test

The V-funnel test was performed to measure the filling ability of the newly produced SCGC. Table 4.4 shows the V-funnel test results for all mixes.

Table 4.4. V Funnel test results

#	Mix No.	Base Material %	Mix Code	Test Result Sec
1	M1	*CG-100S*	CG-100S-9	21.15
2	M2		CG-100S-12	17.76
3	M3		CG-100S-16	14.31
4	M4	*CM-100S*	CM-100S-9	23.08
5	M5		CM-100S-12	22.61
6	M6		CM-100S-16	20.87
7	M7	*CGM-100S*	CG-M100S-9	22.84
8	M8		CGM-100S-12	21.94
9	M9		CGM-100S-16	19.12
10	M10	*CG-50S-50F*	CG-50S-50F-9	6.86
11	M11		CG-50S-50F-12	6.68
12	M12		CG-50S-50F-16	6.32
13	M13	*CM-50S-50F*	CM-50S-50F-16	13.65
14	M14		CM-50S-50F-16	12.1
15	M15		CM-50S-50F-16	10.21
16	M16	*CGM-50S-50F*	CGM-50S-50F-9	9.85
17	M17		CGM-50S-50F-12	8.95
18	M18		CGM-50S-50F-16	8.1

4.1.4. L Box Test

To measure the passing ability of SCGS, an L-box test was performed; table 4.5 shows the L-box test results for all mixes.

Table 4.5. L-Box test Results

#	Mix No.	Base material %	Mix Code	Test Result
1	M1	*CG-100S*	CG-100S-9	0.84
2	M2		CG-100S-12	0.86
3	M3		CG-100S-16	0.88
4	M4	*CM-100S*	CM-100S-9	0.82
5	M5		CM-100S-12	0.83
6	M6		CM-100S-16	0.85
7	M7	*CGM-100S*	CG-M100S-9	0.83
8	M8		CGM-100S-12	0.84
9	M9		CGM-100S-16	0.86
10	M10	*CG-50S-50F*	CG-50S-50F-9	0.94
11	M11		CG-50S-50F-12	0.95
12	M12		CG-50S-50F-16	0.98
13	M13	*CM-50S-50F*	CM-50S-50F-16	0.88
14	M14		CM-50S-50F-16	0.90
15	M15		CM-50S-50F-16	0.92
16	M16	*CGM-50S-50F*	CGM-50S-50F-9	0.90
17	M17		CGM-50S-50F-12	0.92
18	M18		CGM-50S-50F-16	0.94

4.2. Compressive strength of SCGC

All mixes were tested for compressive strength at ages 7 days, 14 days, 28 days, and 90 days, and Table 4.6 illustrates the compressive strength test results.

Table 4.6. Compressive strength test results

#	Mix No.	Base %	Mix Code	Test Result			
				7 Days	14 Days	28 Days	90 Days
				MPa	MPa	MPa	MPa
1	M1	*CG-100S*	CG-100S-9	*14.50*	*32.16*	*48.22*	*59.54*
2	M2		CG-100S-12	*15.13*	*33.20*	*50.29*	*62.41*
3	M3		CG-100S-16	*13.36*	*29.95*	*44.61*	*57.83*
4	M4	*CM-100S*	CM-100S-9	*12.49*	*27.68*	*43.14*	*53.70*
5	M5		CM-100S-12	*12.77*	*28.38*	*44.99*	*55.58*
6	M6		CM-100S-16	*11.82*	*26.27*	*42.35*	*49.28*
7	M7	*CGM-100S*	CG-M100S-9	*12.81*	*26.50*	*42.51*	*50.09*
8	M8		CGM-100S-12	*13.29*	*27.02*	*43.56*	*53.13*
9	M9		CGM-100S-16	*12.05*	*25.61*	*42.09*	*49.45*
10	M10	*CG-50S-50F*	CG-50S-50F-9	*10.11*	*14.98*	*22.13*	*44.86*
11	M11		CG-50S-50F-12	*10.32*	*15.59*	*23.60*	*47.49*
12	M12		CG-50S-50F-16	*10.18*	*14.48*	*21.18*	*43.52*
13	M13	*CM-50S-50F*	CM-50S-50F-16	*10.42*	*15.05*	*22.15*	*44.19*
14	M14		CM-50S-50F-16	*10.63*	*15.21*	*22.67*	*46.13*
15	M15		CM-50S-50F-16	*10.39*	*14.12*	*21.30*	*42.90*
16	M16	*CGM-50S-50F*	CGM-50S-50F-9	*9.47*	*13.77*	*21.22*	*39.64*
17	M17		CGM-50S-50F-12	*10.21*	*14.15*	*22.01*	*44.61*
18	M18		CGM-50S-50F-16	*10.12*	*13.56*	*21.06*	*39.81*

4.3. Axial Loading for CFST

4.3.1. Short Columns

The loading capacity for the short columns was performed. Table 4.7 shows the axial loading capacity of short columns and comparing the test results with the design codes.

Table 4.7. Short columns axial loading test

#	Column	P Exper. KN	AISC KN	P/AISC	EC4 KN	P/EC4
1	C-101-3-454	755	606	1.25	624	1.21
5	C-101-6-454	1398	1068	1.34	1086	1.30
2	C-114-3-513	932	734	1.27	757	1.23
6	C-114-6-513	1522	1261	1.24	1284	1.20
3	C-127-3-571	995	874	1.14	903	1.10
7	C-127-6-571	1625	1465	1.12	1494	1.08
4	C-139-3-625	1082	1013	1.07	1048	1.03
8	C-139-6-625	1723	1663	1.12	1698	1.08

4.3.2. Long Columns

The loading capacity for the long columns was performed. Table 4.8 shows the axial loading capacity of short columns and comparing the test results with the design codes.

Table 4.8. Long columns axial loading

#	Column	P Exper. KN	AISC KN	P/AISC	EC4 KN	P/EC4
1	C-101-3-454	719	598	1.20	624	1.15
5	C-101-6-454	1407	1052	1.34	1086	1.30
2	C-114-3-513	936	724	1.29	757	1.24
6	C-114-6-513	1541	1242	1.24	1284	1.20
3	C-127-3-571	1021	862	1.18	903	1.13
7	C-127-6-571	1610	1443	1.12	1494	1.08
4	C-139-3-625	1108	999	1.11	1048	1.06
8	C-139-6-625	1835	1639	1.12	1698	1.08

5. DISCUSSION

5.1. Fresh properties of SCGCs

Passing ability and flowability test outcomes of the SCGC mixes were compatible with the EFNARC specifications. SCGC mixes' flow diameters were higher than the minimum flow diameter of 550 mm. No bleeding and segregation were observed in the SCGC mixes. In addition, resulting slump flow diameters were also compatible with the EN 12350-8 standard. Furthermore, the setting and/or hardening time for SCGC mixes decreased by adding 50% FA. Researchers studied the use of SCGC in ambient environments (Nuruddin et al., 2011; Mo et al., 2014). The use of GGBS and/or FA increases the probability of the use of SCGC under an ambient environment.

Moreover, the flowability of SCGC decreased with an increase in the aggregate size, and the flowability of crushed aggregate was less than that of crushed marble due to the high absorption of crushed aggregate. The flowability of combined aggregate was similar to that of crushed marble aggregate.

5.1.1. Fresh unit weight

The fresh unit weight of SCGC was measured during the research, as shown in Table 4.1; the fresh unit weight for all mixtures was valid from 2298 kg/m^3 to 2393 kg/m^3, the variation in fresh unit weight between the mixture groups was influenced mainly by coarse aggregate type, mixtures containing crushed gravel coarse aggregate performed a higher amount of fresh unit weight compared with mixtures containing marble coarse aggregate due to the variation of coarse aggregate density, crushed gravel aggregate's density was higher than marble coarse aggregate. Compared with conventional Portland cement self-compacting concrete, the fresh unit weight of self-compacting geopolymer concrete of 2335 kg/m^3 was closer to that of traditional self-compacting concrete.

Table 5.1. Fresh unit weight of self-compacting geopolymer concrete

#	Mix No.	Base Material %	Mix Code	Test Result Kg/m^3
1	M1	*CG-100S*	CG-100S-9	2375
2	M2		CG-100S-12	2373
3	M3		CG-100S-16	2393
4	M4	*CM-100S*	CM-100S-9	2338
5	M5		CM-100S-12	2314
6	M6		CM-100S-16	2352
7	M7	*CGM-100S*	CG-M100S-9	2330
8	M8		CGM-100S-12	2321
9	M9		CGM-100S-16	2352
10	M10	*CG-50S-50F*	CG-50S-50F-9	2358
11	M11		CG-50S-50F-12	2341
12	M12		CG-50S-50F-16	2323
13	M13	*CM-50S-50F*	CM-50S-50F-16	2317
14	M14		CM-50S-50F-16	2308
15	M15		CM-50S-50F-16	2331
16	M16	*CGM-50S-50F*	CGM-50S-50F-9	2298
17	M17		CGM-50S-50F-12	2284
18	M18		CGM-50S-50F-16	2318

5.1.2. Slump flow and T500

Fig. 5.1 shows the combined effect of aggregate size and base material on T500mm durations. T500mm duration is the recorded time for fresh geopolymer concrete to reach 500 mm. Using fly ash as a base material significantly affected T500 duration when compared to mixes without FA. Furthermore, the effect of aggregate size on T500 duration presents no significant effect compared to binder materials. Mix CG-100S-9, with no FA, records the maximum time of 5.65 sec to reach T500mm, while using 50% of FA, which contains the same size of aggregate (mix CG-50S-50F-9), records the minimum time of 2.23 sec. This indicates that the flow ability increased by about 2.5 times, proving the binder materials' effect. Increasing the aggregate maximum size from 9mm to 12mm and 16mm decreased the duration due to decreasing the total aggregate surface area. Moreover, using different types of aggregate with the same grading and binder materials had no significant effect on the duration of flow ability.

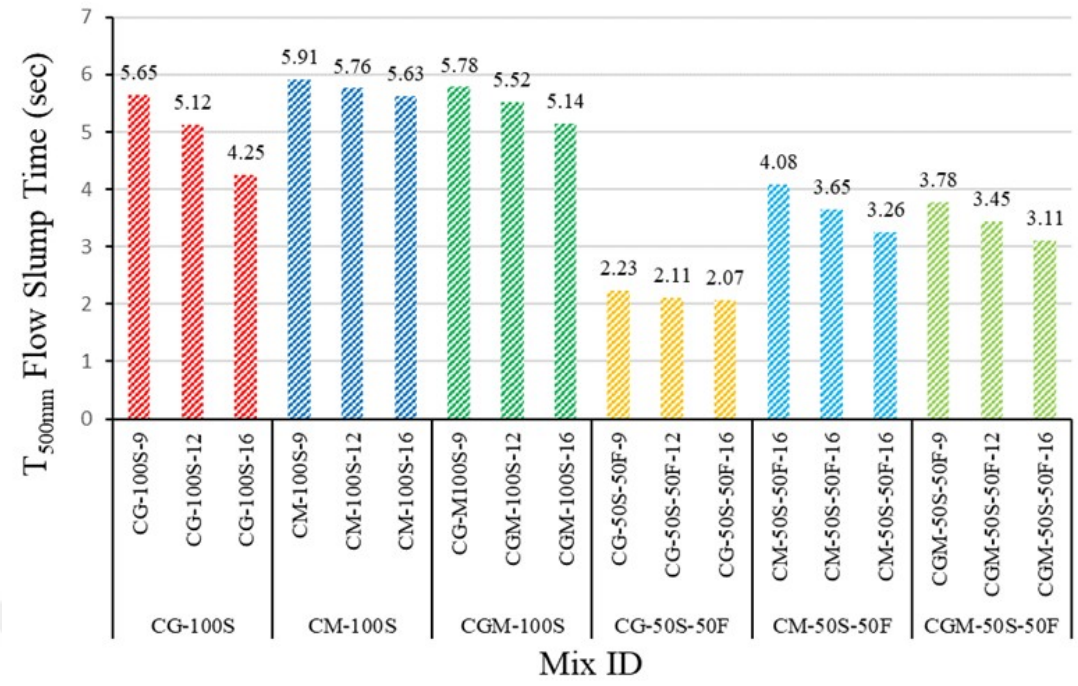

Figure 5.1. Time required passing (500 mm Dia.) Circle

The same concept was used with the flow test for T500mm, influencing the effect of base material, as shown in Fig. 5.2. The flow ability of self-consolidating geopolymer concrete increased, regardless of aggregate type or grading. The influence of using 50% FA increased the flow from 685mm to 778mm because of the flow tests for mixture CG-100S-9 and mixed CG-50S-50F-9, respectively, with minor changes due to changes in aggregate type and aggregate size.

Fig. 5.3 represents the flow test for self-compacting geopolymer concrete. It indicates the ideal distribution of the aggregate particles through all parts and achieves better homogeneity and uniformity of the concrete.

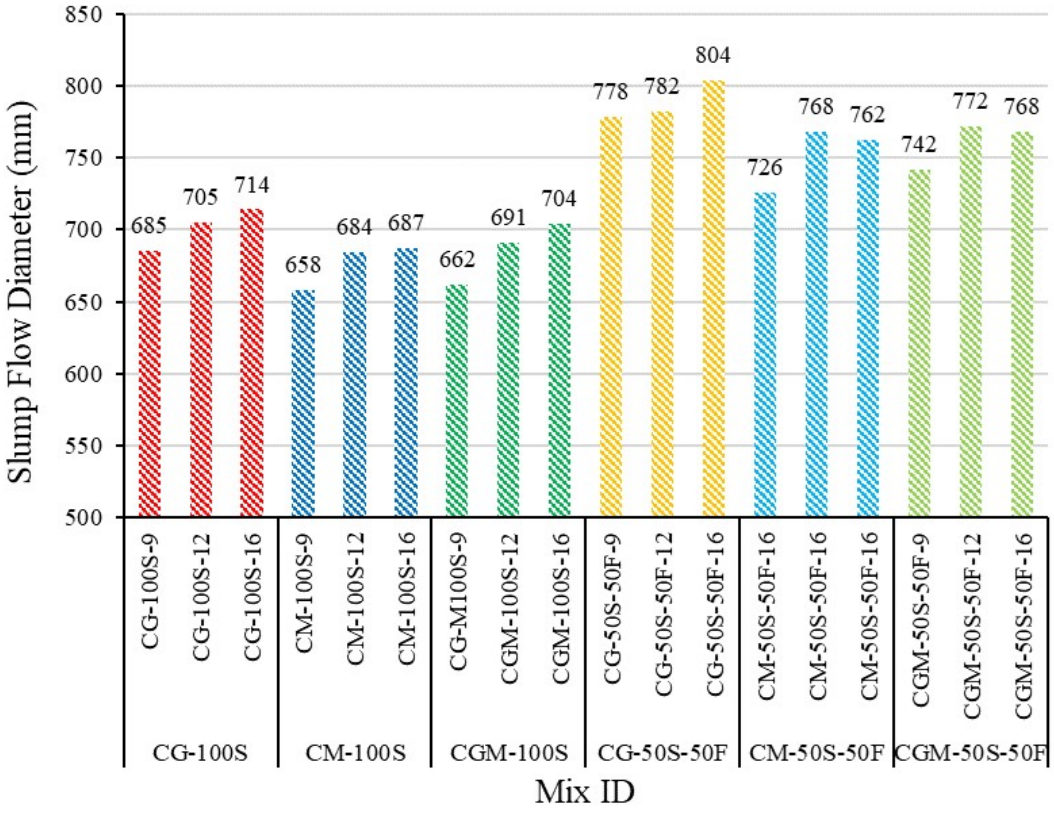

Figure 5.2. Variation of slump flow diameter

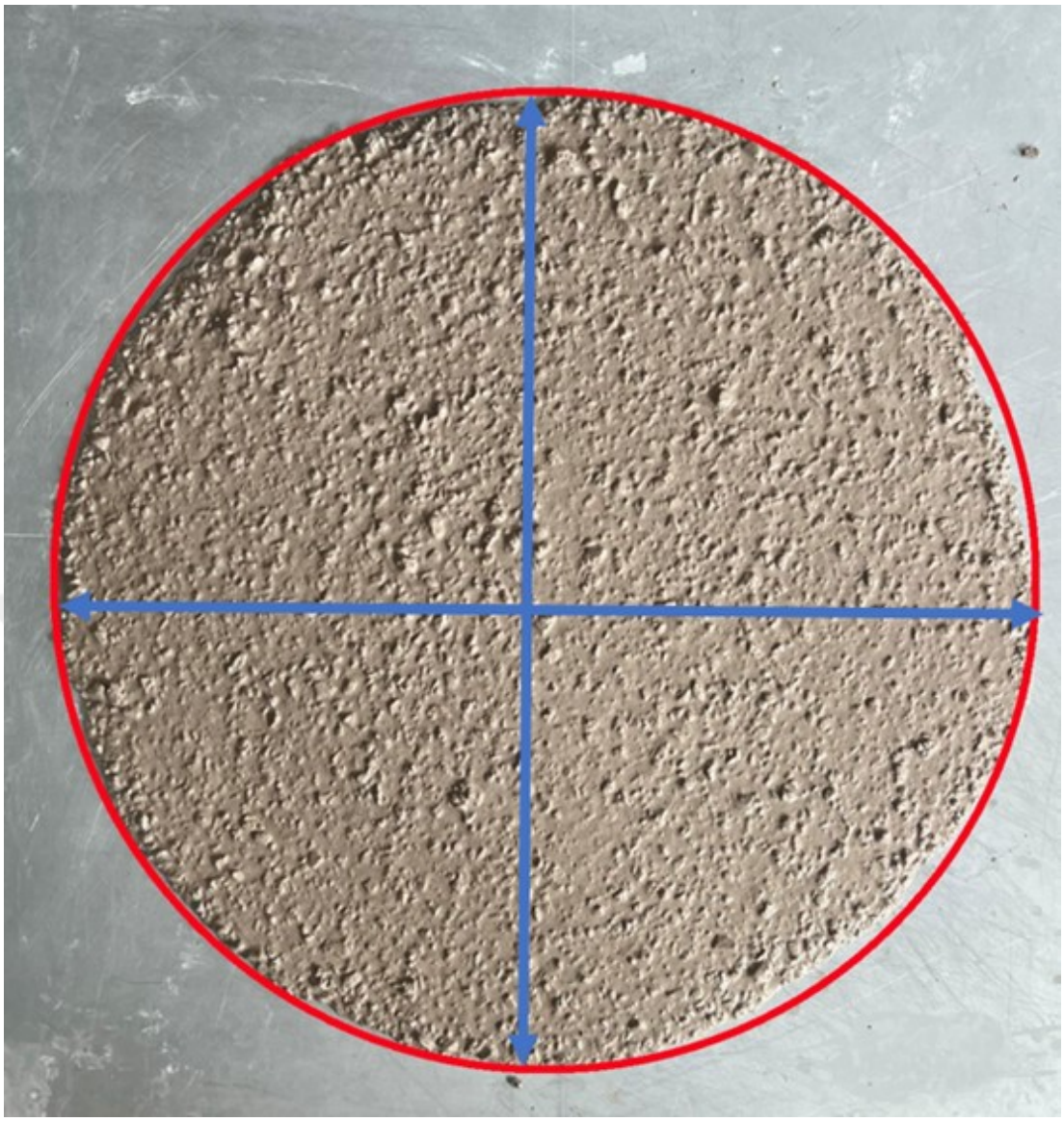

Figure 5.3. Flow test of self-compacting geopolymer concrete

Fig. 5.4 shows the correlation between T500mm time and slump flow of the self-consolidating geopolymer concrete and shows the flow improvement for the mixes with changing the aggregate size, aggregate type, and the superior effect of the base material.

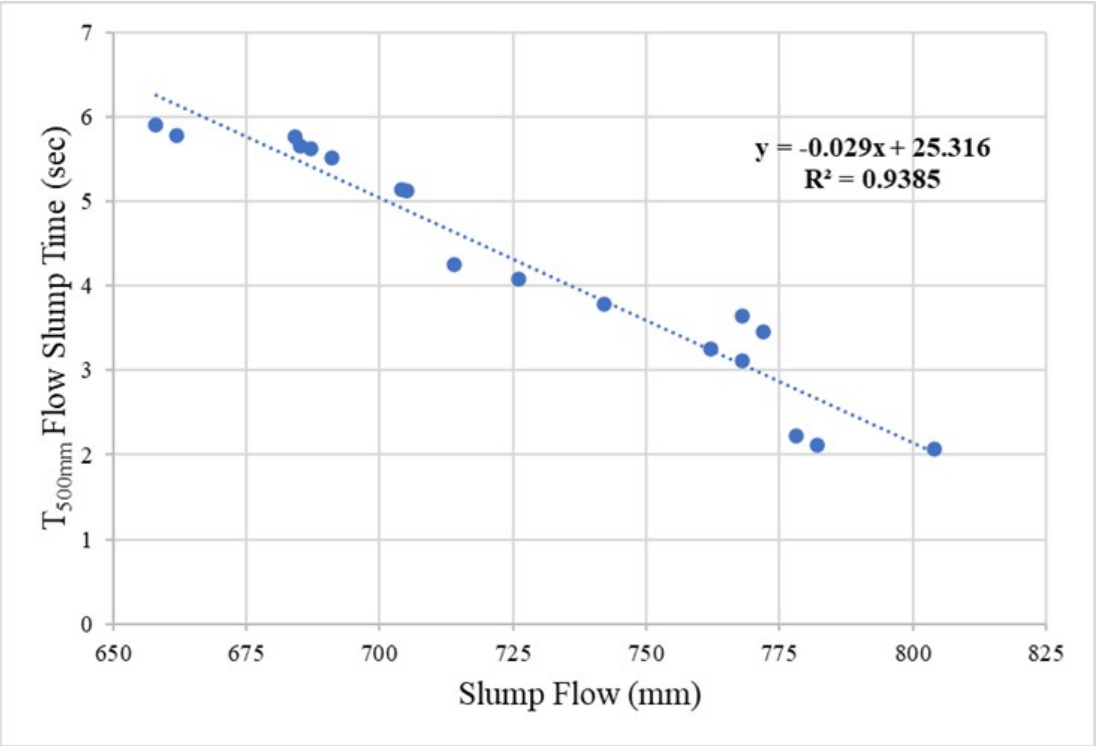

Figure 5.4. Correlation between T500 And Flow test

5.1.3. V-funnel test

V-funnel flow duration results for each mix illustrated in Fig. 5.5 match the viscosity class according to EFNARC. Binder materials significantly influenced the flow time; the use of 50% FA significantly improved the flow of the mix and decreased the viscosity without bleeding or segregation. Moreover, increasing the aggregate size reduced the flow time, while changing the type of aggregate from crushed gravel to crushed marble decreased the flow due to the surface roughness of the aggregate particles. At the same time, as observed at T500mm and slump flow, changing the aggregate size improved the flowability without any bleeding, separation of aggregate particles, or segregation.

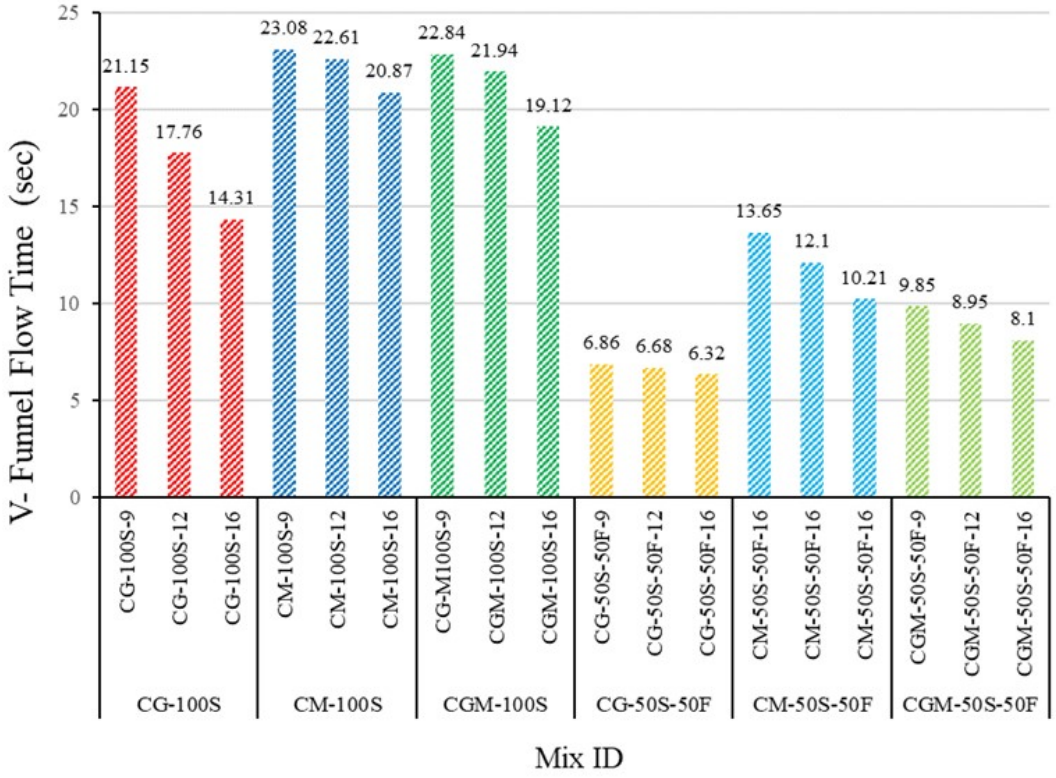

Figure 5.5. Variation of V-funnel flow time

Even though all mixes satisfy EFNARC's limitation for self-consolidating requirements, Figs. 5.5 and . 5.6 show that the tendency for flowability improvement is due to increasing the aggregate size and aggregate type and influencing 50% of FA as a base material, the linear relation between T500mm with flow slump and flow slump with V-funnel shows a constant enhancement of flow during the mixes' groups.

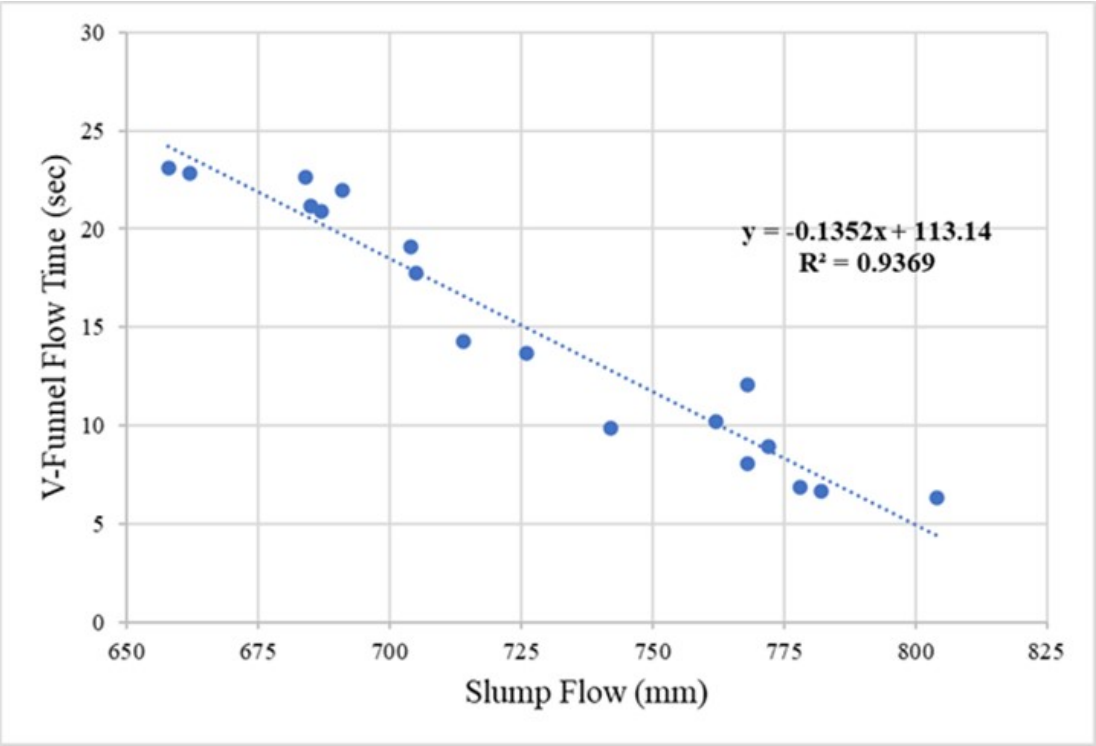

Figure 5.6. Correlation between Slump flow test and V-Funnel test

5.1.4. L box test

To specify the passing ability of all mixes, the L-box three-bar test, which simulates the concrete pass ability for more congested reinforcement EFNARC, has been performed; Fig. 5.7 illustrates the passing ability of the L-box three bars' results.

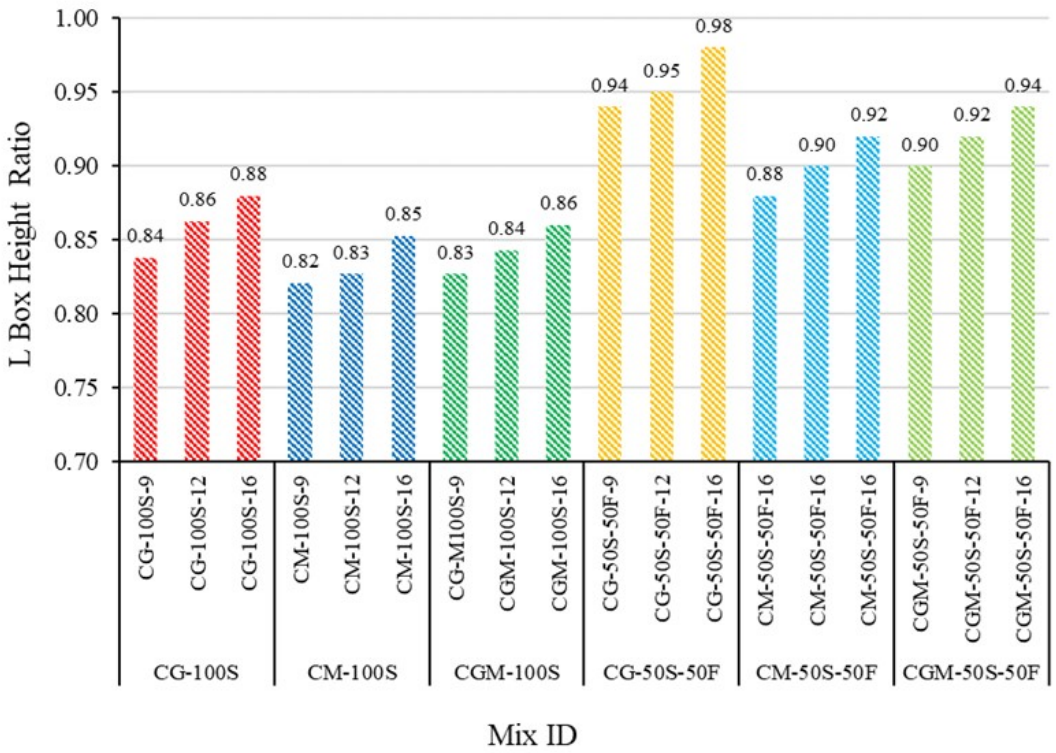

Figure 5.7. Variation of L-box height ratio

Based on EFNARC requirements, H2/H1 ratio for the L-box test must be equal to or greater than 0.8 to ensure and certify self-consolidating requirements and passing ability, as shown in the L-box test results illustrated in Fig. 5.8 all mixes fulfil the EFNARC passing ability's requirements, the mixes with 50% FA base materials gives more flow ability, and increasing aggregate size enhanced the flowability of the self-consolidating geopolymer concrete.

Based on Fig. 5.8, all test results were in the VS2/VF2 viscosity class. According to EFNARC, a mix in the VS1/VF1 viscosity class has a better filling ability for congested reinforcement areas. Still, we must avoid the possibility of bleeding and segregation. The VS2/VF2 class is classified as having good bleeding and segregation resistance with low pressure on formwork; however, the VS2/VF2 class tends to have insufficient surface finish properties or may suffer from flow stoppage in congested reinforcement.

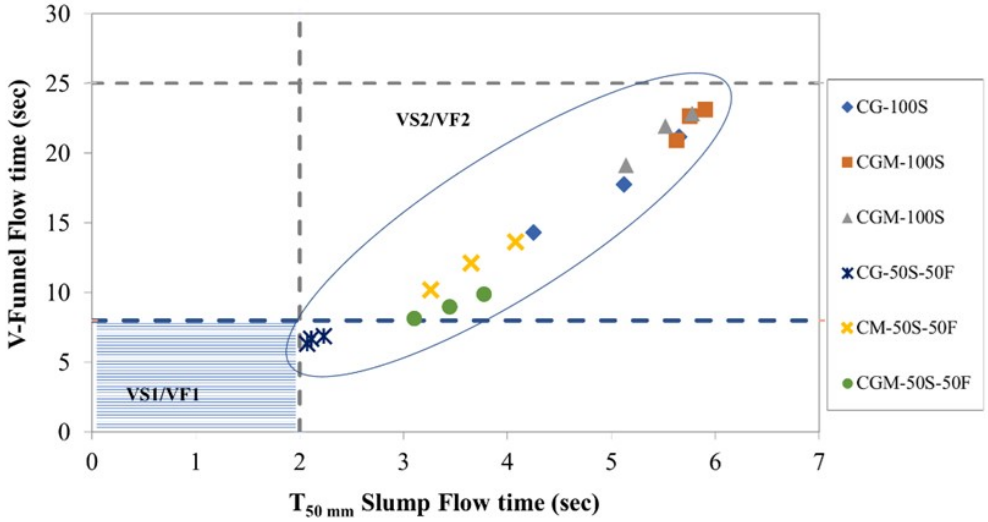

Figure 5.8. V-Funnel Flow time vs T500 Flow time

5.2. Compressive strength of SCGCs

The most important characteristic of conventional and geopolymer concrete, which is responsible for concrete durability, is compressive strength, which is employed to resist the loads. Based on the requirements of construction industries and limitations for self-consolidating requirements in congested reinforcement research on producing new construction material and/or developing materials, the first characteristic to be studied is the compressive strength to predict the durability of newly created material. Therefore, in the study stage, the effects of the type and size of aggregate and their impact on the compressive strength of the geopolymer concrete are studied, too.

Fig. 5.9 illustrates the compressive strength results for all mixes; it can be noticed that the compressive strength of all mixes changed with changes in aggregate size at the same group of aggregate type, regardless of the base material. At an early age, because of ambient curing, the compressive strength of mixes which contained 100% GGBS increased than the mixes containing 50% GGBS and 50% FA due to geopolymerization and alkaline activation for the slag, which was faster than fly ash. The results show that crushed gravel in the mixes gave higher compressive strength than crushed marble mixes; the rough surface texture of the crushed gravel particles attributed to this effect, which gives a stronger bond between aggregate particles and paste than crushed marble, which has smooth surface texture (Golewski, 2023b; Boğa and Şenol, 2023; Mohammed et al., 2022)

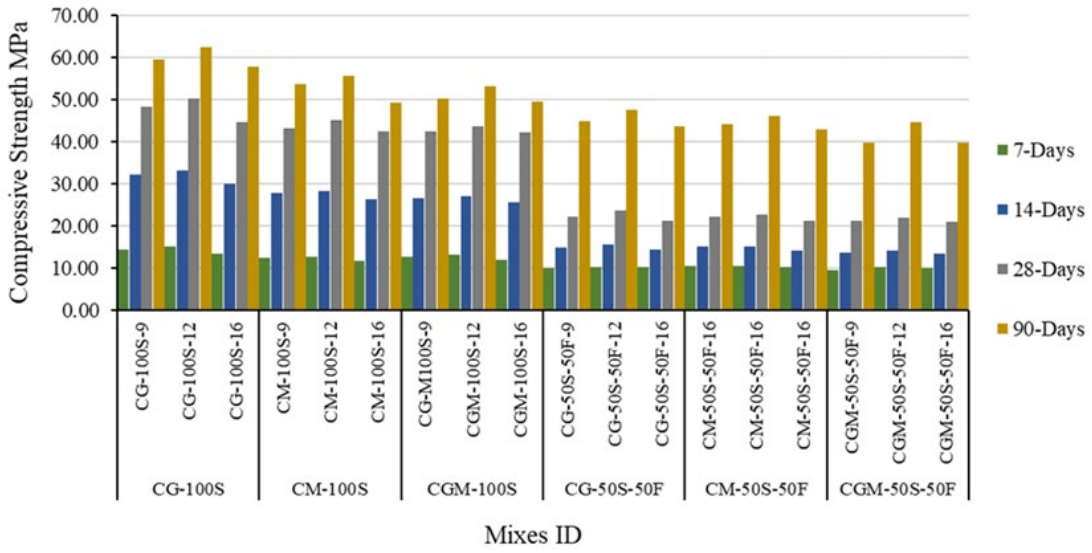

Figure 5.9. The 7-, 14-, 28- and 90-days compressive strength values of SCGC

Concrete strength is the maximum load it can withstand before rupturing or failing. Factors such as manufacturing method, aggregate properties, curing conditions, gel/space ratio, water/cement ratio, aggregate/binder ratio, and concrete age directly impact its strength. In contrast, workability does not have a direct effect. In compression tests, three loading types are commonly employed: uniaxial loading, which yields the most conservative results and can lead to shear, tension, or combined failure; biaxial loading; and triaxial loading.

The compressive strength of self-consolidating geopolymer concrete (SCGC) is influenced by aggregate size and type, similar to traditional Portland cement concrete. Achieving optimal aggregate particle distribution is crucial for attaining the required workability and flow, which are essential for SCGC to fill formwork without vibration. Proper aggregate distribution enhances packing density within the concrete matrix, reducing voids and improving compressive strength.

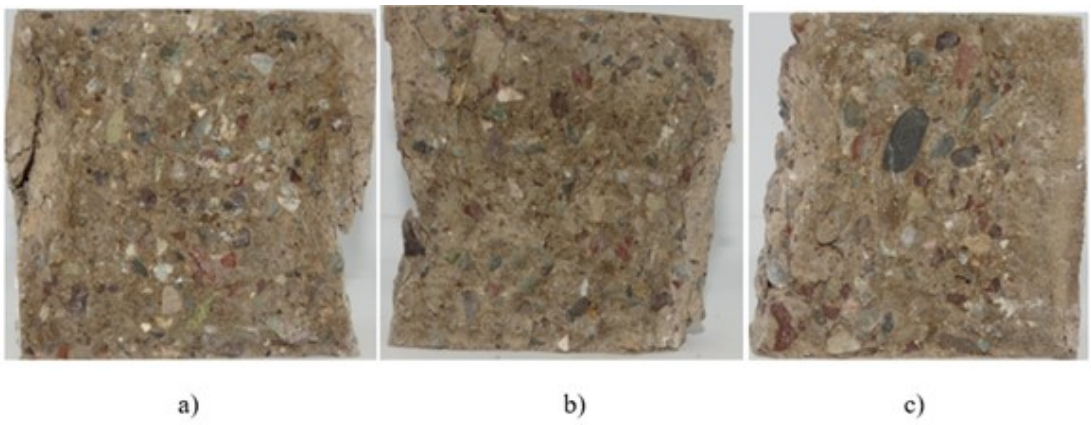

Figure 5.10. Crushed gravel aggregate particle distribution a) 9mm, b) 12mm, c) 16mm inside hardened self-consolidating concrete made with base material 100% GGBS after failure under compression.

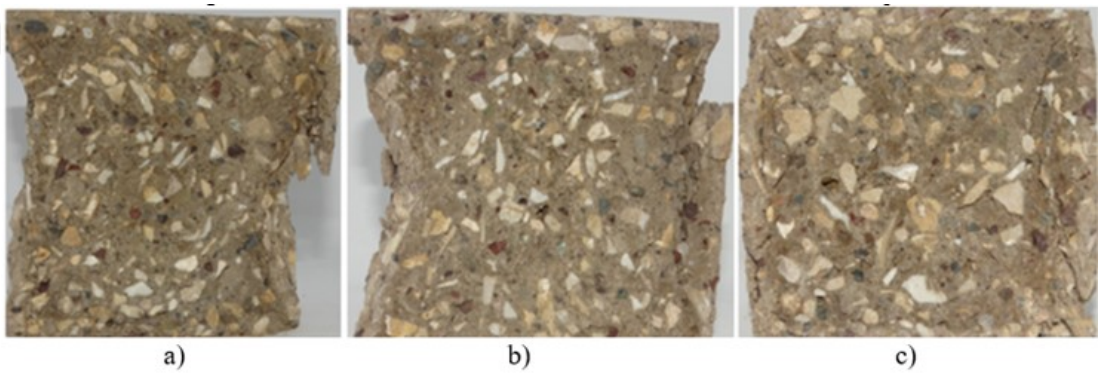

Figure 5.11. Crushed marble aggregate particle distribution a) 9mm, b) 12mm, c) 16mm inside hardened self-consolidating concrete made with base material 100% GGBS after failure under compression

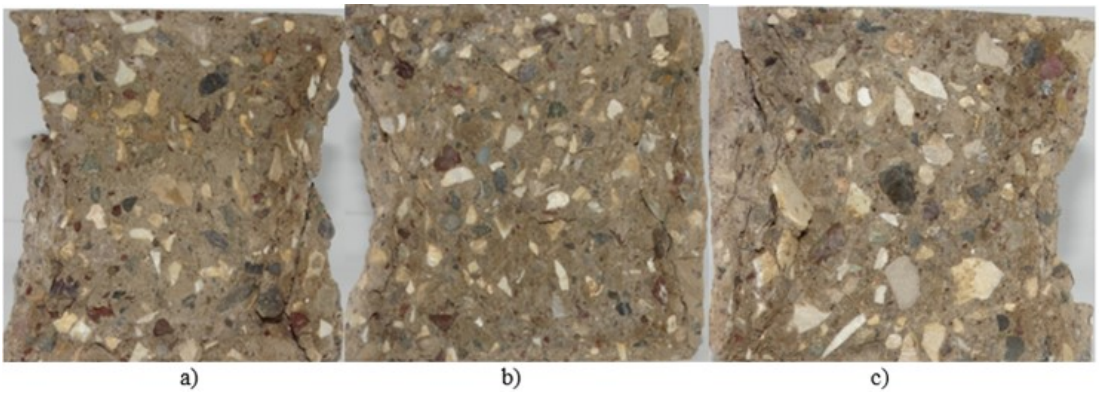

Figure 5.12. Crushed gravel-marble aggregate particle distribution a) 9mm, b) 12mm, c) 16mm inside hardened self-consolidating concrete made with base material 100% GGBS after failure under compression

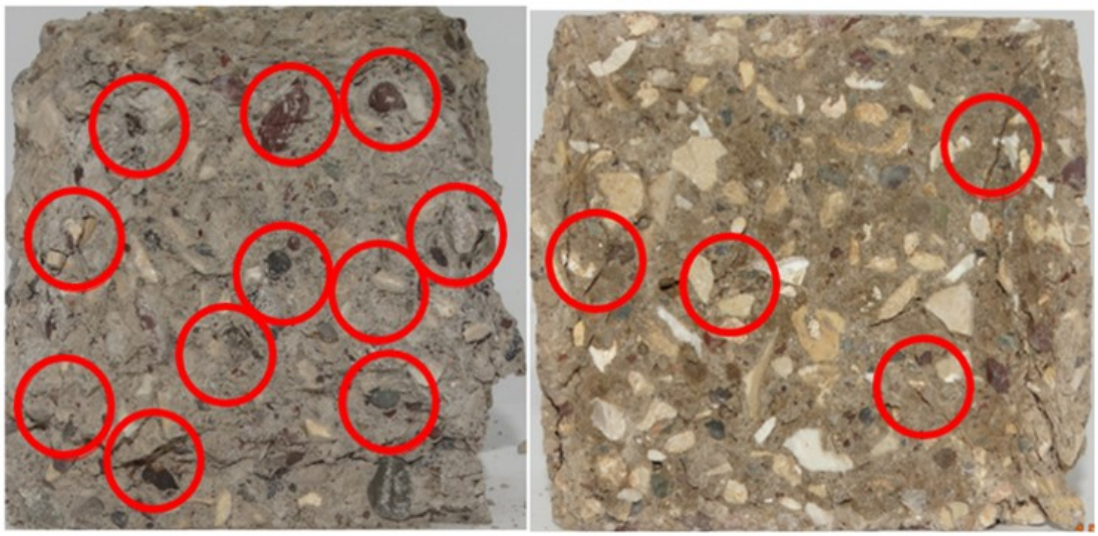

Figure 5.13. Crushed aggregate particles under compression. a) Crushed gravel, b) Crushed marble

Furthermore, aggregate size affects the interfacial transition zone (ITZ) between aggregates and the binder matrix, influencing binding strength. The quality of this transition zone is affected by aggregate size, as seen in Figure 5.13, where crushed aggregate particles within SCGC samples contributed to its strength.

Figure 5.14 displays cross-sections of broken specimens that have been examined and magnified. These cross-sections reveal that the crushed gravel aggregate particles played a significant role in enhancing the concrete bond. This is attributed to the strong bond between the geopolymer paste and the rough-surfaced gravel aggregate particles and the inherent strength of these particles. As a result, the strength of the SCGC made with crushed gravel aggregates is superior to that of the SCGC made with crushed marble aggregates, which have a smoother surface and lower strength. Prior research has established that aggregates' size and texture impact concrete's mechanical characteristics (Güneyisi et al., 2014; Gesoğlu et al., 2013; Han et al., 2003).

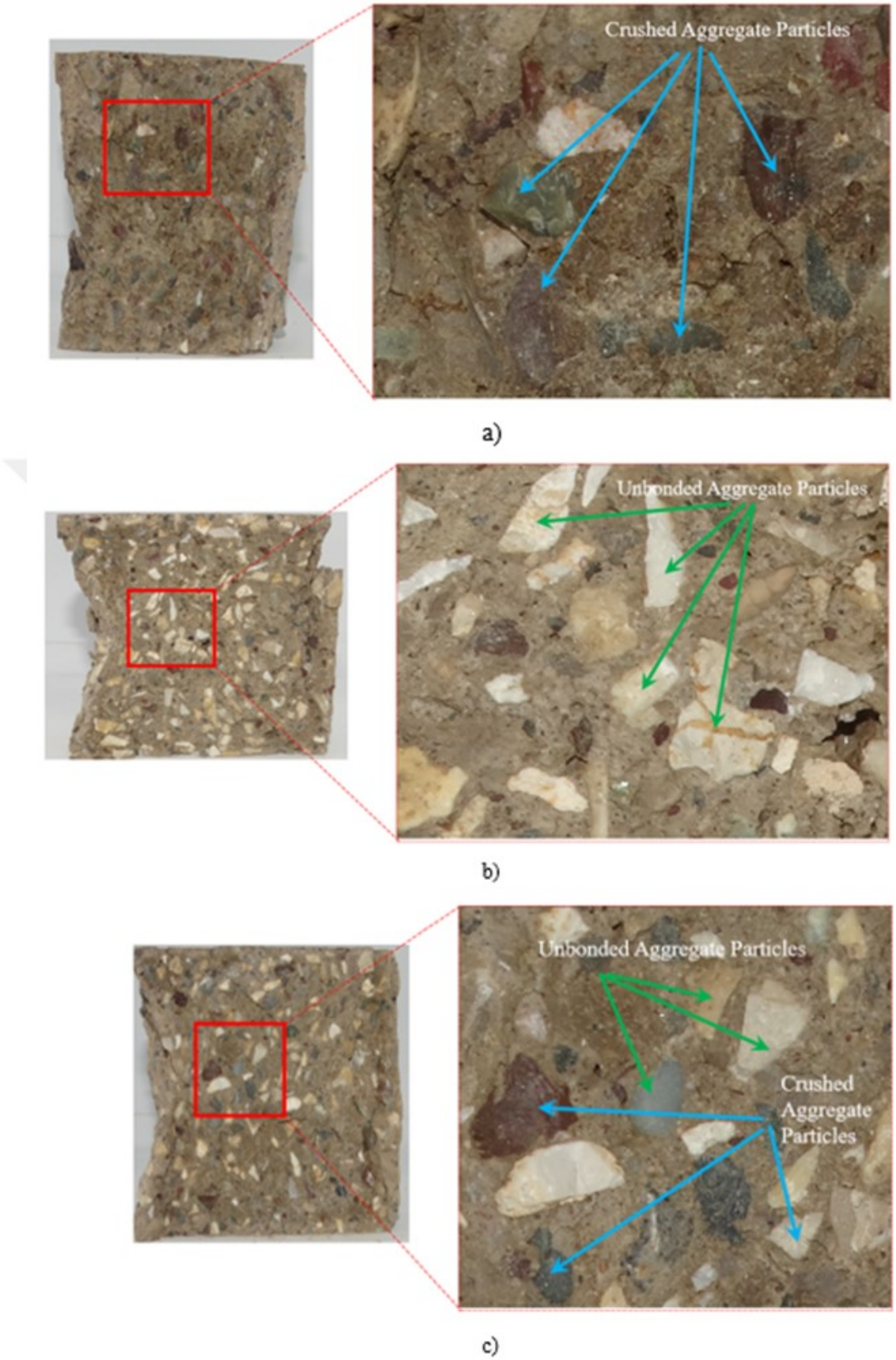

Figure 5.14. Cross-section of SCGC samples, a) 12mm Crushed gravel, b) 12

Crushed marble, c) 12 mm Mixed crushed gravel and marble aggregate

Summarising the mentioned results. The following could be concluded from the findings:

The SCGC mixes demonstrated excellent passing ability and flowability, adhering strictly to EFNARC requirements, with flow diameters above the minimum requirement of 550 mm. No occurrences of bleeding or segregation were detected in the SCGC mixes, and their fresh properties were fully compliant with the EN 12350-8 standard, showcasing the accuracy and dependability of our study.

EFNARC has verified that all A-ASCC mixes, except mix CG-50S-50F, are classified within the VS2/VF2 viscosity class. This classification indicates that these mixes have excellent resistance to bleeding and segregation and low formwork pressure, as determined by v-funnel and slump-flow tests.

Additionally, the study found that the aggregate's size and type can influence the compressive strength of self-consolidating geopolymer concrete (SCGC). Attaining the requisite workability and flow is of utmost importance, as it is essential for SCGC to fill formwork without the need for vibration. The optimal distribution of aggregate particles in self-consolidating concrete (SCGC) improves the compactness of the concrete structure, resulting in a substantial increase in its compressive strength.

5.3. Self-compacting geopolymer concrete-filled steel tubes

This section includes the deformation behaviour study of self-compacting geopolymer concrete-filled tubes CFST loaded axially; the aim is to evaluate the deformation performance and load-carrying capacity of CFST with two length-to-diameter (D/L) rations, four different tube diameters, and two different wall thicknesses as well. A self-compacting geopolymer concrete with a compressive strength of 45 MPa was used.

5.3.1. Deformation behaviour of CFST

5.3.1.1. Empirical equations for composite columns

The behaviour of circular long and short columns under axial loading was determined as a function of axial compression loading versus shortening and lateral displacement until failure according to the length, diameter, and mechanical

properties of the columns as a composite column. Observing the deformation curves can also capture the behaviour of concrete cores. The strength index (SI) was used to compare the performance of columns. In previous literature, SI was used as an indicator to evaluate the performance of composite columns and was defined as follows (Shi et al., 2015).

$$SI = \frac{N_u}{A_s f_y + 0.95 A_c f_c} \tag{5.1}$$

Where N_u is the experimental compression capacity of the GCFST, the factor 0.95 is used to calculate the cross-sectional strength to compensate for the uncertainties inherent in concrete.

Based on the L/D ratio, the specimens were classified into two groups: L/D = 4.5 and L/D=2.0; according to the literature, when L/D > 4 is classified as long, and L/D ≤ 4 is classified as short (Ekmekyapar and Al-Eliwi, 2016; Li et al., 2015).

5.3.1.2. Load deformation behaviour of short columns

Columns with 2D height are classified as short columns, and the failure mode for this group of columns included crushing concrete and yielding steel tubes. It was expected that local buckling would occur at the ends of the columns for this group. The thickness of the steel tubes is the critical factor influencing the variation in results and the manner of deformation. According to Table 5.1, which presents steel tube parameters, the yield strength of steel tubes with a thickness of 3 mm is lower than that of steel tubes with a thickness of 6 mm. Fig. 5.15 displays several examples of columns in this group after the loading process until they reach the point of failure.

Figure 5.15. The failure mode of short column specimens

This group of columns consists of two tubes of thickness with two different yield strengths; the performance of tubes with a thickness of 6mm is greater than that of tubes of thickness of 3mm, as shown in Figure 5.16 and Figure 5.17, illustrating the compression load-shortening curves. As shown in Figures 5.16 and 5.17, compression load increased with increasing the diameter of the columns from the shortening curves, showing that the shortening of higher thicknesses is less than the lower thickness up to the ultimate loading due to better confinement and provides better ductility. The strength index of this group of columns varies from 1.03 to 1.3 depending on the column diameter, which means a suitable confinement parameter for all diameters with fixing the compressive strength of the geopolymer concrete. The ultimate compression load for SCGC-C-101-3-202 was 755 KN; at this load, the shortening was about 10mm, compared with SCGC-C-101-6-202 which has the same diameter as the ultimate compression load of 1398 Kn, the shortening at the ultimate load was about 5. mm, this was observed for the other higher-diameter samples. C-139-3-278 sample shortening was about 10 mm at the ultimate loading of 1082 KN, while C-139-6-278 was about 5 mm at the ultimate load of 1723 KN.

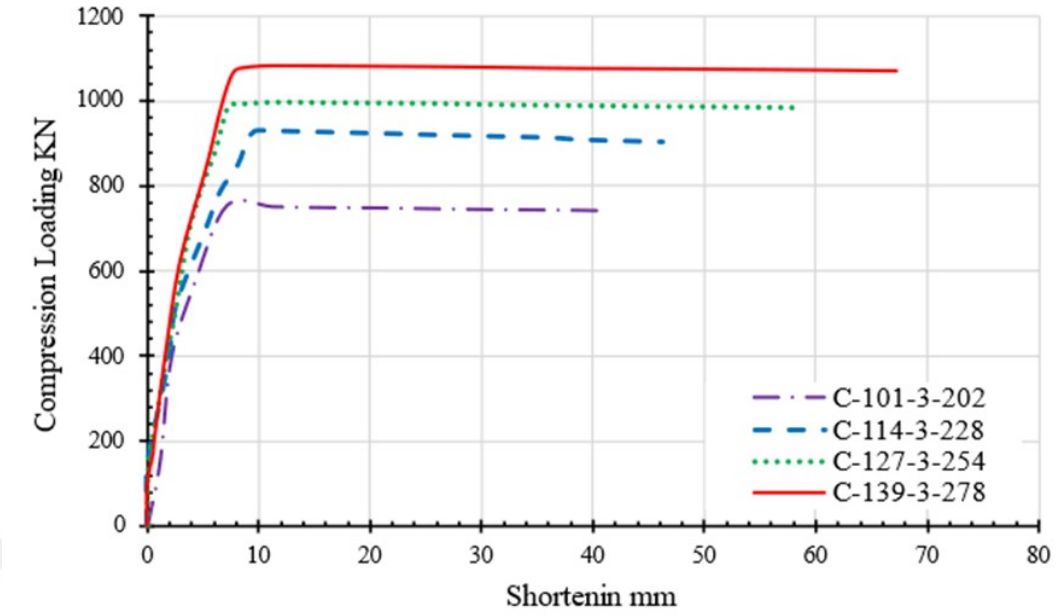

Figure 5.16. Compression loading vs axial shortening curve for 3mm thickness tubes

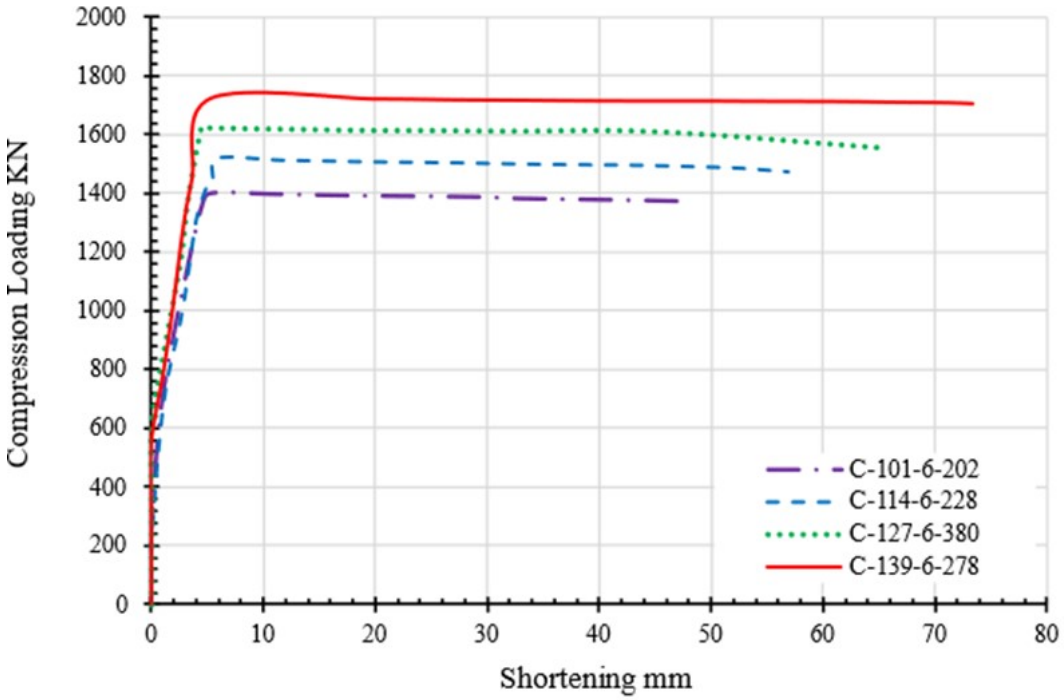

Figure 5.17. Compression loading vs axial shortening curve for 6mm thickness tubes

Figures 5.18 and 5.19 show that even the lateral deformation (local buckling) curves for 6mm thickness samples provide better ductility and uniform, smooth curves with equal total deformation at the failure of the sample other than samples of

3mm thickness that provide different lateral deformation curve shapes and amounts.

Placing concrete infill in axially loaded components avoids inward buckling of the steel tube wall, as illustrated in Figures 5.20 and 5.21. GCFST members exhibit more excellent ductility in their post-buckling behaviour than equivalent HSS members. This can be attributed to the bigger wavelength of the buckling mode, the spreading of plastic deformation, and a modest increase in the moment of inertia of the steel tube caused by the outward buckling shape (Shi et al., 2015; De Oliveira et al., 2009).

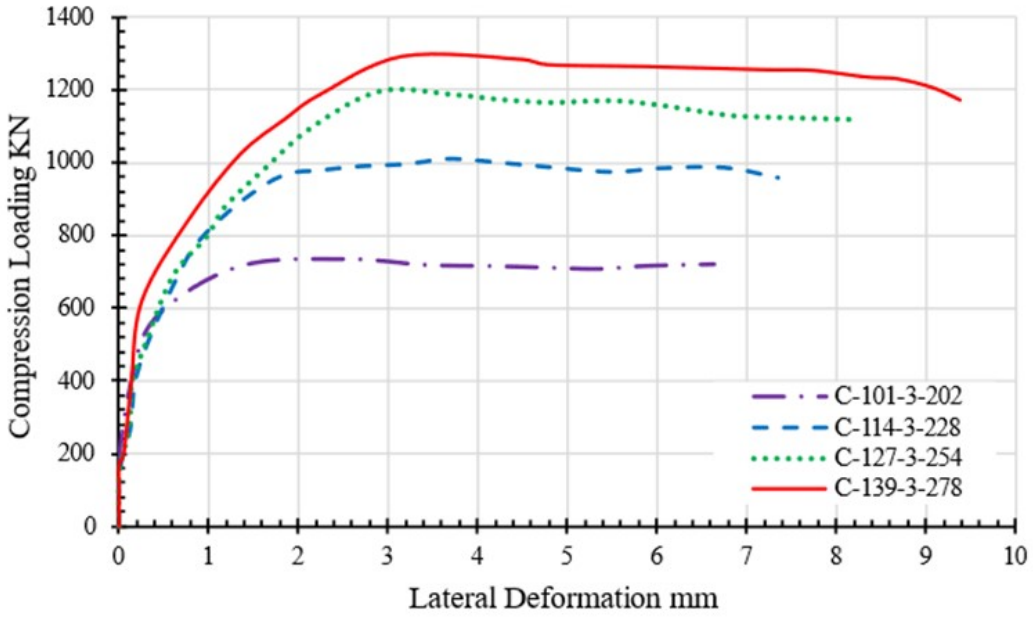

Figure 5.18. Compression loading vs lateral deformation curve for 3mm thickness tubes

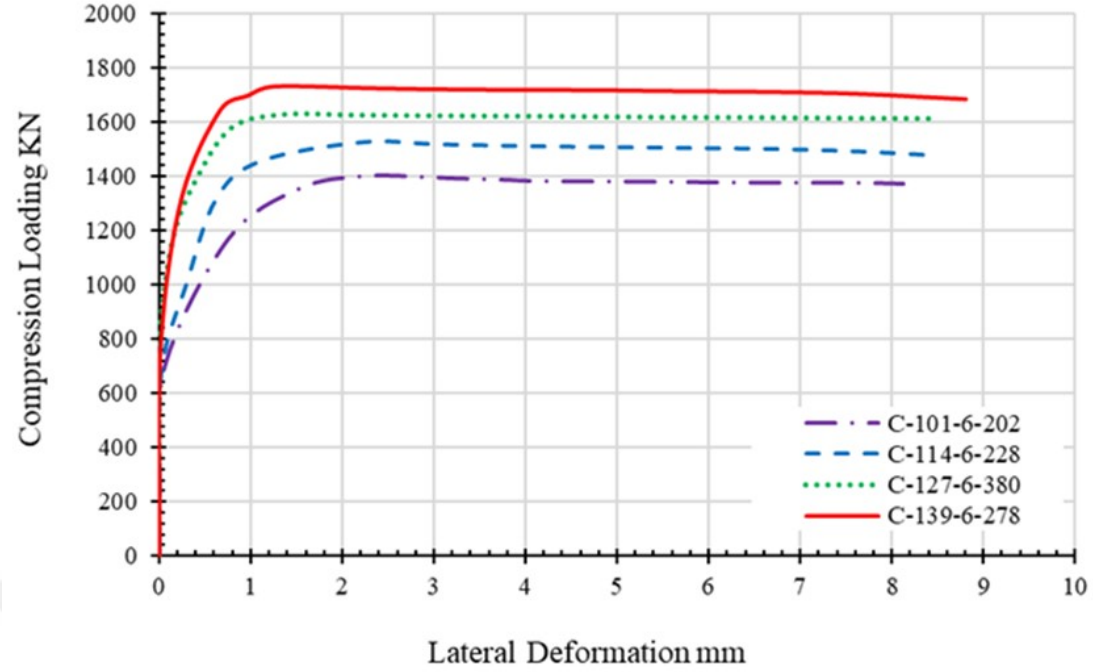

Figure 5.19. Compression loading vs lateral deformation curve for 6mm thickness tubes

a) Buckled shape for a hollow tube. b) Buckled shape for a filled tube.

Figure 5.20. Experimental photo of effects of concrete infill on the local buckling of hollow tubes

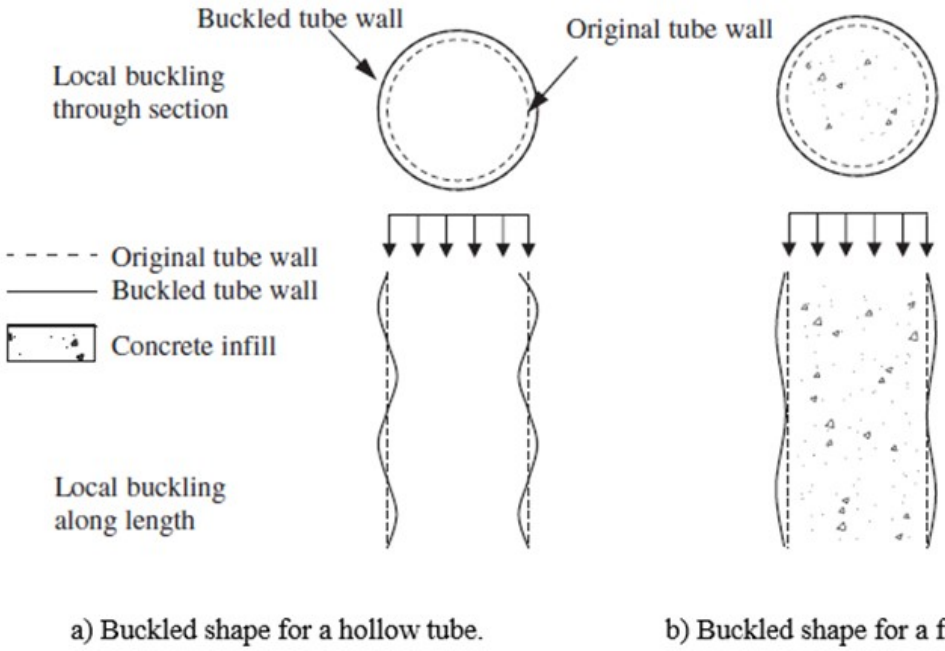

Figure 5.21. Effects of concrete infill on the local buckling of hollow tubes

Figure 5.17 shows that samples with a thickness of 6 mm and a yield strength of 450 MPa provide excellent performance due to increasing the initial stiffness. From the shortening-loading curves, it can be shown that the ultimate load of specimens with a 6mm thickness is greater than the sample having the same diameter but less thickness. The ultimate compression capacity of sample C-101-3-202 is 735 Kn, while the ultimate compression capacity of sample C-101-6-202 is 1395 Kn, and both samples have the same diameter. Regarding the strength index, SI samples with a thickness of 6mm and a yield strength of 450 MPa are larger than samples with a 3mm thickness and yield strength of 330 MPa; SI for sample C-101-3-202 is 1.24, while the SI of sample C-101-6-202 is 1.3. Previous research concluded that increasing the tube thickness increased the compression loading capacity (Mustapha et al., 2021).

The modes of failure of the specimens have significance in evaluating the performance of GCFST columns. Regardless of the significant difference in the ultimate compression capacity between the samples having a thickness of 6 mm and the samples having a thickness of 3mm, there is also a difference between the failure modes of the columns with a thickness of 6mm and 3mm. In contrast, figure 5.5 shows the clear difference between samples with the same diameter but different thicknesses.

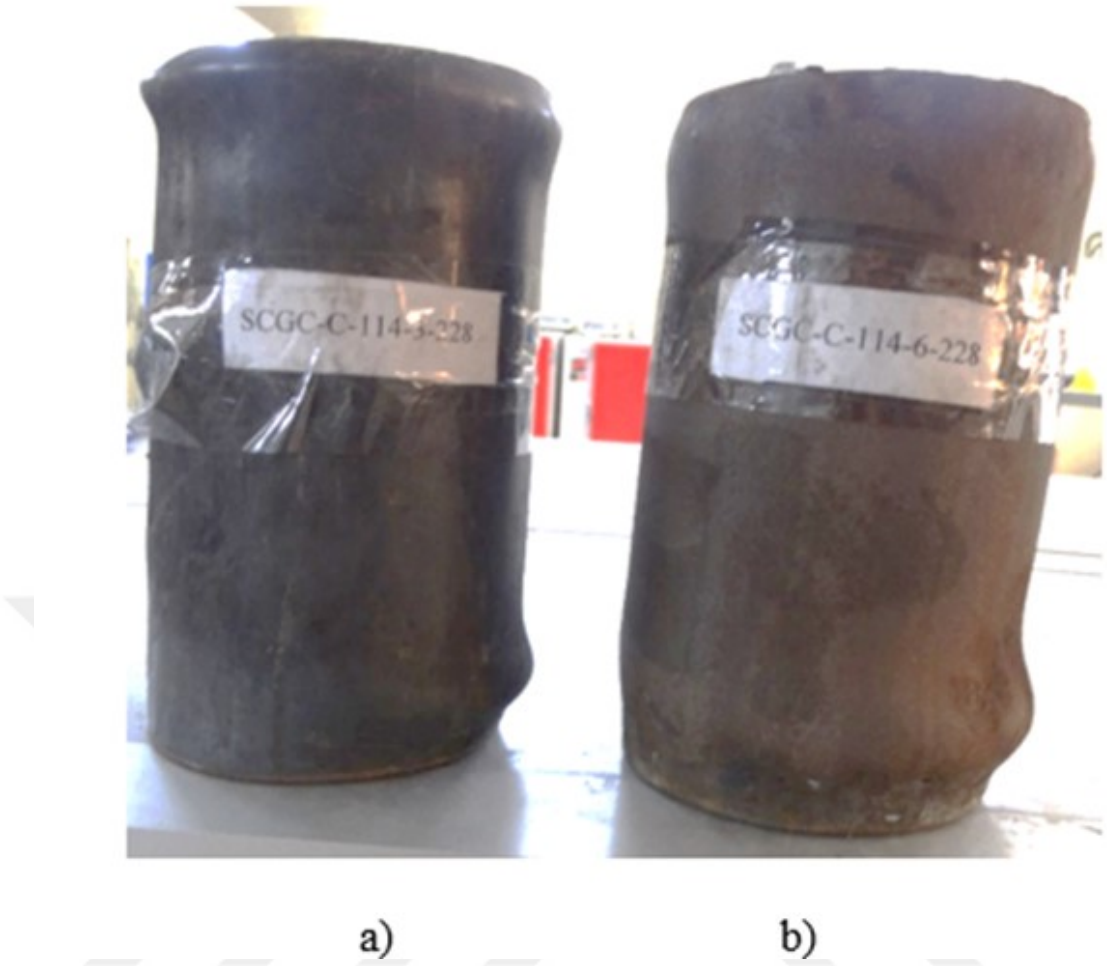

Figure 5.22. Failure mode of a) C-114-3-228 b) C-114-6-228

The specimens in this group exhibited outward local buckling behaviour in steel tubes, which consisted of expanding outward; Figure 5.8 illustrates the local buckling or expanding of the sample under the compression load of this group.

5.3.1.3. Load deformation behaviour of long columns

The columns with a height of 4.5D are classified as long columns. Figure 5.9 illustrates the failure mode of a sample of columns in this group; the prevalence of failure was more pronounced in this group of columns. Shortening and crippling are observed.

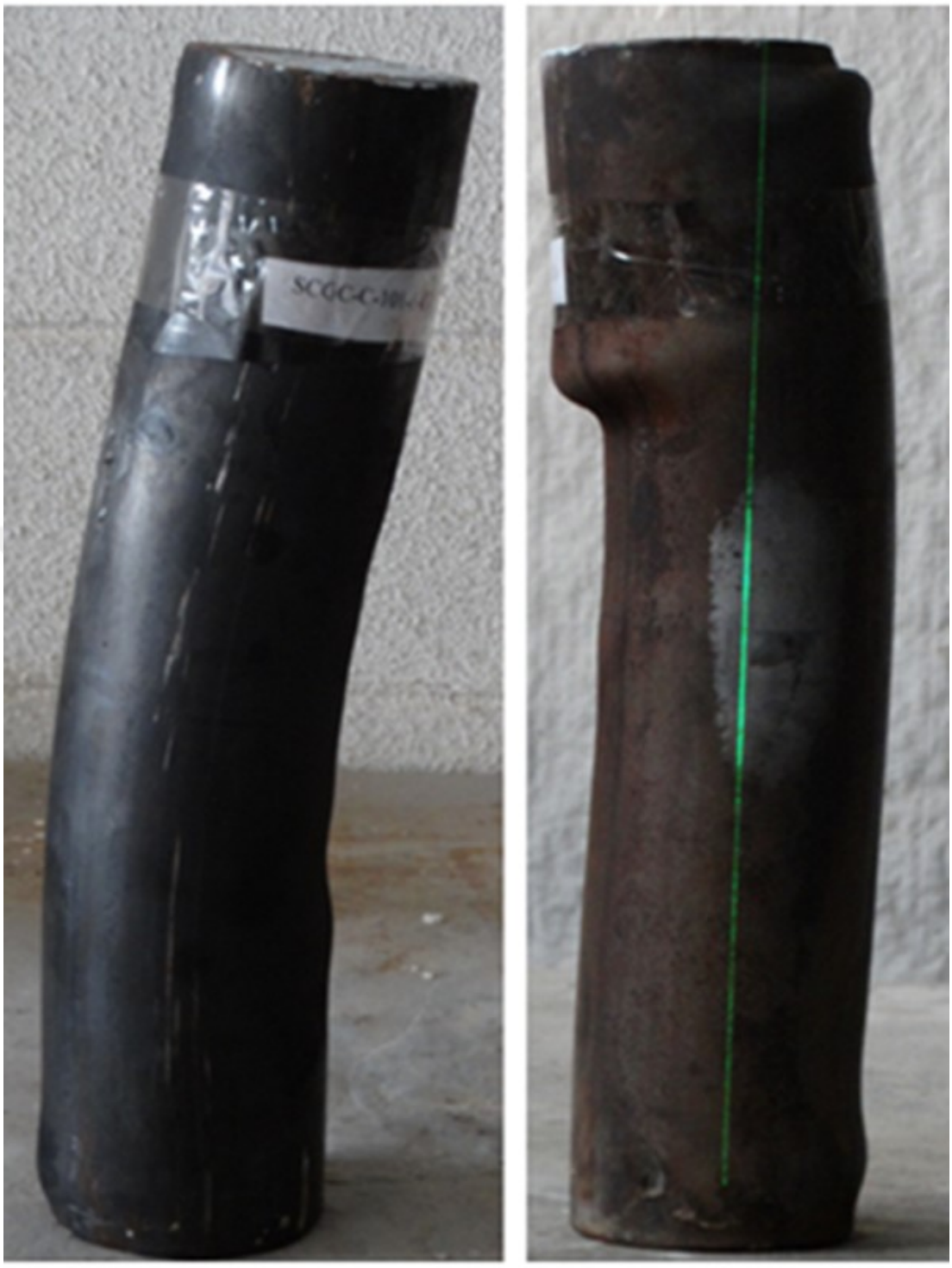

Figure 5.23. Failure mode for long columns a) C-101-3-454, b) C-101-6-454.

Figure 5.23 Sample a) C-101-3-454 concaved very clearly to the side under axial load, which means global buckling was observed in addition to local buckling from the lateral deformation curve represented in Figures 5.24 and 5.25; global buckling or lateral deformation for samples with 3mm thickness of 3 mm was

more than that of samples with a thickness of 6mm due to the confinement performance of thicker tubes, Figure 5.26 confirms the confinement after opening the failed sample laterally.

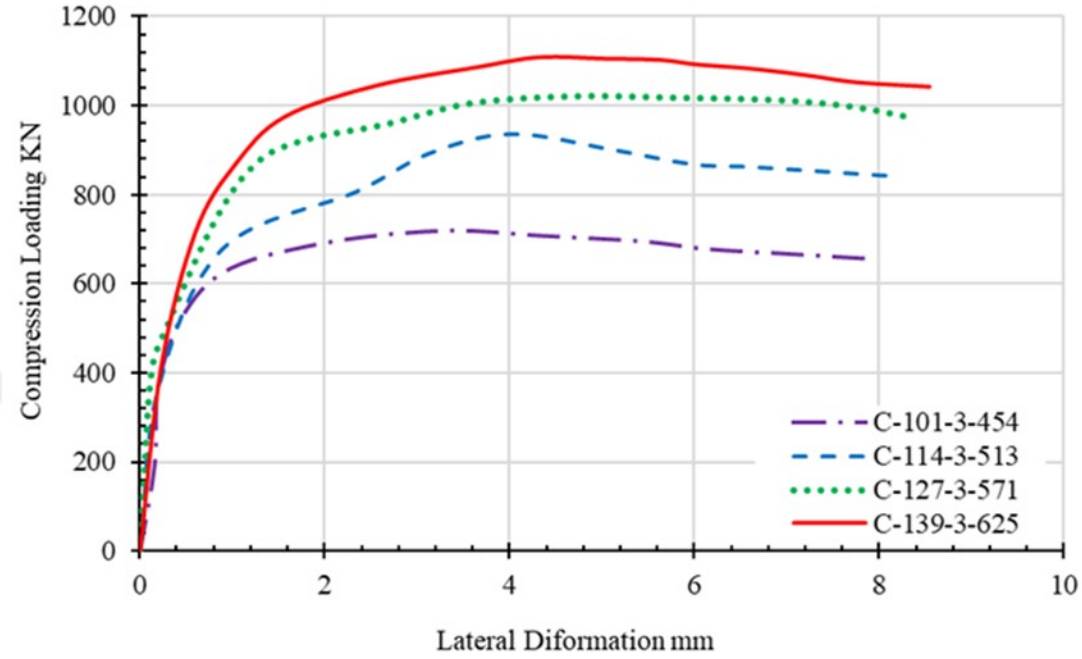

Figure 5.24. Compression loading vs lateral deformation curve for 3mm thickness tubes

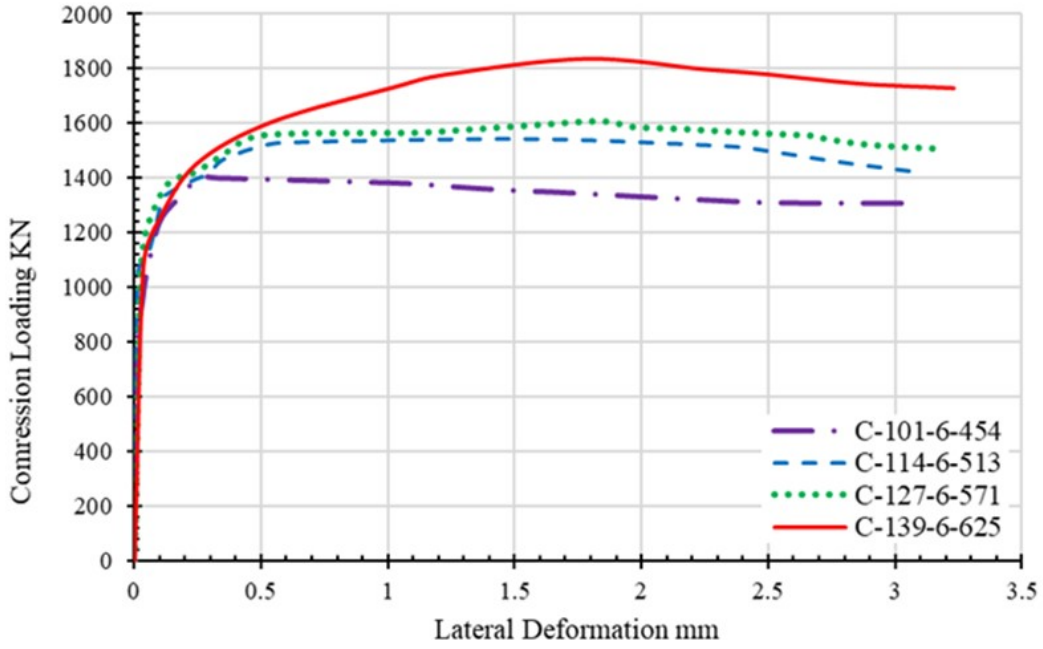

Figure 5.25. Compression loading vs lateral deformation curve for 3mm thickness tubes

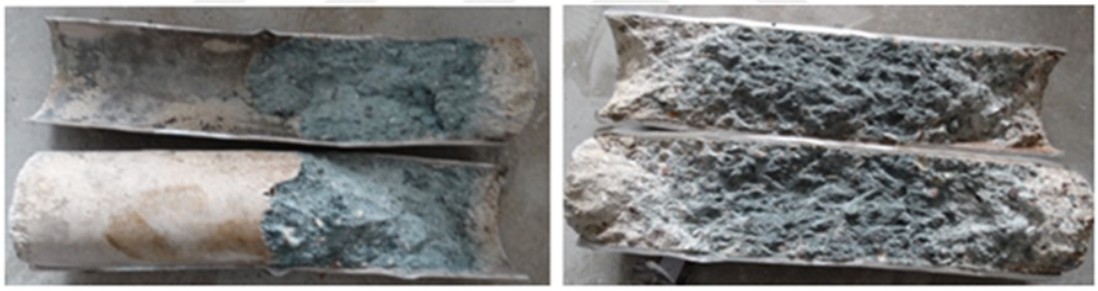

Figure 5.26. Failure mode a) C-114-3-228, b) C-114-6-228

Due to good confinement, the geopolymer concrete inside the tube was crushed under compression load for samples with a tube thickness of 6mm and acted as a composite member. Meanwhile, the geopolymer concrete was crushed partially for tubes with a thickness of 3 mm. It was easy to separate the geopolymer concrete from the tubes.

Ultimate compression load for samples C-101-3-454, C-114-3-513, C-127-3-572, and C-139-3-625 was 719KN, 936 KN, 1021 KN, and 1108 KN, respectively, where the SI was 1.18, 1.27, 1.16, 1.09 comparing with short column group there was no significant variation in the compression capacity. Still, the shortening compression loading curves represent the behaviour of the samples and withstanding with continuous sample loading. It was observed that the compression

load curve was approximately smooth for the short columns with a constant amount of loading, while for the long columns, the curve was decreased till the sample failed.

The SI of the short-column and long-column groups are almost close; therefore, SI values cannot be the decisive parameter for confinement. Considering the tube thickness, the L/D ratio is vital in describing the failure mode, deformation curve, and failure mode (Buckling type).

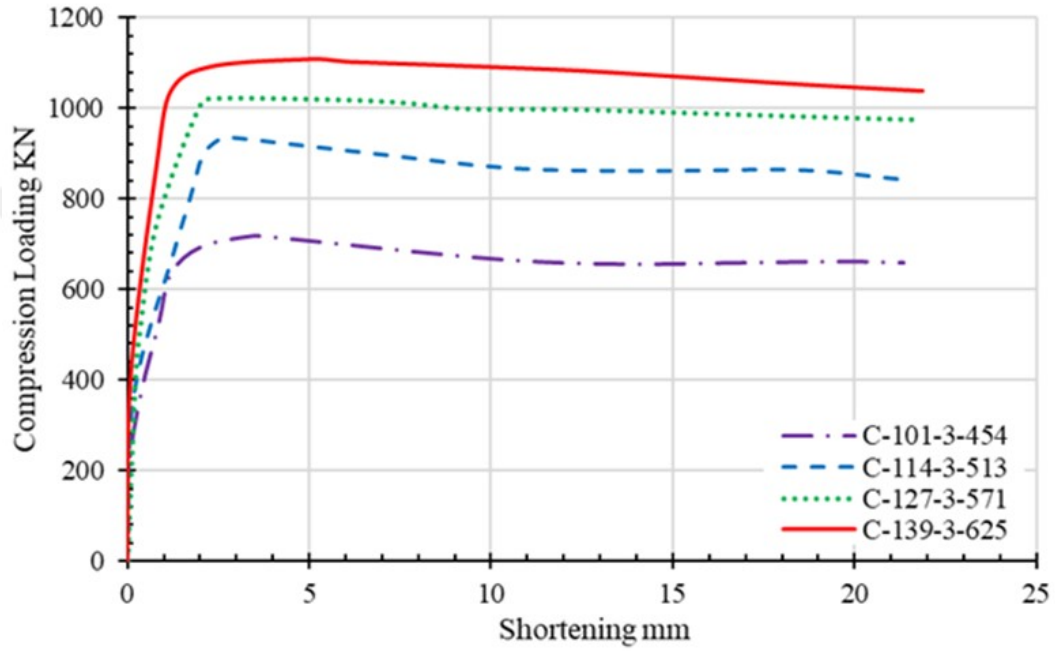

Figure 5.27. Compression loading vs axial shortening curve for 3mm thickness tubes

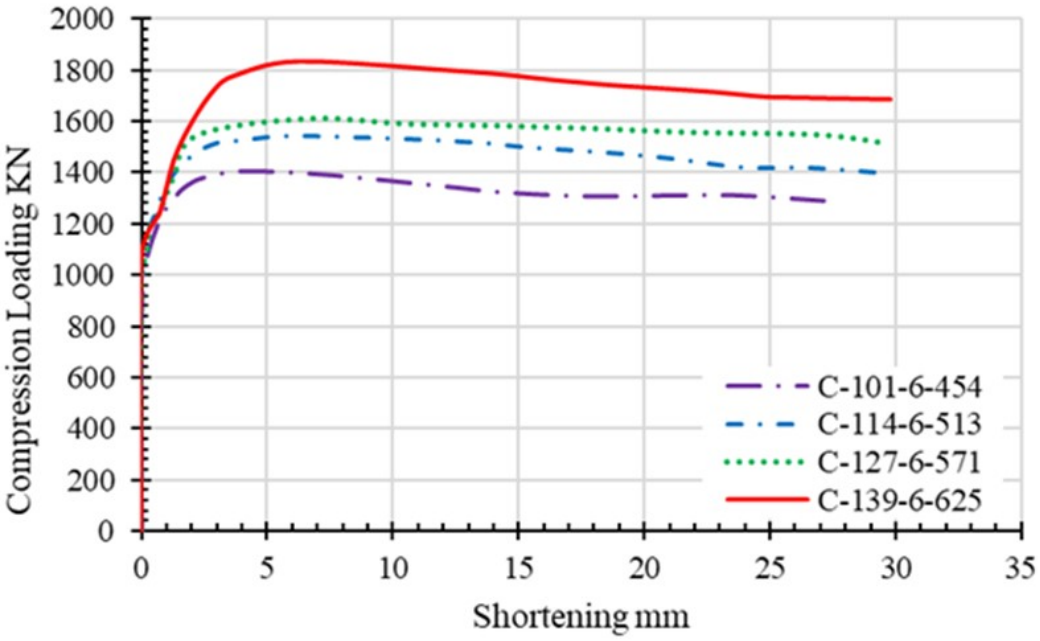

Figure 5.28. Compression loading vs axial shortening curve for 6mm thickness tubes

Figures 5.27 and 5.28 show the compression loading vs. axial deformation of the 3mm tube thickness and 6mm tube thickness, as it was for short columns; the higher thickness tube columns provide the more withstanding capability, and the axial deformation at the ultimate load is less than that for columns with 3mm tube thickness. The deformation curves illustrate that the 6mm tube thickness provides more ductility due to better confinement.

The test results showed good performance in using self-compacting geopolymer concrete filling steel tubes as a composite material; the conclusions below can be drawn.

Compression loading compared to axial deformation curves demonstrated that columns with greater tube thickness exhibit superior confinement and enhance ductility performance. The maximum tube thickness during compression loading resulted in the least axial distortion at the ultimate load.

Only local buckling was found for both tube thicknesses in the short-column group. Testing is necessary to examine global buckling and determine the concrete core capacity of long columns under loading conditions. Long columns may experience global buckling, which decreases column stress before the concrete core reaches its full capacity.

5.4. Standards and design codes for composite columns

This section includes a comparison of columns' performance with international codes. The ultimate loading capacity of the columns is to be compared with two codes, the American code ANSI/AISC 360-16 and European specifications for composite structural design for steel structures EC4. The AISC 360-10 formulations, widely used in the industry, must thoroughly address the confinement effect to ensure the safety and reliability of geopolymer concrete-filled steel tubes. The codes calculate the capacity of concrete-filled steel tubes subjected to axial loads. Considering geopolymer concrete as an alternative to conventional concrete, comparing the study results for geopolymer products with standard codes for regular concrete is necessary.

5.4.1. Design code AISC/ ANSI 360-16

ANSI/AISC 360-16 depends on the structural design of the steel, using the permissible stress or the limited state of the section. At the same time, the Eurocode 4 relies on the limited design state with the possibility of service and safety of the section. The adopted codes in this research depend on the mechanical properties of the materials used and the geometrical properties of the columns, and there are significant differences in the restrictions imposed on the design specifications. Table 5.2 illustrates the material properties and geometrical limitations for composite sections.

Table 5.2. Codes limitations of design specifications

Parameter	Member	AISC 360-16	EC4
fy (MPa)	Structural steel tube	$fy \leq 525$	$235 \leq fy \leq 460$
fc (MPa)	Normal concrete	$21 \leq fc \leq 70$	$20 \leq fc \leq 60$
Steel amount %	Structural steel tube	$\delta \geq 1$ gross section area	$0.2 \leq \delta \leq 0.9$
t mm	Structural steel tube	$t \geq \frac{Dfy}{0.15E}$	$t \geq \frac{Dfy}{(90*235)}$
Slenderness		KL/r ≤ 200	$\lambda \leq 2$

AISC 360-16 defines the composite cross-section strength Pno below (eq. 5.2) for compact sections:

$$P_{no} = A_s f_y + C A_c f_c \tag{5.2}$$

C= 0.95 for circular sections

The ultimate compression capacity P of steel tube-filled concrete, according to AISC 360-16, is determined by (eq. 5.3)

$$P = \phi_c P_n \tag{5.3}$$

Where ϕ_c is the safety coefficient = 0.75 (load and resistance factor design LRFD).

$$P_n = P_{no}\left[0.658^{\frac{P_{no}}{P_e}}\right] when \frac{P_{no}}{P_e} \leqslant 2.25 \tag{5.4}$$

$$P_n = 0.877 P_e when \frac{P_{no}}{P_e} > 2.25 \tag{5.5}$$

Where P_e is Euler critical load as per AISC 360-16, which is calculated by Eq. (6.5),

$$P_e = \frac{\pi^2 E I_{eff}}{L^2} \tag{5.6}$$

$(EI)_{eff}$ is the effective stiffness of the composite section and is given by eq. (5.7)

$$EI_{eff} = E_s I_s + C3 E_c I_c \tag{5.7}$$

E_s and E_c are the elastic moduli of steel tube and concrete, respectively, where

I_s and I_c are the steel and concrete moments of inertia, and C3 is the coefficient for calculating the adequate rigidity of the filled composite compression member.

$$C3 = 0.45 + 3\left[\frac{A_s + A_{sr}}{A_g}\right] \leq 0.9 \tag{5.8}$$

AISC 360-16 classified the concrete-filled steel tubes depending on the D/t ratio to consider the local buckling effect into three classifications: compact if the D/t ratio is lower than $\lambda_p = 0.15Es/f_y$; non-compact if D/t is greater than λ_p but less than $\lambda_r=0.19E_s/f_y$; and slender when the D/t ratio is more significant than λ_r.

Based on the D/t ratio and steel tube properties, this research sample is classified as compact and eq. 5.2 is used to calculate the section strength.

5.4.2. Eurocode EC4

Eurocode EC4 defines the strength of composite columns as a plastic resistance to compression $N_{pI,Rd}$, which is equal to the combined resistance of circular steel tubes and concrete cores.

$$N_{PI,Rd} = A_c f_c + A_s f_y \tag{5.9}$$

Rectangular and square steel tubes provide smaller confinement than the circular section, and that reduction factor is used for these sections for a concrete strength of 0.85 in eq. 5.9.

The increase in concrete strength resulting from confinement can be considered for circular steel concrete-filled tubes, considering that the relative slenderness does not exceed 0.5.

$$N_{NP,Rd} = \eta A_s f_y + A_c f_c \left[1 + \eta c \frac{t f_y}{D f_c}\right] \tag{5.10}$$

Where t is the steel tube thickness, η_c=0, and η_a=1.0 are the concrete and steel confinement factors for loaded columns with eccentricity less than 10% and the

slenderness ratio λ less than 0.5.

$$\lambda = \sqrt{\frac{N_{PI,Rd}}{N_{cr}}} \tag{5.11}$$

Where $N_{pI,Rd}$ is the column plastic resistance founded by eq. (5.11), and N_{cr} is the Euler critical buckling load of columns found by eq. 5.6.

Where EI is the member's calculated effective stiffness as determined by equation 5.12.

$$EI = E_c I_s + K_e E_c I_c \tag{5.12}$$

E_s and E_c are the modulus of elasticity of steel tubes and concrete, respectively. I_s and I_c are the moment of inertia of steel tubes and concrete. K is the correction factor EC4, considered 0.6.

5.4.3. Comparison of the results with the design codes

It is essential to assess the columns' performance by comparing the experimental performance with the requirements of the international codes. Examining the prediction to test result ratios could reveal whether these approaches could be used for design purposes.

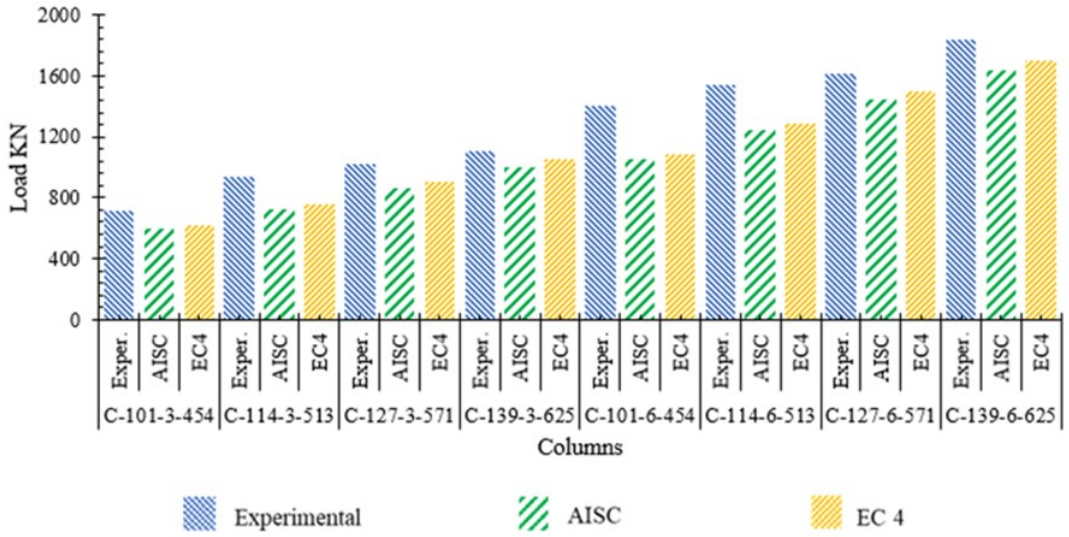

Figure 5.29. Comparison of experimental results with codes for long columns group

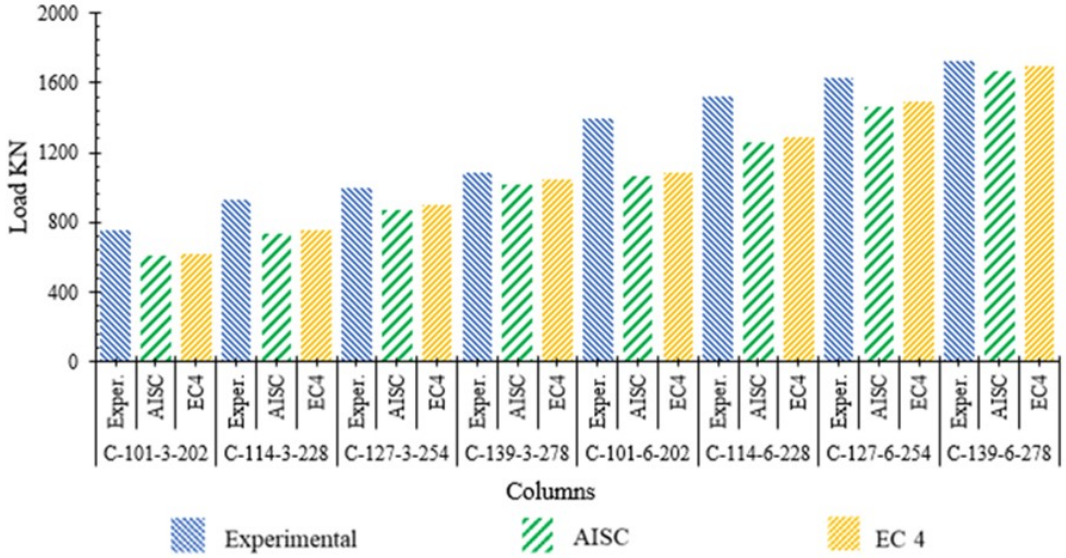

Figure 5.30. Comparison of experimental results with codes for short columns group

The comparison between the experimental results and the standard AISC and EC4 codes presented in Figures 5.29 and 5.30 for all columns of the experimental result is higher than the required columns' capacity compared with the codes. For both groups, short and long, the higher tube thickness provides a higher compression loading capacity. The D/L ratio provides less variation when D/L is increased; at certain L/D, the compression loading capacity decreases with decreasing the tube thickness.

Table 5.3. Comparison of experimental results with the code design formulation

Column	t (mm)	f_y MPa	*SI*	F_{Exp} KN	F_{exp}/AISC	$F_{exp.}$/EC4
SCGC-C-101-3-202	3	330	1.24	755	1.246	1.210
SCGC-C-101-6-202	6	450	1.3	1398	1.309	1.287
SCGC-C-101-3-454	3	330	1.18	719	1.202	1.156
SCGC-C-101-3-454	6	450	1.31	1407	1.338	1.295
SCGC-C-114-3-228	3	330	1.26	932	1.269	1.230
SCGC-C-114-6-228	6	450	1.2	1522	1.207	1.185
SCGC-C-114-3-513	3	330	1.27	936	1.292	1.235
SCGC-C-114-6-513	6	450	1.22	1541	1.241	1.200
SCGC-C-127-3-254	3	330	1.13	995	1.138	1.101
SCGC-C-127-6-254	6	450	1.11	1625	1.109	1.087
SCGC-C-127-3-572	3	330	1.16	1021	1.184	1.130
SCGC-C-127-6-572	6	450	1.09	1610	1.115	1.077
SCGC-C-139-3-278	3	330	1.06	1082	1.067	1.032
SCGC-C-139-6-279	6	450	1.03	1723	1.035	1.014
SCGC-C-139-3-625	3	330	1.09	1108	1.109	1.057
SCGC-C-139-6-625	6	450	1.10	1835	1.119	1.080

As illustrated in Table 5.2, the experimental results showed good agreement with the code formulation. For all columns, the comparison factor between the experimental result and the codes is greater than 1, which means excellent confinement performance is fulfilled.

6. CONCLUSION

Summarizing the test results, the following could be concluded from the findings:

The SCGC mixes showcased passing ability and flowability in strict accordance with EFNARC specifications, with flow diameters surpassing the minimum requirement of 550 mm. The SCGC mixes did not show any signs of bleeding or segregation, and their fresh properties were exactly the same as the EN 12350-8 standard. This shows that our research was accurate and trustworthy.

While aggregate had a lesser effect on fresh characteristics than basic materials, the incorporation of fly ash yielded a substantial enhancement in fresh properties, with improvements of approximately 50% to 60% observed for both aggregate type/size and the use of fly ash, respectively.

Additionally, it was noted that the flowability of SCGC decreased with larger aggregate sizes, with crushed aggregate showing lower flowability than crushed marble due to higher absorption. However, the flowability of combined aggregate resembled that of crushed marble.

EFNARC confirmed that, except for mix CG-50S-50F, all A-ASCC mixes fell within the VS2/VF2 viscosity class, indicating good resistance to bleeding and segregation and low formwork pressure, as per v-funnel and slump-flow tests.

The study revealed that both aggregate size and type could significantly impact the compressive strength of self-consolidating geopolymer concrete. This understanding of the key factors influencing SCGC performance is crucial for its practical application in construction projects, making the audience feel well-informed.

Remarkably, the compressive strength of SCGC exhibited superior improvements in an ambient environment, particularly at the age of 90 days, surpassing the enhancements observed at earlier ages (7, 14, and 28 days). These findings underscore the potential of SCGC for practical application in construction projects, making the audience feel optimistic about its performance.

Moreover, aggregate size influences the interfacial transition zone (ITZ)

between aggregates and the binder matrix, impacting the binding strength. Crushed aggregate particles inside SCGC enhance compressive strength by improving the quality of this transition zone.

Incorporating crushed gravel in mixes resulted in substantially higher compressive strength than crushed marble. This enhancement can be attributed to the rough and uneven texture of crushed gravel particles, facilitating a stronger connection with the paste, unlike the smooth surface texture of crushed marble.

As a result, the optimal aggregate size was 12 mm, and crushed gravel showed optimum performance compared to other types of aggregate and mixing. Fly ash improved the fresh properties, and GGBS significantly enhanced the compressive strength of SCGC.

Self-compacting geopolymer concrete could be used as an alternative to ordinary Portland concrete as a part of composite material with steel tubes; the ambient curing for the self-compacting geopolymer concrete using GGBFS as a base material in producing self-compacting geopolymer concrete provides excellent compressive strength at the age of 28 days.

Compression loading versus axial deformation curves showed that the highest tube thickness performs better confinement and increases the ductility performance of the columns. The highest tube thickness during compression loading performed the lowest axial deformation at the ultimate load.

In the short column group, only local buckling was observed for both tube thicknesses. Long columns require testing to investigate global buckling to investigate the concrete core capacity during loading. Global buckling may occur for long columns, reducing the column stress before the concrete core develops its capacity.

The D/L is a critical parameter in investigating the column capacity to indicate the relative slenderness of the columns, while the tube thickness improves the confinement of the self-compacting geopolymer concrete steel filled tube.

The comparison of test results with the standard codes presents satisfactory results, mainly for the long columns group; for long columns, the ratio from experimental results to the code's predictions is about 1.1, but for short columns, it

reached 1.28.

As the slenderness of the column grows, the predictions made by EC4 and AISC 360-10 become more accurate. While both codes yield conservative results for slenderness ratios greater than 1.0, AISC 360-10 outperforms the other code in this range and provides predictions more closely aligned with the test results of the specimens examined in this study.

Overall, EC4 predictions demonstrate significantly improved concurrence with the test findings and provide reasonable forecasts for CFST columns that possess features outside the limitations of their intended applications. Hence, the application boundaries of EC4 could be expanded to encompass the resolution of more extensive column configurations. AISC 360-16 provides cautious outcomes for self-compacting geopolymer concrete steel filled tube columns that possess properties both within and beyond the limitations of their intended use. Therefore, it is necessary to reassess the confinement impact of circular tubes in the AISC 360-16 equations.

7. RECOMMENDATIONS

Based on the experimental outcomes of this study, the potential field of future studies is recommended:

- To find out exactly how the type of aggregate affects the new properties of self-compacting geopolymer concrete, a rheological study is suggested.
- Influencing ambient-cured self-compacting geopolymer concrete to produce a composite beam and composite girders and studying the flexural strength.
- Tests are to be conducted on rectangular or square sections of self-compacting geopolymer concrete steel-filled tubes to understand their behaviour under axial loading.
- It is strongly recommended that biaxial-loaded self-compacting geopolymer concrete steel filled tube be studied to investigate its deformations.
- Finite element analysis is recommended to simulate the deformation behaviour of a self-compacting geopolymer concrete steel filled tube, comparing the results with experimental and code equations.

REFERENCES

Adam, A. A., Amiri, N. H., Suarnita, I. W., & Rupang, N. (2016). The effect of lime addition on the setting time and strength of ambient cured fly ash based geopolymer binder. *MATEC Web of Conferences*, *47*, 01015. https://doi.org/10.1051/matecconf/20164701015

Al-Saadi, A. U., Aravinthan, T., & Lokuge, W. (2018). Structural applications of fibre reinforced polymer (FRP) composite tubes: A review of columns members. Composite Structures, 204, 513-524.

American Institute of Steel Construction AISC. (2016). *AISC 360-16: An American National Standard Specification for Structural Steel Buildings*. AISC.

American Society for Testing and Materials ASTM. (2012). *ASTM C618: Standard Specification for Coal Fly Ash and Raw or Calcined Natural Pozzolan for Use in Concrete*. ASTM International.

American Society for Testing and Materials ASTM. (2002). *ASTM C138: Standard Test Method for Density (Unit Weight), Yield, and Air Content (Gravimetric) of Concrete*. ASTM International.

American Society for Testing and Materials ASTM. (2016). *ASTM E8/E8M-16: Standard test methods for tension testing of metallic materials*. ASTM International. https://doi.org/10.1520/E0008_E0008M-16

American Society for Testing and Materials ASTM. (2002). *Standard Specification for Concrete Aggregates* (ASTM C33-02). ASTM International.

ASTM International. (2003). *ASTM C39/C39M-01: Standard Test Method for Compressive Strength of Cylindrical Concrete Specimens*. ASTM International.

Bartos, P. (1992). Fresh Concrete: Workability and Tests.

Boğa, A. R., & Şenol, A. F. (2023). The effect of waste marble and basalt aggregates on the fresh and hardened properties of high strength self-compacting concrete. *Construction and Building Materials*, *363*, 129715. https://doi.org/10.1016/j.conbuildmat.2022.129715

British Standards Institution BSI. (1990). *BS 812-110: Methods for Determination of Aggregate Crushing Value (ACV)*. BSI.

Brykov, A. S. (2004). Formation of Concentrated Polysilicate Solutions from Stabilized Silica Sols. *Colloid Journal*, *66*(4), 430–434. https://doi.org/10.1023/b:coll.0000037448.08034.50

Davidovits, J. (1994). High-alkali cements for 21st century concretes. Special Publication, 144, 383-398.

Davidovits, J. (1982). U.S. Patent No. 4,349,386. Washington, DC: U.S. Patent and Trademark Office.

De Oliveira, W. L. A., De Nardin, S., De Cresce El Debs, A. L. H., & Debs, M. K. E. (2009). Influence of concrete strength and length/diameter on the axial

capacity of CFT columns. *Journal of Constructional Steel Research*, *65*(12), 2103–2110. https://doi.org/10.1016/j.jcsr.2009.07.004

Deb, P. S., Nath, P., & Sarker, P. K. (2014). The effects of ground granulated blast-furnace slag blending with fly ash and activator content on the workability and strength properties of geopolymer concrete cured at ambient temperature. *Materials & Design (1980-2015)*, *62*, 32–39. https://doi.org/10.1016/j.matdes.2014.05.001

Diaz-Loya, E. I., Allouche, E. N., & Vaidya, S. (2011). Mechanical properties of Fly-Ash-Based geopolymer concrete. *ACI Materials Journal*, *108*(3). https://doi.org/10.14359/51682495

Druta, C. (2003). *Tensile strength and bonding characteristics of self-compacting concrete*. https://doi.org/10.31390/gradschool_theses.4228

Dubey, R., & Kumar, P. (2012). Effect of superplasticizer dosages on compressive strength of self compacting concrete. *International Journal of Civil and Structural Engineering*, *3*(2), 360–366. https://www.indianjournals.com/ijor.aspx?target=ijor:ijcse&volume=3&issue=2&article=009

Duxson, P., Fernández-Jiménez, A., Provis, J. L., Lukey, G. C., Palomo, A., & Van Deventer, J. S. J. (2006). Geopolymer technology: the current state of the art. *Journal of Materials Science*, *42*(9), 2917–2933. https://doi.org/10.1007/s10853-006-0637-z

EFNARC. (2005). *The European Guidelines for Self-Compacting Concrete: Specification, Production, and Use*. EFNARC.

Ekmekyapar, T., & Al-Eliwi, B. J. (2016). Experimental behaviour of circular concrete filled steel tube columns and design specifications. *Thin-Walled Structures*, *105*, 220–230. https://doi.org/10.1016/j.tws.2016.04.004

Erniati, M. W. T., Djamaluddin, R., & Sampebulu, V. (2006). Compressive Strength and Slump Flow of Self Compacting Concrete Uses Fresh Water and Sea Water.

European Committee for Standardization CEN. (2000). *EN 206-1: Concrete – Part 1: Definitions, specifications and quality control*. CEN.

European Committee for Standardization CEN. (2004). *Eurocode 4: Design of composite steel and concrete structures. Part 1-1: General rules and rules for buildings*. CEN.

Fletcher, R. A., MacKenzie, K. J., Nicholson, C. L., & Shimada, S. (2005). The composition range of aluminosilicate geopolymers. *Journal of the European Ceramic Society*, *25*(9), 1471–1477. https://doi.org/10.1016/j.jeurceramsoc.2004.06.001

German Standardization Body (Beuth Verlag). (2009). *EN 12350: Testing Fresh Concrete*. Beuth Verlag.

Gesoğlu, M., Güneyisi, E., Alzeebaree, R., & Mermerdaş, K. (2013). Effect of silica

fume and steel fiber on the mechanical properties of the concretes produced with cold bonded fly ash aggregates. *Construction and Building Materials*, *40*, 982–990. https://doi.org/10.1016/j.conbuildmat.2012.11.074

Giannopoulou, I., & Panias, D. (2007, September). Structure, design and applications of geopolymeric materials. In Proceedings of the 3rd International Conference on Deformation Processing and Structure of Materials (Vol. 636876, p. 8).

Golewski, G. L. (2023a). Concrete Composites Based on Quaternary Blended Cements with a Reduced Width of Initial Microcracks. *Applied Sciences*, *13*(12), 7338. https://doi.org/10.3390/app13127338

Golewski, G. L. (2023). Study of strength and microstructure of a new sustainable concrete incorporating pozzolanic materials. Structural Engineering and Mechanics, An Int'l Journal, 86(4), 431-441.

Golewski, G. L. (2023b). The Effect of the Addition of Coal Fly Ash (CFA) on the Control of Water Movement within the Structure of the Concrete. *Materials*, *16*(15), 5218. https://doi.org/10.3390/ma16155218

Golewski, G. L. (2023c). Assessing of water absorption on concrete composites containing fly ash up to 30 % in regards to structures completely immersed in water. *Case Studies in Construction Materials*, *19*, e02337. https://doi.org/10.1016/j.cscm.2023.e02337

Gülşan, M. E., Alzeebaree, R., Rasheed, A. A., Niş, A., & Kurtoğlu, A. E. (2019). Development of fly ash/slag based self-compacting geopolymer concrete using nano-silica and steel fiber. *Construction and Building Materials*, *211*, 271–283. https://doi.org/10.1016/j.conbuildmat.2019.03.228

Güneyisi, E., Gesoğlu, M., Mohamadameen, A., Alzeebaree, R., Algın, Z., & Mermerdaş, K. (2014). Enhancement of shrinkage behavior of lightweight aggregate concretes by shrinkage reducing admixture and fiber reinforcement. *Construction and Building Materials*, *54*, 91–98. https://doi.org/10.1016/j.conbuildmat.2013.12.041

Han, T. S., Feenstra, P. H., & Billington, S. L. (2003). Simulation of highly ductile Fiber-Reinforced Cement-Based composite components under cyclic loading. *ACI Structural Journal*, *100*(6). https://doi.org/10.14359/12841

Hardjito, D., & Rangan, B. V. (2005). DEVELOPMENT AND PROPERTIES OF LOW-CALCIUM FLY ASH-BASED GEOPOLYMER CONCRETE. *Curtin University of Technology*. https://www.geopolymer.org/dl/?get=curtin-flyash-GP-concrete-report.pdf

Hardjito, D., & Rangan, B. V. (2005). Development and properties of low-calcium fly ash-based geopolymer concrete.

Hemmings, R. T. (1989). Fly ash and coal conversion by-products : characterization, utilization and disposal V : symposium held December 1-3, 1988, Boston, Massachusetts, U.S.A. In *Materials Research Society eBooks*. http://ci.nii.ac.jp/ncid/BA07604077

Hoang, A. L., & Fehling, E. (2017). Numerical study of circular steel tube confined concrete (STCC) stub columns. *Journal of Constructional Steel Research*, *136*, 238–255. https://doi.org/10.1016/j.jcsr.2017.05.020

Hu, W., Nie, Q., Huang, B., Shu, X., & He, Q. (2018). Mechanical and microstructural characterization of geopolymers derived from red mud and fly ashes. *Journal of Cleaner Production*, *186*, 799–806. https://doi.org/10.1016/j.jclepro.2018.03.086

Jang, J., & Lee, H. (2015). Effect of fly ash characteristics on delayed high-strength development of geopolymers. *Construction and Building Materials*, *102*, 260–269. https://doi.org/10.1016/j.conbuildmat.2015.10.172

Khaleel, O., Al-Mishhadani, S., & Razak, H. A. (2011). The effect of coarse aggregate on fresh and hardened properties of Self-Compacting Concrete (SCC). *Procedia Engineering*, *14*, 805–813. https://doi.org/10.1016/j.proeng.2011.07.102

Khan, Q. S., Sheikh, M. N., & Hadi, M. N. (2016). Axial compressive behaviour of circular CFFT: Experimental database and design-oriented model. *Steel and Composite Structures*, *21*(4), 921–947. https://doi.org/10.12989/scs.2016.21.4.921

Khan, Q. S., Sheikh, M. N., & Hadi, M. N. (2020). Experimental results of circular FRP tube confined concrete (CFFT) and comparison with analytical models. *Journal of Building Engineering*, *29*, 101157. https://doi.org/10.1016/j.jobe.2019.101157

Koleżyński, A., Król, M., & Żychowicz, M. (2018). The structure of geopolymers – Theoretical studies. *Journal of Molecular Structure*, *1163*, 465–471. https://doi.org/10.1016/j.molstruc.2018.03.033

Lai, Z., & Varma, A. H. (2018). High-Strength Rectangular CFT members: database, modeling, and design of short columns. *Journal of Structural Engineering*, *144*(5). https://doi.org/10.1061/(asce)st.1943-541x.0002026

Lai, Z., Varma, A. H., & Griffis, L. G. (2016). Analysis and design of Noncompact and Slender CFT Beam-Columns. *Journal of Structural Engineering*, *142*(1). https://doi.org/10.1061/(asce)st.1943-541x.0001349

Lai, Z., Varma, A. H., & Zhang, K. (2014). Noncompact and slender rectangular CFT members: Experimental database, analysis, and design. *Journal of Constructional Steel Research*, *101*, 455–468. https://doi.org/10.1016/j.jcsr.2014.06.004

Lai, Z., Yan, J., Wang, Y., Dong, C., & Weng, X. (2023). Axial compressive behavior and design of high-strength square concrete-filled steel tube short columns with embedded GFRP tubes. *Journal of Constructional Steel Research*, *207*, 107955. https://doi.org/10.1016/j.jcsr.2023.107955

Lata, P., & Kaur, I. (2019). Thermomechanical interactions in transversely isotropic magneto thermoelastic solid with two temperatures and without energy

dissipation. *Steel and Composite Structures*, *32*(6), 779–793. https://doi.org/10.12989/scs.2019.32.6.779

Li, N., Lu, Y., Li, S., & Liang, H. (2015). Statistical-based evaluation of design codes for circular concrete-filled steel tube columns. *Steel and Composite Structures*, *18*(2), 519–546. https://doi.org/10.12989/scs.2015.18.2.519

Malhotra, V. M. and A. A. Ramezanianpour (2004). Fly Ash in Concrete. Ottawa, Ontario, Canada, CANMET

Malhotra, V. M. (1999). Making Concrete "Greener" with Fly Ash. *ACI Concrete International*, *21*(5), 61–66. https://trid.trb.org/view/504169

Mathew, G., & Issac, B. M. (2020). Effect of molarity of sodium hydroxide on the aluminosilicate content in laterite aggregate of laterised geopolymer concrete. *Journal of Building Engineering*, *32*, 101486. https://doi.org/10.1016/j.jobe.2020.101486

Mccaffrey, R. (2002). Climate change and the cement industry. Global cement and lime magazine (environmental special issue), 15, 19.

Mo, B., Zhu, H., Cui, X., He, Y., & Gong, S. (2014). Effect of curing temperature on geopolymerization of metakaolin-based geopolymers. *Applied Clay Science*, *99*, 144–148. https://doi.org/10.1016/j.clay.2014.06.024

Mohammed, M., Geremew, A., Mohammed, M., & Jemal, A. (2022). A study on the applicability of scoria gravel an alternative base course material through blending with marble waste aggregate. *Heliyon*, *8*(11), e11742. https://doi.org/10.1016/j.heliyon.2022.e11742

Moukannaa, S., Loutou, M., Benzaazoua, M., Vitola, L., Alami, J., & Hakkou, R. (2018). Recycling of phosphate mine tailings for the production of geopolymers. *Journal of Cleaner Production*, *185*, 891–903. https://doi.org/10.1016/j.jclepro.2018.03.094

Mustapha, F. A., Sulaiman, A., & Mohamed, R. N. (2021). Performance of fly ash and silica fume self-compacting concrete filled steel tube stub columns under axial compression. *IOP Conference Series Materials Science and Engineering*, *1144*(1), 012012. https://doi.org/10.1088/1757-899x/1144/1/012012

Nguyen, A. D., & Škvára, F. (2016). The influence of ambient pH on fly ash-based geopolymer. *Cement and Concrete Composites*, *72*, 275–283. https://doi.org/10.1016/j.cemconcomp.2016.06.010

Nuruddin, M. F., Demie, S., Ahmed, M. F., & Shafiq, N. (2011). Effect of superplasticizer and NAOH molarity on workability, compressive strength and microstructure properties of Self-Compacting geopolymer concrete. *World Academy of Science, Engineering and Technology, International Journal of Environmental, Chemical, Ecological, Geological and Geophysical Engineering*, *5*(3), 187–194. https://doi.org/10.5281/zenodo.1062742

Okamura, H., & Ouchi, M. (2003). Self-compacting concrete. Journal of advanced concrete technology, 1(1), 5-15.

Okamura, H., & Ouchi, M. (1998). Self-compacting high performance concrete. *Progress in Structural Engineering and Materials*, *1*(4), 378–383. https://doi.org/10.1002/pse.2260010406

Ouchi, M. (2000). Self-compacting concrete-development, applications and investigations. NORDIC CONCRETE RESEARCH-PUBLICATIONS-, 23, 29-34.

Pade, C., Larsen, F., Luping, T., Karlsson, M., Carlström, S., & Johansen, K. (2005). Self-compacting concrete: test methods for SCC. Nordic Innovation Centre, Danish Technological Institute, Project, (02128), 31.

Palomo, A., Grutzeck, M. W., & Blanco, M. T. (1999). Alkali-activated fly ashes: A cement for the future. Cement and concrete research, 29(8), 1323-1329.

Provis, J. L., & Van Deventer, J. S. J. (2009). *Geopolymers : structure, processing, properties and industrial applications*. https://binamarga.pu.go.id/bintekjatan/otomasi/index.php?p=show_detail&id=20657&keywords=

Rahi, R. A., Azizli, K., Man, Z., Rahmiati, T., & Nuruddin, M. (2014). Effect of sodium hydroxide concentration on the mechanical property of non sodium silicate fly ash based geopolymer. *Journal of Applied Sciences*, *14*(23), 3381–3384. https://doi.org/10.3923/jas.2014.3381.3384

Rangan, V. (2008). Low-Calcium, Fly-Ash-Based geopolymer concrete. In *CRC Press eBooks*. https://doi.org/10.1201/9781420007657.ch26

Resheidat, M., & Alzyoud, S. A. (2008). SCC Development in Jordan. ICCBT 2008–A–(29), 319-332.

Roy, D. M. (1999). Alkali-activated cements Opportunities and challenges. *Cement and Concrete Research*, *29*(2), 249–254. https://doi.org/10.1016/s0008-8846(98)00093-3

Sakino, K., Nakahara, H., Morino, S., & Nishiyama, I. (2004). Behavior of centrally loaded Concrete-Filled Steel-Tube short columns. *Journal of Structural Engineering*, *130*(2), 180–188. https://doi.org/10.1061/(asce)0733-9445(2004)130:2(180

Salehi, S., Khattak, M. J., Rizvi, H., Karbalaei, S., & Kiran, R. (2017). Sensitivity analysis of fly ash geopolymer cement slurries: Implications for oil and gas wells cementing applications. *Journal of Natural Gas Science and Engineering*, *37*, 116–125. https://doi.org/10.1016/j.jngse.2016.11.025

Shi, X., Wang, Q., Zhao, X., & Collins, F. G. (2015a). Structural behaviour of geopolymeric recycled concrete filled steel tubular columns under axial loading. *Construction and Building Materials*, *81*, 187–197. https://doi.org/10.1016/j.conbuildmat.2015.02.035

Shi, X., Wang, Q., Zhao, X., & Collins, F. G. (2015b). Structural behaviour of

geopolymeric recycled concrete filled steel tubular columns under axial loading. *Construction and Building Materials*, *81*, 187–197. https://doi.org/10.1016/j.conbuildmat.2015.02.035

Shilar, F. A., Ganachari, S. V., Patil, V. B., Khan, T. Y., & Khadar, S. D. A. (2022). Molarity activity effect on mechanical and microstructure properties of geopolymer concrete: A review. Case Studies in Construction Materials, 16, e01014.

Sood, H., Khitoliya, R. K., & Pathak, S. S. (2009). Incorporating European standards for testing self-compacting concrete in Indian conditions. International Journal of Recent Trends in Engineering, 1(6), 41.

Sosa, I., Tamayo, P., Sainz-Aja, J. A., Thomas, C., Setién, J., & Polanco, J. A. (2021). Durability aspects in self-compacting siderurgical aggregate concrete. Journal of Building Engineering, 39, 102268.

Szabó, L., Hidalgo, I., Císcar, J. C., Soria, A., & Russ, P. (2003). Energy consumption and CO2 emissions from the world cement industry. European Commission Joint Research Centre, Report EUR, 20769.

Tao, Z., Katwal, U., Uy, B., & Wang, W. (2021). Simplified nonlinear simulation of rectangular Concrete-Filled Steel tubular columns. *Journal of Structural Engineering*, *147*(6). https://doi.org/10.1061/(asce)st.1943-541x.0003021

Temuujin, J., Van Riessen, A., & MacKenzie, K. (2010). Preparation and characterisation of fly ash based geopolymer mortars. *Construction and Building Materials*, *24*(10), 1906–1910. https://doi.org/10.1016/j.conbuildmat.2010.04.012

Tho-In, T., Sata, V., Boonserm, K., & Chindaprasirt, P. (2018). Compressive strength and microstructure analysis of geopolymer paste using waste glass powder and fly ash. *Journal of Cleaner Production*, *172*, 2892–2898. https://doi.org/10.1016/j.jclepro.2017.11.125

Van Jaarsveld, J., Van Deventer, J., & Lukey, G. (2002). The effect of composition and temperature on the properties of fly ash- and kaolinite-based geopolymers. *Chemical Engineering Journal*, *89*(1–3), 63–73. https://doi.org/10.1016/s1385-8947(02)00025-6

Varma, A. H., Sause, R., Ricles, J. M., & Li, Q. (2005). Development and validation of fiber model for High-Strength Square Concrete-Filled Steel Tube Beam-Columns. *ACI Structural Journal*, *102*(1). https://doi.org/10.14359/13532

Wang, H., Feng, G., Qi, T., Gao, X., Wang, C., Wang, L., & Zhang, Z. (2023). Influence of the use of corn straw fibers to connect the interfacial transition zone with the mechanical properties of cemented coal gangue backfill. *Construction and Building Materials*, *367*, 130334. https://doi.org/10.1016/j.conbuildmat.2023.130334

Wang, Y., Lin, H., Lai, Z., Li, D., Zhou, W., & Yang, X. (2022). Flexural behavior of High-Strength rectangular Concrete-Filled Steel tube members. *Journal of*

Structural Engineering, *148*(1). https://doi.org/10.1061/(asce)st.1943-541x.0003192

Xiong, M., Xiong, D., & Liew, J. R. (2017). Axial performance of short concrete filled steel tubes with high- and ultra-high- strength materials. *Engineering Structures*, *136*, 494–510. https://doi.org/10.1016/j.engstruct.2017.01.037

Xu, H., & Van Deventer, J. (2000). The geopolymerisation of alumino-silicate minerals. *International Journal of Mineral Processing*, *59*(3), 247–266. https://doi.org/10.1016/s0301-7516(99)00074-5

Young, B., & Ellobody, E. (2006). Experimental investigation of concrete-filled cold-formed high strength stainless steel tube columns. *Journal of Constructional Steel Research*, *62*(5), 484–492. https://doi.org/10.1016/j.jcsr.2005.08.004

Young, J. F. (1998a). The Science and technology of civil engineering materials. *Choice Reviews Online*, *35*(10), 35–5678. https://doi.org/10.5860/choice.35-5678

Young, J. F. (1998b). The Science and technology of civil engineering materials. *Choice Reviews Online*, *35*(10), 35–5678. https://doi.org/10.5860/choice.35-5678

Zhuang, X. Y., Chen, L., Komarneni, S., Zhou, C. H., Tong, D. S., Yang, H. M., Yu, W. H., & Wang, H. (2016). Fly ash-based geopolymer: clean production, properties and applications. *Journal of Cleaner Production*, *125*, 253–267. https://doi.org/10.1016/j.jclepro.2016.03.019

Zrar, Y. J., Younis, K. H., & Sherwani, A. F. H. (2023). Properties of sustainable self-compacted concrete with recycled concrete and waste tire crumb rubber aggregates. *Construction and Building Materials*, *407*, 133524. https://doi.org/10.1016/j.conbuildmat.2023.133524

Zribi, M., Samet, B., & Baklouti, S. (2019). Effect of curing temperature on the synthesis, structure and mechanical properties of phosphate-based geopolymers. *Journal of Non-Crystalline Solids*, *511*, 62–67. https://doi.org/10.1016/j.jnoncrysol.2019.01.032